Surfactant Based Enhanced Oil Recovery and Foam Mobility Control

1st Annual Technical Report

Reporting Period Start Date: July 2003

Reporting Period End Date: June 2004

Principal Authors:

George J. Hirasaki, Rice University

Clarence A. Miller, Rice University

Gary A. Pope, The University of Texas

Richard E. Jackson, INTERA

Date Report was Issued: July 2004

DE-FC26-03NT15406

Rice University
Department of Chemical Engineering, MS-362
6100 Main Street
Houston, TX 77005-1892

The University of Texas
Department of Petroleum Engineering
P.O. Box 7726
Austin, TX 78713-7726

INTERA, Inc.
9111A Research Blvd.
Austin, TX 78758

DISCLAIMER

This report was prepared as an account of work sponsored by an agency of the United States Government. Neither the United States Government nor any agency thereof, nor any of their employees, make any warranty, expressed or implied, or assumes any legal liability or responsibility for the accuracy, completeness, or usefulness of any information, apparatus, product, or process disclosed, or represents that its use would not infringe privately owned rights. References herein to any specific commercial product, process, or service by trade name, trademark, manufacturer, or otherwise does not necessarily constitute or imply its endorsement, recommendation, or favoring by the United States Government or any agency thereof. The views and opinions of authors expressed herein do not necessarily state or reflect those of the United States Government or and agency thereof.

ABSTRACT

Surfactant flooding has the potential to significantly increase recovery over that of conventional waterflooding. The availability of a large number of surfactant structures makes it possible to conduct a systematic study of the relation between surfactant structure and its efficacy for oil recovery. Also, the addition of an alkali such as sodium carbonate makes possible in situ generation of surfactant and significant reduction of surfactant adsorption. In addition to reduction of interfacial tension to ultra-low values, surfactants and alkali can be designed to alter wettability to enhance oil recovery.

An alkaline surfactant process is designed to enhance spontaneous imbibition in fractured, oil-wet, carbonate formations. It is able to recover oil from dolomite core samples from which there was no oil recovery when placed in formation brine.

Mobility control is essential for surfactant EOR. Foam is evaluated to improve the sweep efficiency of surfactant injected into fractured reservoirs.

UTCHEM is a reservoir simulator specially designed for surfactant EOR. A dual-porosity version is demonstrated as a potential scale-up tool for fractured reservoirs.

TABLE OF CONTENTS

TABLE OF TABLES

Task 1.0 Improved surfactants and formulations

Task 2 Phase behavior, adsorption, and composition changes during displacement

Subtask 2.3 Surfactant-enhanced spontaneous imbibition experiments

Subtask 2.5 Adsorption

Task 4: Simulation of Field-Scale Processes

TABLE OF FIGURES

Task 1.0 Improved surfactants and formulations

Task 2 Phase behavior, adsorption, and composition changes during displacement

Subtask 2.3 Surfactant-enhanced spontaneous imbibition experiments

Subtask 2.5 Adsorption

Task 3 Foam for Mobility Control

Task 4: Simulation of Field-Scale Processes

INTRODUCTION

Oil recovery by primary depletion and waterflooding recovers only about one third of the original in place, on the average. The remaining oil can be categorized into: (1) the residual oil in the regions swept by water and (2) the movable oil in the regions unswept or poorly swept by water. This project uses surfactants to reduce the residual oil saturation by both interfacial tension reduction and wettability alteration, the latter in cases where wettability is responsible for retaining oil in the matrix. A factor in the sweep efficiency of a reservoir is the mobility ratio between the resident fluids and the injected fluids. Polymer solution is the traditional method for mobility control in surfactant flooding. This project will evaluate foam as an alternate or supplement to polymer for mobility control. Our objective is to economically increase the recovery efficiency beyond that achieved by waterflooding.

Both unfractured and fractured formations will be addressed in this project. The driving force for displacement of oil in unfractured systems is primarily the pressure gradient developed by displacing fluids from the injection well to the production well. This pressure gradient may be only a small contributor in fractured formations. In this case, spontaneous imbibition is needed to exchange the injected fluid and oil between the fracture and matrix. The driving force for spontaneous imbibition includes capillary pressure gradients and buoyancy, or gravity drainage. The contribution due to capillary pressure gradients may be diminished because of low interfacial tension.

Both sandstone and carbonate formations will be considered. Carbonate formation usually tend to be more oil-wet and fractured compared to sandstone formations. In either case, surfactant adsorption on the mineral surfaces must be minimized. Sodium carbonate is used with anionic surfactants in carbonate formations to reduce adsorption. The alkalinity of the sodium carbonate also generates surfactants in situ by reacting with the naphthenic acids in the crude oil.

Scale-up from the laboratory to the field is a necessary part of developing an enhanced oil recovery process. The tool for this scale-up in the reservoir simulator, UTCHEM.

EXECUTIVE SUMMARY

Twenty four surfactants are compared for their efficacy for oil recovery by surfactant flooding. Surfactant structure – performance relationships are needed for applications with a specified crude oil composition, brine salinity, reservoir temperature, formation mineralogy, and recovery mechanism. The surfactants are characterized by the optimal salinity for different pure hydrocarbon oils, the solubilization ratio, which is an estimator of the level of interfacial tension at optimal conditions, and whether it forms viscous gel or liquid crystalline phases that cause slow emulsion coalescence.

An alkaline surfactant process is being developed for enhanced spontaneous imbibition in a fractured, oil-wet, carbonate formation. The carbonate ion of sodium carbonate is a potential determining ion in carbonate formations such as calcite and dolomite. Alteration of the mineral surface to a negative charge aids in the wettability alteration and makes a dramatic reduction in the adsorption of anionic surfactants. Calcium ion concentration is sequestered because of the low solubility product of calcium carbonate. Also the alkali raises the pH, which results in sponification of naphthenic acids to naphthenic soap, a natural surfactant. The naphthenic soap is usually too lypophilic by itself and addition of a synthetic surfactant is needed. Ultra-low interfacial tensions are possible at synthetic surfactant concentrations as low as 0.05%. However, the system is complex because it is a mixture of two surfactants with very different properties. This results in the optimal salinity that depends on the water/oil ratio and surfactant concentration. However, these dependencies can be correlated by the ratio of natural surfactant/synthetic surfactant.

It is argued that capillarity, governed by wettability and interfacial tension, is responsible for retaining oil in the oil-wet matrix when a fractured, carbonate formation is waterflooded. This is demonstrated by observations with a calcite plate, either in a horizontal configuration or in a narrow, vertical gap. Replacement of brine with alkaline surfactant solution results in mobilization of oil by buoyancy or gravity drainage.

Spontaneous imbibition did not occur when partially oil saturated, dolomite core samples were placed in an imbibition cell filled with brine. Spontaneous imbibition occurred when the brine was replaced with alkaline surfactant solution. Scaling of the rate of recovery indicated that dominant mechanism for recovery was gravity drainage.

Surfactant retention by adsorption and phase trapping determine the amount of surfactant required for a surfactant enhanced oil recovery process. We show that the adsorption of anionic surfactants on calcite and dolomite can be reduced by an order of magnitude by addition of sodium carbonate.

Mobility control is recognized as an essential element of surfactant EOR. Surfactant injection into fractured formations imposes a severe challenge for reservoir conformance or sweep efficiency. The volumetric flow rate into a set of

parallel fractures is proportional to the third power of the fracture width. This will result in large fractures acting as “thief zones” and small fractures being bypassed. Foam has the potential to improve the liquid distribution in fractured systems. For bubbles of the same size, the apparent viscosity is higher in larger fractures compared to smaller fractures. We have verify that the model developed for foam in capillaries can be extended to flow between parallel plates. Our next task is to demonstrate that better sweep efficiency is possible with the use of foam.

The reservoir simulator, UTCHEM will be used as the tool to scale-up from laboratory experiments to field design. The effect of changing wettability in naturally fractured systems is demonstrated by 2-D areal and vertical simulations with UTCHEM.

Task 1.0 Improved surfactants and formulations

Subtask 1.1. Identifying and synthesizing improved, cost-effective surfactants

Start Date: June 2003 Proposed Completion Date: May 2004

Introduction. After 1990, oil companies drastically scaled back research on surfactants, but we and other academic researchers continued to make progress in finding better surfactants for both groundwater cleanup and EOR (Jayanti *et al.*, 2002). The search for better surfactants must take into account (1) the anticipated EOR approach, (2) the chemical/physical conditions in reservoirs, (3) economic factors, and (4) commercial availability. For example, the alkaline surfactant (AS) EOR approach utilizes anionic surfactants under alkaline conditions to minimize surfactant adsorption onto mineral surfaces and to generate additional surfactants *in situ* by reacting with naphthenic acids in the crude oil to create soaps. The second consideration, chemical/physical conditions in the reservoirs, includes sandstone vs carbonate formations, crude oil characteristics, fractured vs unfractured formations, aqueous phase chemistry, and temperature. These varied reservoir parameters may necessitate the use of a surfactant tailoring approach, which simply means that a surfactant or mixture of surfactants that works in one oil reservoir may not be effective in another. Although it is highly desirable to identify a single surfactant or general surfactant chemical structure for all reservoirs, the site-to-site variations require a "toolbox" of efficient surfactants rather than just one. We have already experienced this problem while screening surfactants for the Yates field of West Texas and the Cedar Creek field in Montana. In the low temperature Yates field, surfactants belonging to the class known as branched alcohol, propoxy sulfates can be used. However, the high temperature (220 F) in the Cedar Creek field precludes the use of sulfates because of their susceptibility to hydrolysis (Talley, 1988). The case-by-case evaluation of EOR candidates for effective surfactants can be an impediment to widespread adoption of chemical EOR. It would be of great practical advantage if surfactant selection and evaluation could be simplified to a relatively small number of surfactants belonging to a single chemical class with very high performance characteristics. Consequently, we are considering new surfactant molecules that would be more universal in their application but still expect different classes will be needed for low temperature and high temperature applications.

The economics and commercial availability of new surfactants are as important as their performance if EOR is to become commercial on a large scale. We are incorporating this philosophy into the identification of more effective surfactants through the following guidelines:

- Surfactants must be capable of being produced in large-scale at U.S. plants and using existing chemical technology. Selected manufacturers such as Harcros and Stepan will be queried on their ability to produce good-performing surfactants that are not in their inventories.

- A protocol for determining the manufacturer's cost for surfactant production should be applied to laboratory-synthesized surfactants used in these studies.
- Manufacturers' costs should not exceed approximately $1.50 per lb. active using a cost determination formula outlined below.

Manufacturing costs are calculated from the sum of the feedstock and processing costs. Feedstock costs are determined or assumed as:

- Hydrophobe (e.g., alcohol): Chemical Marketing Reporter or quotations;
- Propylene oxide/ ethylene oxide: $0.66/lb (fluctuates with natural gas pricing);
- SO_3: $0.18/lb (Oleum, sulfamic acid, sodium sulfite, sodium bisulfite are similarly priced; exact numbers are available from Chemical Marketing Reporter.);
- NaOH: $0.30/lb.

Processing costs are estimated at:

- Alkoxylation (PO/EO): $0.10/lb based on the number of pounds of alcohol alkoxylate;
- Sulfation/sulfonation + neutralization: $0.15/lb based on the number of pounds of neutralized product;
- Drumming, miscellaneous handling: $0.12/lb

The following figure shows the calculation of costs for a surfactant containing isotridecyl alcohol (TDA) at $0.72/lb plus 4 moles propylene oxide and then sulfated. The nomenclature would be TDA-4PO-SO_4. Molecular weights for the individual components are: TDA = 200; SO_3 = 80; PO = 58; NaOH = 40; TDA-4PO-$S0_4^-Na^+$ = 535.

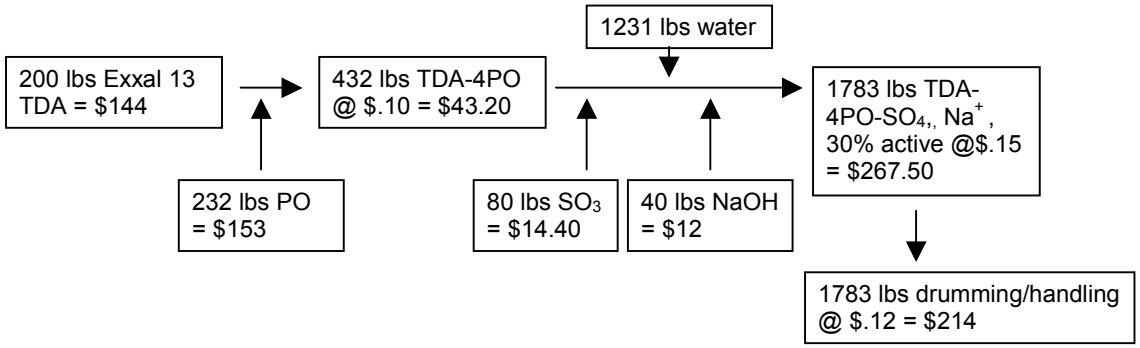

In the cost calculations above, 1783 lb of produced surfactant would cost $848.10, which is $0.48/lb on a 30% active basis or $1.60/lb as 100% active.

References cited:

1. Jayanti, S., L.N. Britton, V. Dwarakanath, and G. Pope. 2002. Laboratory Evaluation of Custom-Designed Surfactants to Remediate NAPL Source Zones. Environ. Sci. Technol. **36:**5491-5497.

2. Talley, L.D. 1988. Hydrolytic Stability of Alkylethoxy Sulfates. SPE Reservoir Engineering, February 1988.

Progress. Procurement of Surfactants. Candidate surfactants were obtained from Harcros, Sasol N.A, Shell and Stepan, and are listed in Table 1. Most of these surfactants belong to the class called alcohol propoxy sulfate. Their overall structure is:

$$\text{(branched alcohol)} - (\text{propoxyl groups})_n - \text{(sulfate)}$$

By varying the number of propoxyl groups the surfactant exhibits varying ratios of hydrophilicity to hydrophobicity (often referred to as the hydrophile:lipophile balance or HLB). However, unlike ethoxyl (EO) moieties the increasing propoxyl (PO) groups increase the hydrophobicity whereas increasing EO groups increase hydrophilicity. Actually, the propoxy chain appears to be equally comfortable on either side of the water:oil interface. This can explain the low interfacial tensions that can be achieved with these surfactants. By varying the alcohol hydrophobe and the number of PO groups, together with shifting the hydrophobicity with increasing cation counterion concentration (i.e., optimal salinity), it should be possible to find the right water:oil phase behavior for any oil. However, these sulfated surfactants are susceptible to hydrolysis at temperatures above 70 C. Therefore, more stable sulfonate surfactants also are being tested for high temperature applications.

Table 1. Candidate Surfactants: Description & Tradenames

Product Name	Alcohol Carbon Chain Length & (Trademark)	Moles PO
TDA-4PO-sulfate (Harcros Chemical)	C_{13}; Isotridecanol (Exxal 13 TDA)	4
TDA-1EO-4PO-sulfate (Harcros Chemical)	C_{13}; Isotridecanol (Exxal 13 TDA)	4
TDA-8PO-sulfate (Harcros Chemical)	C_{13}; Isotridecanol (Exxal 13 TDA)	8
Alfoterra® 13	C_{13}; Isotridecanol (Marlipal™)	3
Alfoterra® 15	C_{13}; Isotridecanol (Marlipal™)	5
Alfoterra® 18	C_{13}; Isotridecanol (Marlipal™)	8
Alfoterra® 23	C_{12} Guerbet (Isofol® 12)	3
Alfoterra® 25	C_{12} Guerbet (Isofol® 12)	5
Alfoterra® 28	C_{12} Guerbet (Isofol® 12)	8
Alfoterra® 33	C_{14} Guerbet (Isofol® 14T)	3
Alfoterra® 35	C_{14} Guerbet (Isofol® 14T)	5
Alfoterra® 38	C_{14} Guerbet (Isofol® 14T)	8
Alfoterra® 43	C_{12} & C_{13} (Isalchem™ 123)	3
Alfoterra® 45	C_{12} & C_{13} (Isalchem™ 123)	5
Alfoterra® 48	C_{12} & C_{13} (Isalchem™ 123)	8
Alfoterra® 53	C_{14} & C_{15} (Isalchem™ 145)	3
Alfoterra® 55	C_{14} & C_{15} (Isalchem™ 145)	5
Alfoterra® 58	C_{14} & C_{15} (Isalchem™ 145)	8
Alfoterra® 63	C_{12} & C_{13} (Safol® 23)	3
Alfoterra® 65	C_{12} & C_{13} (Safol® 23)	5
Alfoterra® 68	C_{12} & C_{13} (Safol® 23)	8
N67-3S	C_{16} & C_{17} (95% branched; Shell)	3
CS-330	C_{12} -3EO-sulfate (Stepan)	3
IOS 15-18	C_{15}-C_{18} Internal Olefin Sulfonate (Shell)	-
Petrostep B100	Alkylbenzene sulfonate (Stepan)	-
Stepantan AS-1246	C_{12} alpha olefin sulfonate (Stepan)	-
Polystep A-16-22	$C_{11\text{-}13}$ br. Alkylbenzene sulfonate (Stepan)	-
Bio-Terge AS-40	$C_{14\text{-}16}$ alpha olefin sulfonate (Stepan)	-

Performance. The first step in the surfactant screening process was to conduct the phase behavior experiments using Decane (alkane carbon number equal to 10) as representative surrogate oil at 60°C. Sodium chloride was used as the electrolyte to control surfactant phase behavior. The initial experiments were conducted at a surfactant concentration of 1.5 wt%. The goal of this step was to identify surfactant formulations that equilibrate rapidly while forming low-viscosity microemulsions. In addition, the optimum oil solubilization parameter, σ*, and salinity, S* were also measured.

Figure 1 shows an example of a phase diagram used for calculating S* and σ* where the oil and water solubilization parameters in the middle phase microemulsion intersect.

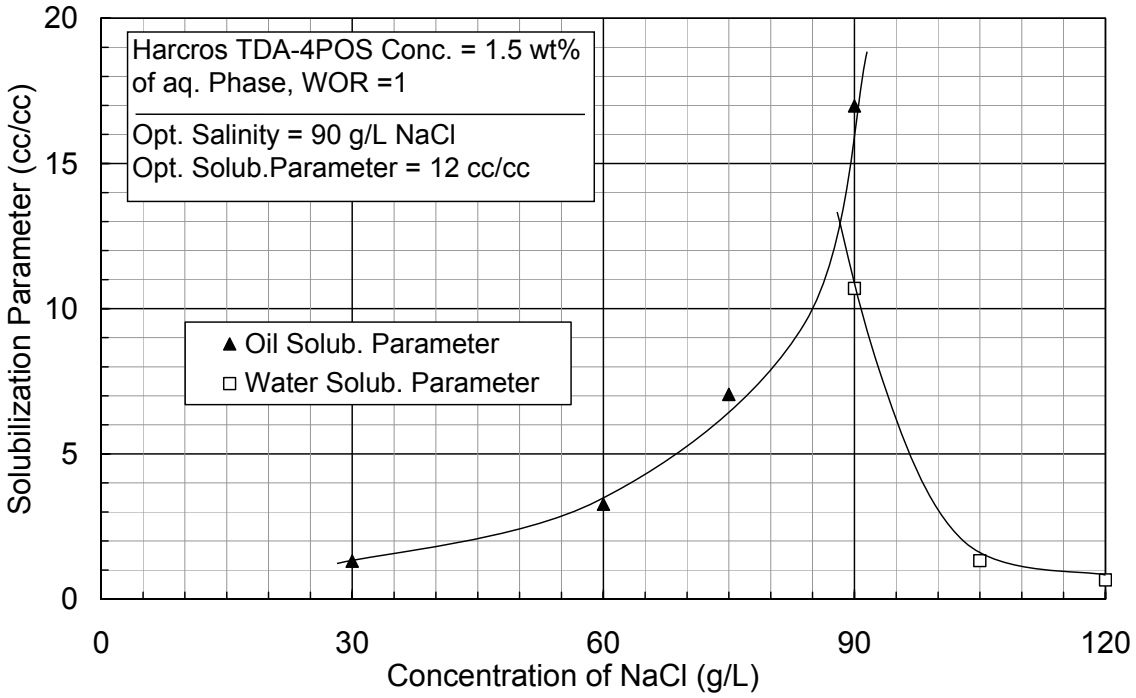

Figure 1. Example of a Phase Diagram

The S* and σ* values obtained from the preliminary screening of Decane with sodium chloride are given in Table 2. The data in Table 2 contain several phase behavior systems that are slow to equilibrate indicated as "not equilibrated". All of these systems contain gels and are unlikely to provide useful phase behavior information other than that they are poor systems and will not be used in further experiments. The surfactant systems marked with two asterisks indicate reasonable systems where one or two of the phase behavior tubes are slower to equilibrate than the rest.

Table 2: Phase Behavior Experiments with Decane, 1.5% Surfactant and 0.05 wt % Na_2CO_3

Product Name	Alcohol Carbon Chain Length & (Trademark)	Optimum Salinity S* (g/L NaCl) @ 60°C	Optimum Oil Solubilization Ratio σ* (cc/cc) @ 60°C
TDA-4PO-sulfate (Harcros Chemical)	C_{13}; Isotridecanol (Ethyl Corp. TDA)	90 and 86*	12 and 13*
TDA-1EO-4PO-sulfate (Harcros Chemical)	C_{13}; Isotridecanol (Ethyl Corp. TDA)	108	6
TDA-8PO-sulfate (Harcros Chemical)	C_{13}; Isotridecanol (Ethyl Corp. TDA)	36	36
Alfoterra® 13	C_{13}; Isotridecanol (Marlipal)	88	16
Alfoterra® 15	C_{13}; Isotridecanol (Marlipal)	68	17
Alfoterra® 18	C_{13}; Isotridecanol (Marlipal)	32	38
Alfoterra® 23	C_{12} (C_6 + C_6) Guerbet (Isofol® 12)	73**	7**
Alfoterra® 25	C_{12} (C_6 + C_6) Guerbet (Isofol® 12)	35**	12**
Alfoterra® 28	C_{12} (C_6 + C_6) Guerbet (Isofol® 12)	Not equilibrated	Not equilibrated
Alfoterra® 33	C_{14} (C_8 + C_6) Guerbet (Isofol® 14T)	32**	3**
Alfoterra® 35	C_{14} (C_8 + C_6) Guerbet (Isofol® 14T)	Not equilibrated	Not equilibrated
Alfoterra® 38	C_{14} (C_8 + C_6) Guerbet (Isofol® 14T)	22**	2**
Alfoterra® 43	C_{12} & C_{13} (Isalchem™ 123)	95**	15**
Alfoterra® 45	C_{12} & C_{13} (Isalchem™ 123)	Not equilibrated	Not equilibrated
Alfoterra® 48	C_{12} & C_{13} (Isalchem™ 123)	Not equilibrated	Not equilibrated
Alfoterra® 53	C_{14} & C_{15} (Isalchem™ 145)	55**	6**
Alfoterra® 55	C_{14} & C_{15} (Isalchem™ 145)	56**	2**
Alfoterra® 58	C_{14} & C_{15} (Isalchem™ 145)	Not equilibrated	Not equilibrated
Alfoterra® 63	C_{12} & C_{13} (Safol® 23)	108	3
Alfoterra® 65	C_{12} & C_{13} (Safol® 23)	95	9
Alfoterra® 68	C_{12} & C_{13} (Safol® 23)	68	5

* - results from two surfactant batches

Viscosity measurements were conducted on select middle phase microemulsions in order to arrive at a salinity concentration that gives good oil solubilization with minimum viscosity. Figures 2 and 3 below show examples where, at 90 g/L NaCl non-Newtonian behavior is observed, yet at 105 g/L (which for this surfactant is pushing it into a Type II microemulsion) has an acceptable viscosity of 1 cp or less.

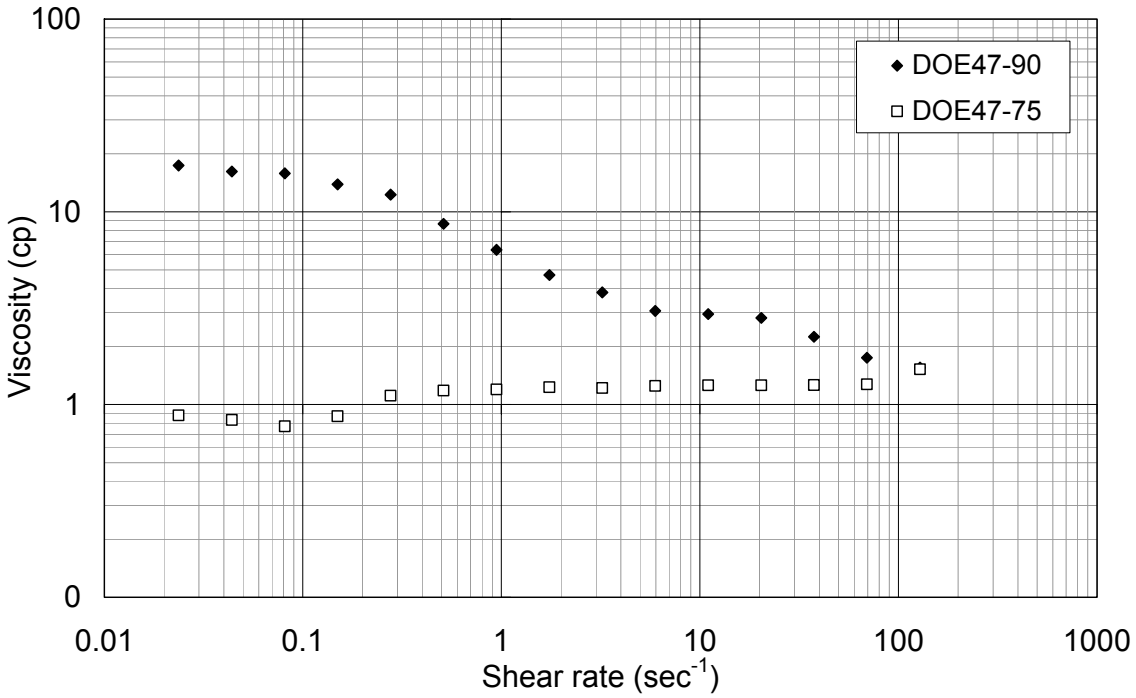

Figure 2. Viscosity vs. Shear Rate for Middle Phase Microemulsion in DOE 47 (Harcros TDA-4PO-sulfate sodium salt) with Decane at 60°C

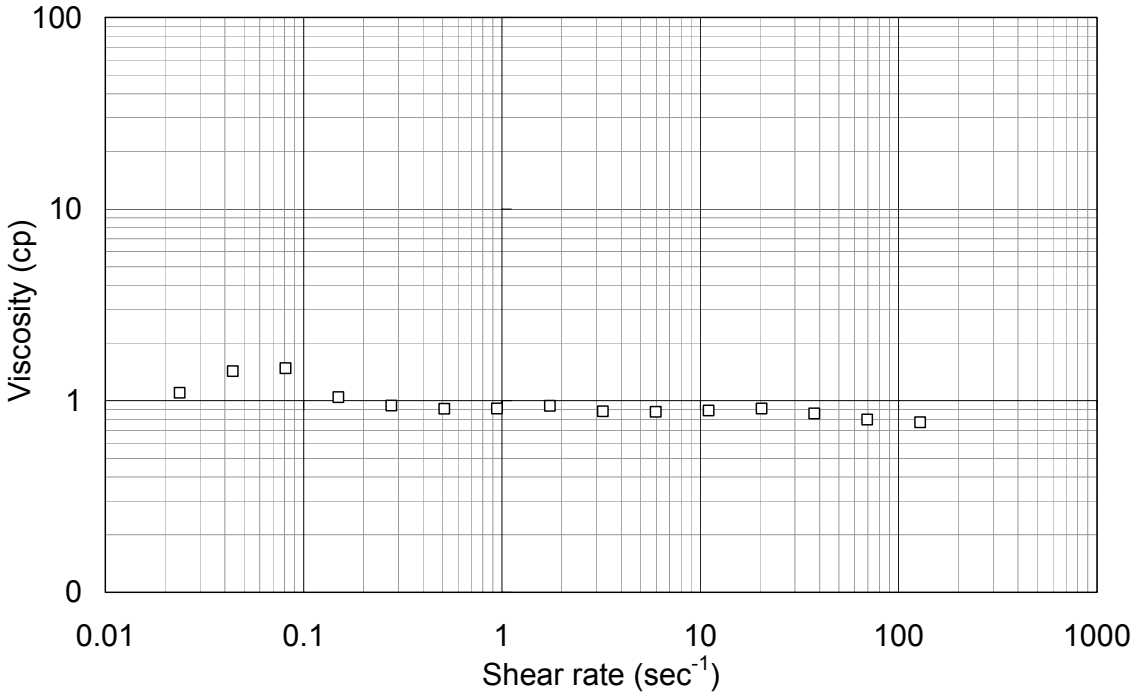

Figure 3. Viscosity vs. Shear Rate for Middle Phase Microemulsion in DOE 52 (Harcros TDA-1EO-4PO-sulfate sodium salt) with Decane at 60°C

The phase behavior experiments with decane identified several promising surfactants for further evaluation, and will be discussed in the next section.

Subtask 1.2 Surfactant tailoring for crude oils and phase behavior
Start Date: June 2003 Proposed Completion Date: May 2004

One of the goals of the work conducted herein was to identify a relationship with surfactant structure and oil EACN. Once such a relationship was developed, the goal was to conduct phase behavior experiments with crude oils and evaluate the performance of the new surfactants with actual crude oils. Two crude oil samples were obtained, one from Burlington Resources, and the other from the Yates field. The Burlington crude oil was from a reservoir in Montana with an ambient temperature of 100^{o}C, so the sulfate surfactants are not applicable. We are currently in the process of tailoring new propoxylated sulfonates that will be applicable at 100^{o}C. A sufficient quantity of Yates crude oil was not available for extensive testing, therefore only preliminary tests were conducted with the Yates oil. We are currently in the process of requesting additional crude oil to complete the phase behavior screening with the Yates oil and provide recommendations for future work at Rice.

Phase behavior experiments were conducted with hexane, octane and decane as surrogate oils for purposes of phase behavior screening. The electrolyte used in the phase behavior experiments with the above surrogate oils was a 9:1 mixture of sodium chloride to calcium chloride to simulate divalent ions in reservoir brines. The base experiments were conducted with octane as the oil and the best experiments were repeated with decane and hexane to obtain phase behavior data as a function of EACN.

All the experiments were conducted at a surfactant concentration of 4 wt% because it is more efficient to first evaluate surfactants at high concentration and then later further test them at low concentrations if justified by the initial results. Tables 3, 4 and 5 summarize the various experiments conducted. Since many formulations exhibited poor phase behavior in terms of equilibration times and high microemulsion viscosities, the phase behavior experiments used secondary butanol (SBA) as a cosolvent. The SBA concentrations were varied between 2 wt% and 8 wt% in the experiments.

Table 3: Phase Behavior Experiments with Hexane, 4% Surfactant, 8% sec-Butanol and 9:1 Mix, NaCl, $CaCl_2$

Product Name	Alcohol Carbon Chain Length & (Trademark)	Optimum Salinity S* (wt% salt) @ 60°C	Optimum Oil Solubilization Ratio σ* (cc/cc) @ 60°C
Alfoterra® 13	C_{13}; Isotridecanol (Marlipal	>1.5	~7
Alfoterra® 15	C_{13}; Isotridecanol (Marlipal)	0.95	10
Alfoterra® 23	C_{12} (C_6 + C_6) Guerbet (Isofol® 12)	>1.5	~10
Alfoterra® 25	C_{12} (C_6 + C_6) Guerbet (Isofol® 12)	1.05	9

Table 4: Phase Behavior Experiments with Octane and 9:1 Mix, NaCl, $CaCl_2$

Product Name	Alcohol Carbon Chain Length & (Trademark)	sec-Butanol (wt %)	Optimum Salinity S* (wt% Salt) @ 60°C	Optimum Oil Solubilization Ratio σ* (cc/cc) @ 60°C
Alfoterra® 23	C_{12} (C_6 + C_6) Guerbet (Isofol® 12)	0	4.2	19.5
Alfoterra® 25	C_{12} (C_6 + C_6) Guerbet (Isofol® 12)	0		Not equilibrated
Alfoterra® 28	C_{12} (C_6 + C_6) Guerbet (Isofol® 12)	0		Not equilibrated
Alfoterra® 23	C_{12} (C_6 + C_6) Guerbet (Isofol® 12)	2	3.9	11
Alfoterra® 23	C_{12} (C_6 + C_6) Guerbet (Isofol® 12)	4	2.95	6.5
Alfoterra® 23	C_{12} (C_6 + C_6) Guerbet (Isofol® 12)	8	2.7	6.5
Alfoterra® 25	C_{12} (C_6 + C_6) Guerbet (Isofol® 12)	2	2.9	7.1
Alfoterra® 25	C_{12} (C_6 + C_6) Guerbet (Isofol® 12)	4	2.1	11
Alfoterra® 25	C_{12} (C_6 + C_6) Guerbet (Isofol® 12)	8	1.8	6.3
Alfoterra® 28	C_{12} (C_6 + C_6) Guerbet (Isofol® 12)	2		Not equilibrated
Alfoterra® 28	C_{12} (C_6 + C_6) Guerbet (Isofol® 12)	4		Not equilibrated
Alfoterra® 28	C_{12} (C_6 + C_6) Guerbet (Isofol® 12)	8		Not equilibrated
Alfoterra® 53	C_{14} & C_{15} (Isalchem™ 145)	0		Not equilibrated
Alfoterra® 55	C_{14} & C_{15} (Isalchem™ 145)	0		Not equilibrated
Alfoterra® 58	C_{14} & C_{15} (Isalchem™ 145)	0		Not equilibrated
Alfoterra® 53	C_{14} & C_{15} (Isalchem™ 145)	2		Not equilibrated
Alfoterra® 53	C_{14} & C_{15} (Isalchem™ 145)	4	2.1	6.5
Alfoterra® 53	C_{14} & C_{15} (Isalchem™ 145)	8	1.6	3.3
Alfoterra® 55	C_{14} & C_{15} (Isalchem™ 145)	2		Not equilibrated
Alfoterra® 55	C_{14} & C_{15} (Isalchem™ 145)	4		Not equilibrated
Alfoterra® 55	C_{14} & C_{15} (Isalchem™ 145)	8		Not equilibrated
Alfoterra® 58	C_{14} & C_{15} (Isalchem™ 145)	2		Not equilibrated
Alfoterra® 58	C_{14} & C_{15} (Isalchem™ 145)	4		Not equilibrated
Alfoterra® 58	C_{14} & C_{15} (Isalchem™ 145)	8		Not equilibrated
Alfoterra® 13	C_{13}; Isotridecanol (Marlipal)	0	4.9	11
Alfoterra® 15	C_{13}; Isotridecanol (Marlipal)	0	2.75	16
Alfoterra® 18	C_{13}; Isotridecanol (Marlipal)	0		Not equilibrated
Alfoterra® 13	C_{13}; Isotridecanol (Marlipal)	2	4.5	8.9
Alfoterra® 13	C_{13}; Isotridecanol (Marlipal)	4	4.22	6.6
Alfoterra® 13	C_{13}; Isotridecanol (Marlipal)	8	3.4	3.4
Alfoterra® 15	C_{13}; Isotridecanol (Marlipal)	2	2.9	10.5
Alfoterra® 15	C_{13}; Isotridecanol (Marlipal)	4	2.3	9.7
Alfoterra® 15	C_{13}; Isotridecanol (Marlipal)	8	2.0	6.3
Alfoterra® 18	C_{13}; Isotridecanol (Marlipal)	2		Not equilibrated
Alfoterra® 18	C_{13}; Isotridecanol (Marlipal)	4	0.6	2.6
Alfoterra® 18	C_{13}; Isotridecanol (Marlipal)	8		Not equilibrated

Table 5: Phase Behavior Experiments with Decane, 4% Surfactant, 8% sec-Butanol and 9:1 Mix, NaCl, $CaCl_2$

Product Name	Alcohol Carbon Chain Length & (Trademark)	Optimum Salinity S* (wt% salt) @ 60°C	Optimum Oil Solubilization Ratio σ* (cc/cc) @ 60°C
Alfoterra® 13	C_{13}; Isotridecanol (Marlipal	5	3.8
Alfoterra® 15	C_{13}; Isotridecanol (Marlipal)	3.1	4.2
Alfoterra® 23	C_{12} (C_6 + C_6) Guerbet (Isofol® 12)	5.3	4
Alfoterra® 25	C_{12} (C_6 + C_6) Guerbet (Isofol® 12)	3.3	4.2

The experiments indicated that the formulations with 3 PO and 5 PO groups rapidly coalesced into stable microemulsions with 8 wt% SBA. However, samples with 8 PO groups were slow to equilibrate even with 8 wt% SBA and useful results were not obtained for analysis.

The above experiments provided valuable correlations between surfactant structure and phase behavior. Figure 4 shows the effect of optimal salinity as a function of the alkane carbon number. Figure 5 indicates that the optimal salinity shows a similar decline with respect to the alkane carbon number for various surfactants. However increasing the number of PO groups reduces the optimal salinity, while increasing coalescence times.

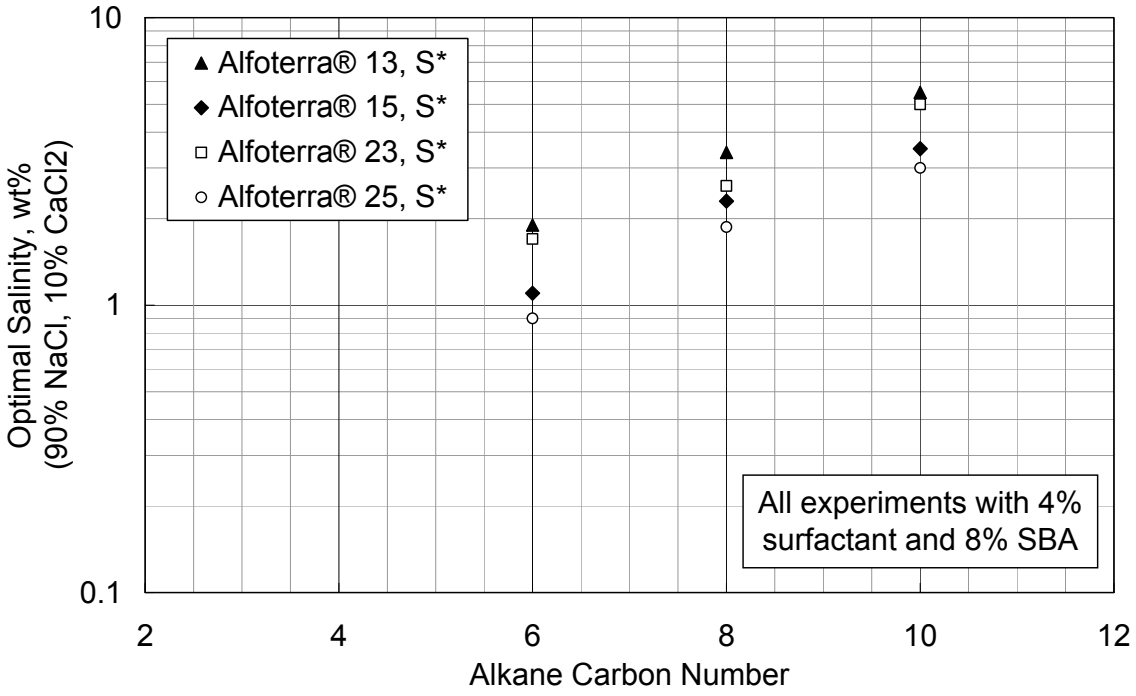

Figure 4. Effect of Alkane Carbon Number on Optimal Salinity with Several Surfactants at 60°C

The effect of PO number on optimal salinity is plotted in Figure 5 and shows a similar decline in optimal salinity for hexane, octane and decane. However, more data is needed with formulations containing a lower number of PO groups to develop trends for future predictions. In general, the number of PO groups did not affect the solubilization parameter, but only affected optimal salinity.

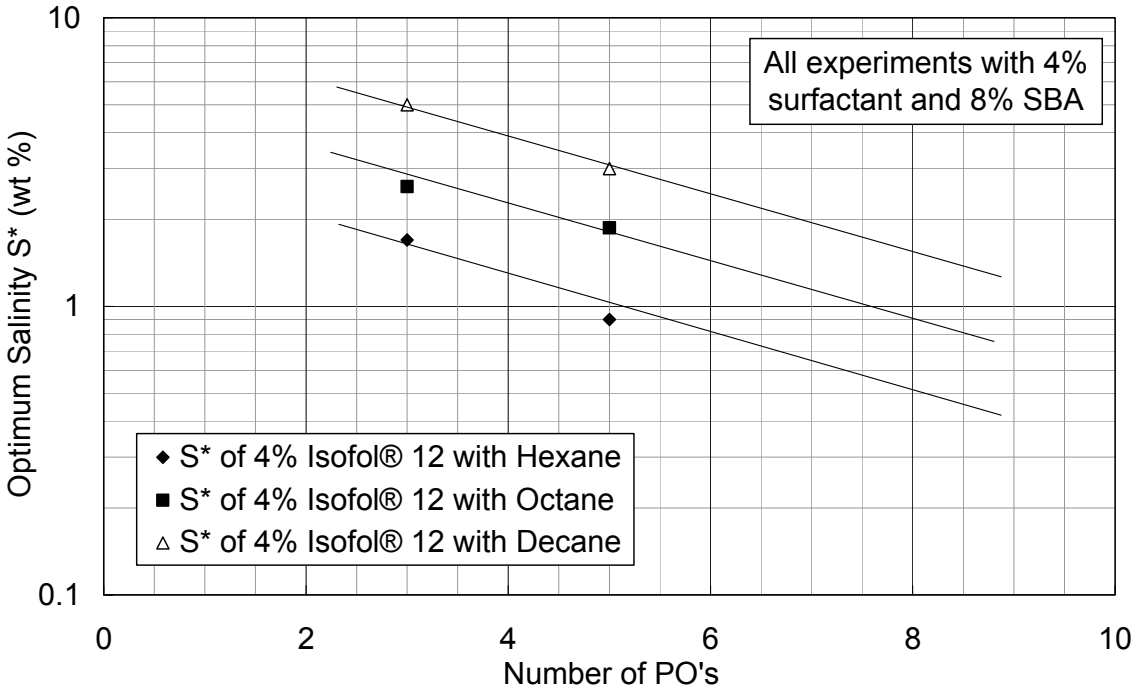

Figure 5. Effect of PO Number on Optimal Salinity at 60°C

In addition to the trends plotted in Figures 4 and 5, the above experiments indicate that when calcium chloride is added to the surfactant formulations, rapid coalescence and equilibration is observed only with the addition of secondary-butanol. Therefore, the next step was to identify co-surfactants that would improve coalescence times and eliminate the use of alcohol, while maintaining rapid coalescence. Table 6 lists the experiments conducted with a range of co-surfactants.

Table 6: Phase Behavior Experiments with Octane and Co-surfactants at 70°C

Alcohol Carbon Chain Length & (Trademark)	Co-Surfactant
2 wt% C_{13}; Isotridecanol -3PO-Sulfate (TDA-3), 2 wt% C_{12} (C_6 + C_6) Guerbet (Isofol® 12)-3PO-Sulfate (L-23)	1 wt% sodium dihexyl sulfosuccinate
2 wt% C_{13}; Isotridecanol -3PO-Sulfate, 2 wt% C_{12} (C_6 + C_6) Guerbet (Isofol® 12)-3PO-Sulfate	0.6 wt% Variquat-CC-9 (polypropoxy quaternary ammonium chloride, MW~400)
2 wt% C_{13}; Isotridecanol -3PO-Sulfate, 2 wt% C_{12} (C_6 + C_6) Guerbet (Isofol® 12)-3PO-Sulfate	0.6 wt% Variquat-CC-32 (polypropoxy quaternary ammonium chloride, MW~1100)

The results with the above experiments indicated that when sodium dihexyl sulfosuccinate was used as a co-surfactant, rapid coalescence was observed, and that sodium dihexyl sulfosuccinate was an excellent surrogate for SBA.

Hence phase behavior experiments were conducted with a formulation containing 2 wt% C_{13}; Isotridecanol -3PO-Sulfate (TDA-3), 2 wt% C_{12} (C_6 + C_6) Guerbet (Isofol® 12)-3PO-Sulfate (L-23), 1 wt% sodium dihexyl sulfosuccinate, using a 9:1 mix of sodium and calcium chloride. The initial screening experiments with Octane showed rapid coalescence into stable microemulsions. The viscosity of the microemulsions at various electrolyte concentrations was measured as a function of the solubilization parameter as shown in Figure 6. These viscosities are acceptably low and further confirm the rapid coalescence into stable microemulsions using sodium dihexyl sulfosuccinate as a co-surfactant.

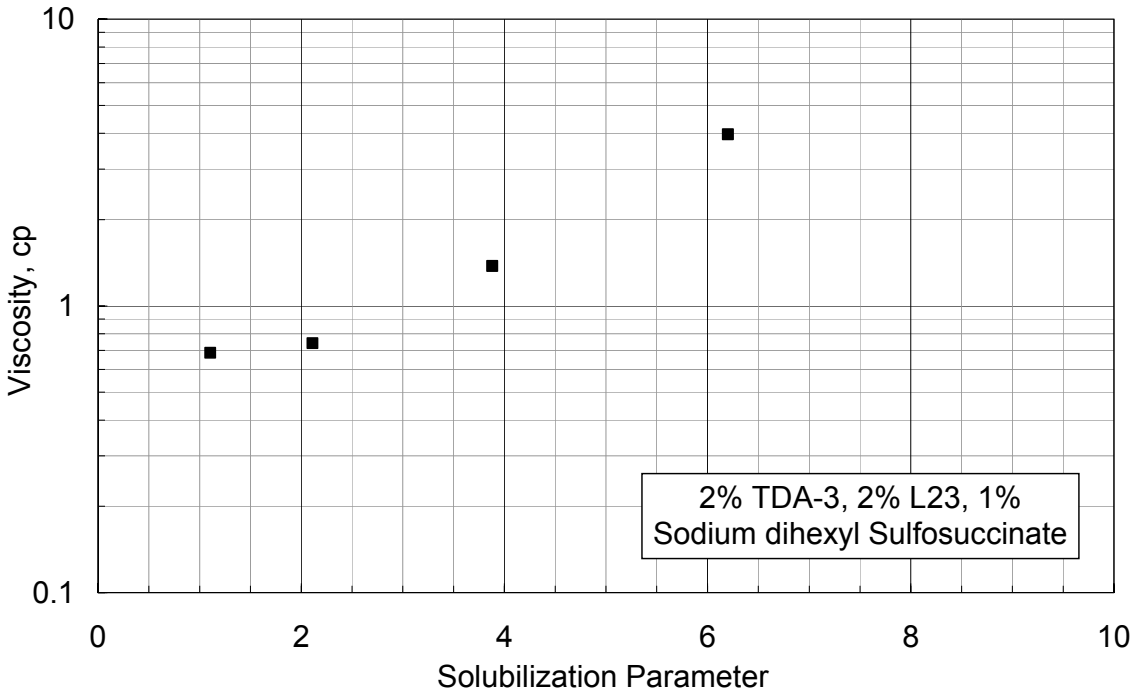

Figure 6. Viscosity of Microemulsions with 2 wt% C_{13}; Isotridecanol -3PO-Sulfate (TDA-3), 2 wt% C_{12} (C_6 + C_6) Guerbet (Isofol® 12)-3PO-Sulfate (L-23), 1 wt% sodium dihexyl sulfosuccinate, using a 9:1 mix of sodium and calcium chloride

Additional phase behavior experiments were conducted with hexane, heptane, octane, nonane and decane to plot the effect of alkane carbon number on optimal salinity for the formulation containing sodium dihexyl sulfosuccinate as shown in Figure 7. The results in Figure 7 indicate an excellent trend of the log of optimal salinity with the alkane carbon number. These results can be used as a predictive guide to surfactant selection for crude oils with various alkane carbon numbers.

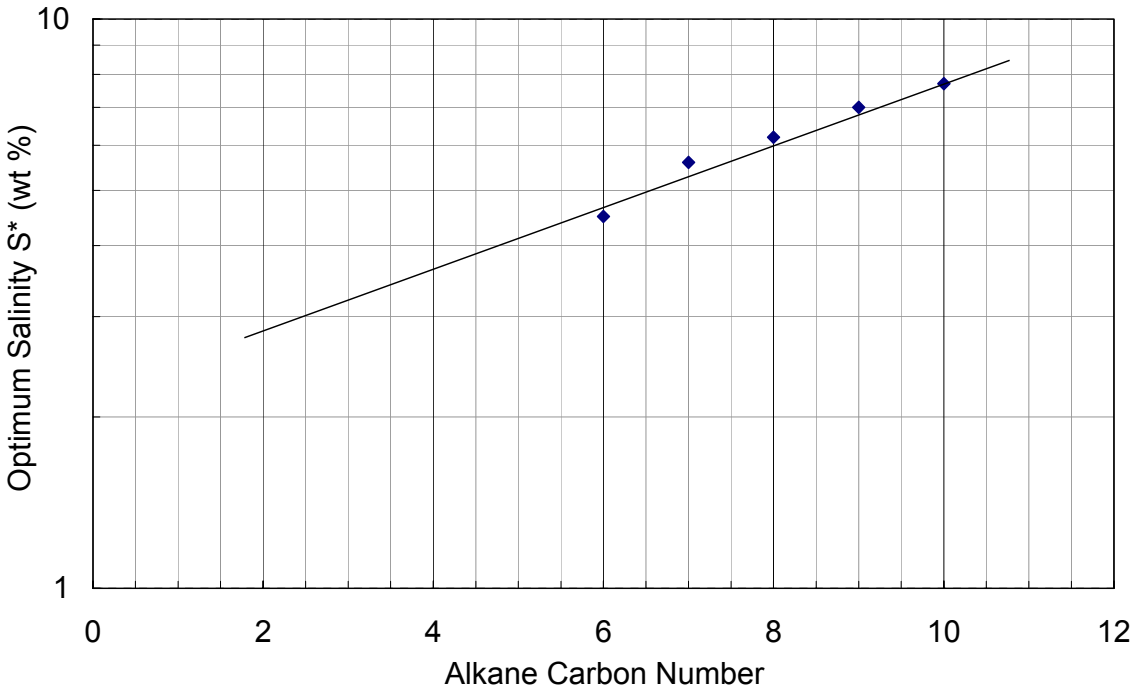

Figure 7. Effect of Alkane Carbon Number on Optimal Salinity with 2 wt% C_{13}; Isotridecanol -3PO-Sulfate (TDA-3), 2 wt% C_{12} (C_6 + C_6) Guerbet (Isofol® 12)-3PO-Sulfate (L-23), 1 wt% sodium dihexyl sulfosuccinate, using a 9:1 mix of sodium and calcium chloride

Summary

In summary, the phase behavior studies conducted identified formulations with excellent phase behavior using various alkanes for surrogate oils. The next step will be to test these formulations with several crude oils. We will conduct such work in Year 2 once crude oil samples are obtained from Yates and Midland Farms or other fields.

Currently, additional work is being carried out to tailor surfactants that are insensitive to the presence of divalent ions and also applicable at higher temperatures compared to the sulfates tested to date. Once such surfactants are obtained, they will be tested with the crude oil provided by Burlington Resources at 100^{o}C. This work will also be conducted during Year 2.

Finally, the ability of these formulations to recover crude oil needs to be tested in corefloods to determine the dynamic performance of the surfactants as well as measure parameters such as surfactant adsorption. During Year 2, a limited number of corefloods will be conducted to evaluate the best surfactants that emerge from the screening studies.

Electrolyte equivalence and PO number

Selected propoxylated-sulfated surfactants were evaluated for assessing (1) equivalences among NaCl and Na_2CO_3 brines and (2) the effect of adding Propoxy (PO) groups to the same lipophile.

Figures 8 and 9 depict phase volume of Alfoterra®53 (C14-C15 PO3) for illustration of how interchangeable NaCl and Na_2CO_3 brines could be on phase behavior studies for WOR=1 at 30°C. To keep interpretation of test results straightforward, brine mixtures of NaCl and Na_2CO_3 were avoided. High pH brines should insure sample integrity by preventing sulfate hydrolysis upon aging. In Fig. 1, one molar Na_2CO_3 was equivalent to ~ 6.3 % NaCl (~1.1 M) for 1.5% Alfoterra®53 against n-Dodecane. In Fig,2, the equivalence appeared to change when using n-Decane and 3.0 % Alfoterra®53; one molar Na_2CO_3 was equivalent to ~ 5.7 % NaCl (~1.0 M). Emulsions are present in the excesse oil and brine phases in these samples, the microemulsion volumes were determined by a high-intensity light beam. The emulsions appeared to be less severe in samples with n-Decane and practically disappeared in samples with n-Hexane and Na_2CO_3 (not shown here). Future work will include approaches on how to lessen the formation of emulsions encountered in the excesses of oil and brine.

Figure 10 depicts the effect of adding PO groups to the same lipophile C14T – ISOFOL. Increasing PO from 3 to 8 groups failed to improve oil solubilization but appeared to promote emulsification of excess phases.

Table 7 is a summary of a quick screening of surfactants of ~3% concentration at WOR=1. The brine was 1M Na_2CO_3 and the oil was n-Hexane at room temperature. Eighteen ALFOTERRA® were compared with TDA-4PO, which is a surfactant with potential for application at Yates field. From test results, ALFOTERRA®13 produced two microemulsions in equilibrium, ALFOTERRA®15 produced a “classical” single-phase microemulsion. Most of the surfactants, 13 of them, produced Winsor-Type II microemulsions. Only three surfactants, including TDA-4PO, produced Winsor-Type I microemulsions. Surfactant solubility in brine was observed before adding n-Hexane to the sample. ALFOTERRA®63 (C12-C13 Safol), forming Type I, was the only one soluble in 1M brine. In spite of forming Type I microemulsions, TDA-4PO formed a very turbid solution.

It is important to find clear surfactant solutions at desirable conditions. So far, the appearance of all surfactant solutions with potential to be effective at Yates field is found to be unclear. Addition of small amount of high molecular weight oils could help to mitigate the variety of problems found when utilizing turbid solutions. Previous experience suggested that addition of a small amount of high molecular weight oil could prevent formation plugging, and high surfactant retention. This idea will be tested in future work.

Table 7. Comparison Among Alfoterra Surfactants and TDA-4PO.

Testing Fluids: n-Hexane and 1M_Na_2CO_3Na at Room Temperature .

			Solubility Test Surfactant (~6%) as is = 1cc 1M Na_2CO_3Na= 5cc		WOR~1 1M_ Na_2CO_3Na : n-Hexan
Product Name	**Alcohol Chain**	**PO's**	**Solubility**	**Appearance**	**Winsor-Type Microemulsion**
ALFOTERRA®13	i-C13OH-TDA	3	n.s.	Very Turbid	**Two micros in Eq.**
ALFOTERRA®15	i-C13OH-TDA	5	n.s.	Very Turbid	**Single phase**
ALFOTERRA®18	i-C13OH-TDA	8	n.s.	Very Turbid	**Type II**
ALFOTERRA®23	C12 - ISOFOL	3	n.s.	Very Turbid	**Type II**
ALFOTERRA®25	C12 - ISOFOL	5	n.s.	Very Turbid	**Type II**
ALFOTERRA®28	C12 - ISOFOL	8	n.s.	Very Turbid	**Type II**
ALFOTERRA®33	C14T - ISOFOL	3	n.s.	Very Turbid	**Type II**
ALFOTERRA®35	C14T - ISOFOL	5	n.s.	Very Turbid	**Type II**
ALFOTERRA®38	C14T - ISOFOL	8	n.s.	Very Turbid	**Type II**
ALFOTERRA®43	C12 & C13 - ISALCHEM	3	n.s.	Very Turbid	**Type II**
ALFOTERRA®45	C12 & C13 - ISALCHEM	5	n.s.	Very Turbid	**Type II**
ALFOTERRA®48	C12 & C13 - ISALCHEM	8	n.s.	Very Turbid	**Type II**
ALFOTERRA®53	C14 & C15 - ISALCHEM	3	n.s.	Very Turbid	**Single phase**
ALFOTERRA®55	C14 & C15 - ISALCHEM	5	n.s.	Very Turbid	**Type II**
ALFOTERRA®58	C14 & C15 - ISALCHEM	8	n.s.	Very Turbid	**Type II**
ALFOTERRA®63	C12 & C13 - SAFOL	3	s	Clear	**Type I**
ALFOTERRA®65	C12 & C13 - SAFOL	5	s.s.	Slightly Turbid	**Type I**
ALFOTERRA®68	C12 & C13 - SAFOL	8	s.s.	Slightly Turbid	**Type II**
TDA-4PO	i-C13	4	n.s	Very Turbid	**Type I**

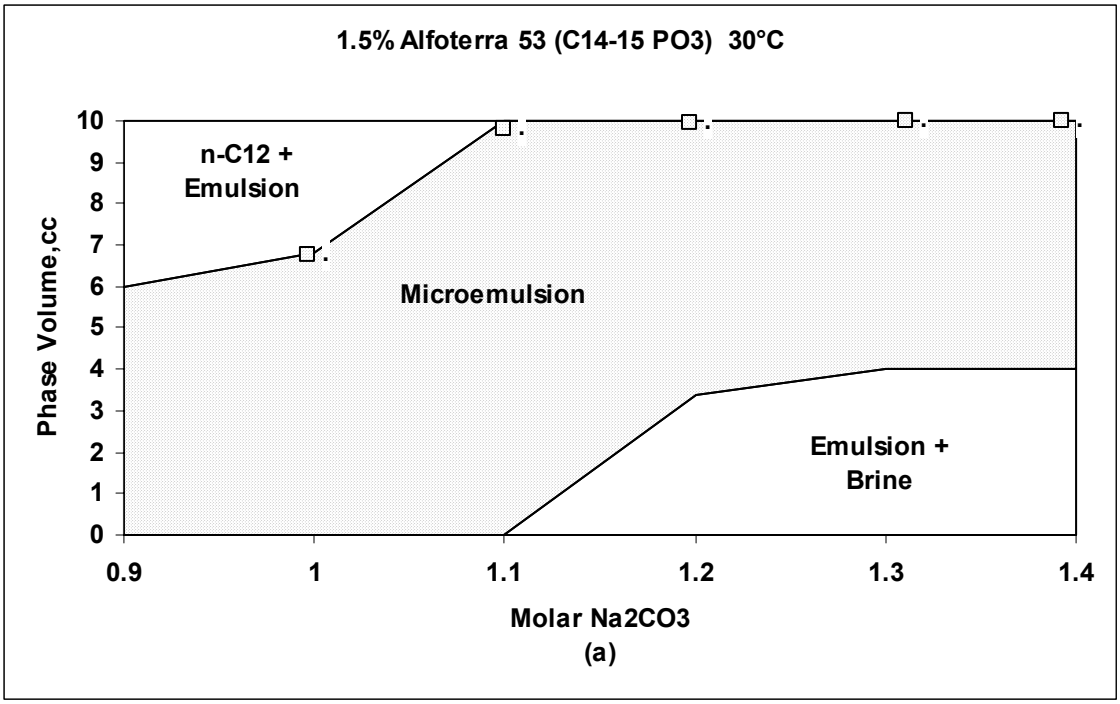

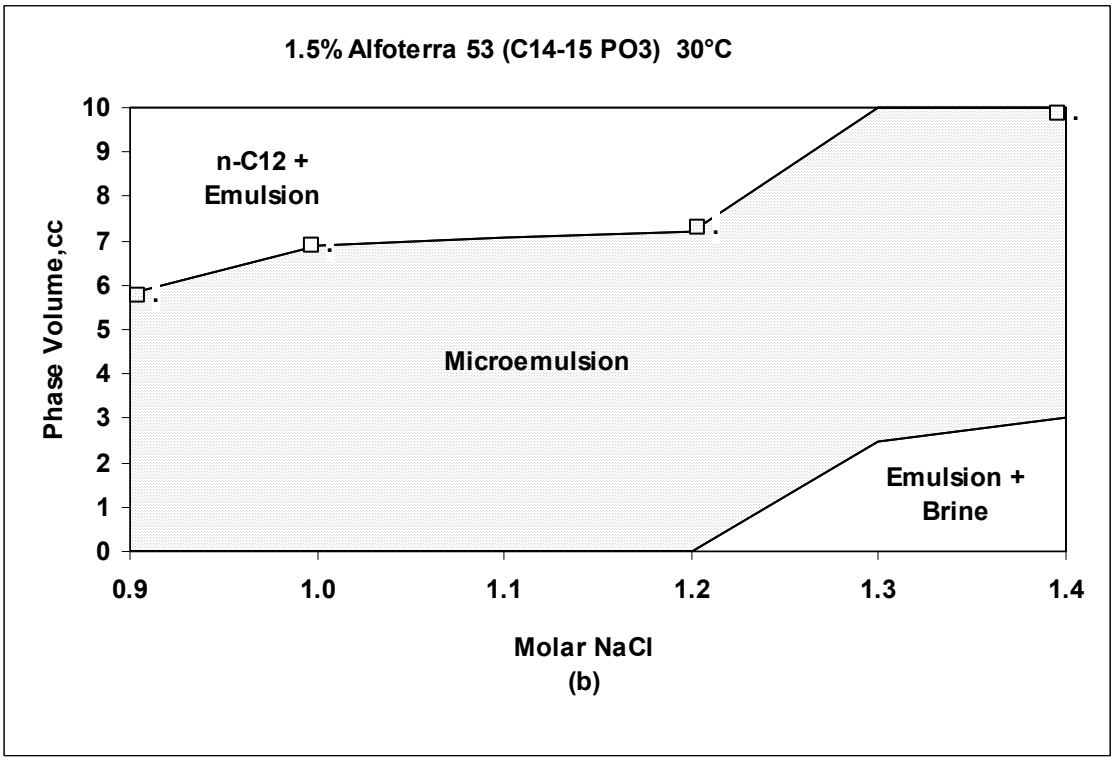

Fig.8- 1.5% Alfoterra 53 (C14-15 PO3) at WOR=1, open squares indicate tested salinity

(a) Na_2CO_3 brines and n-Dodecane

(b) NaCl brines and n-Dodecane

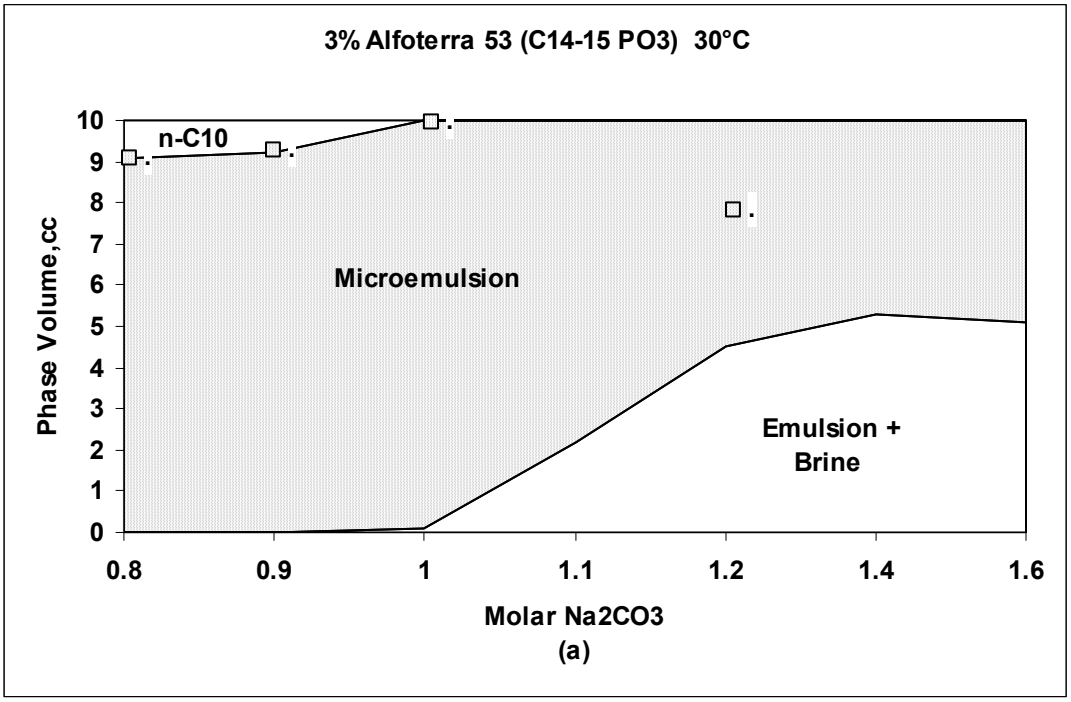

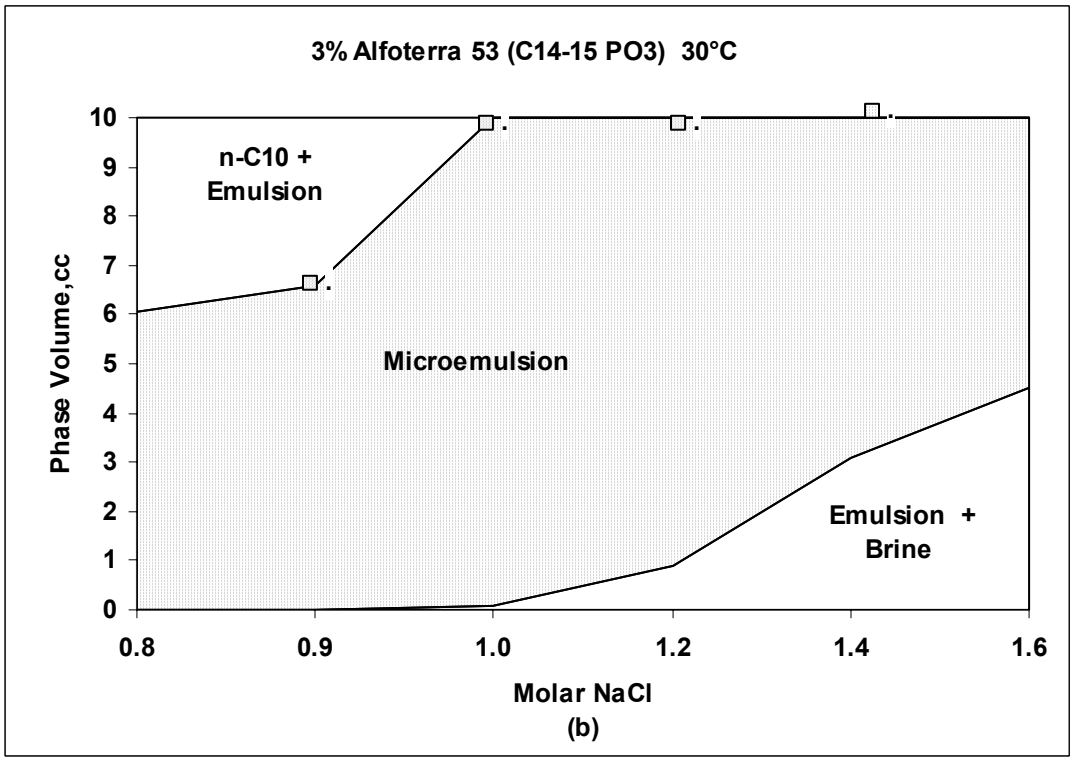

Fig.9- 3% Alfoterra 53 (C14-15 PO3) at WOR=1, open squares indicate tested salinity
(a) Na_2CO_3 brines and n-Decane
(b) NaCl brines and n-Decane

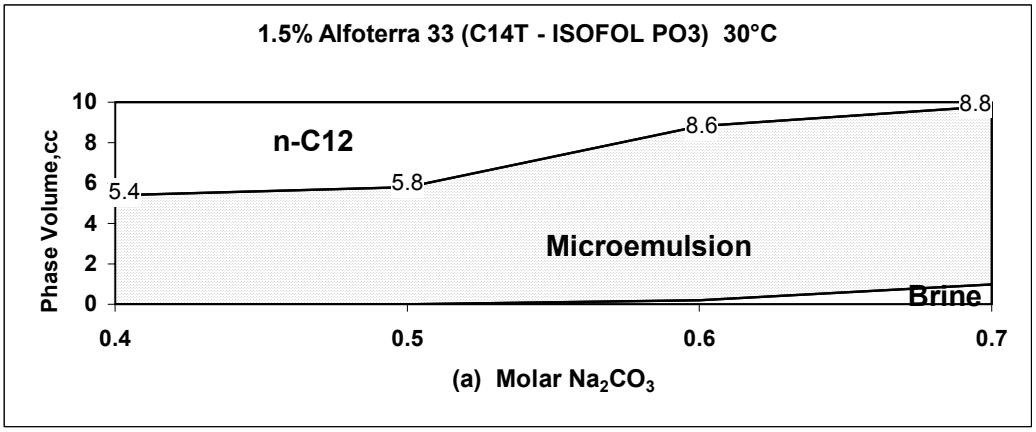

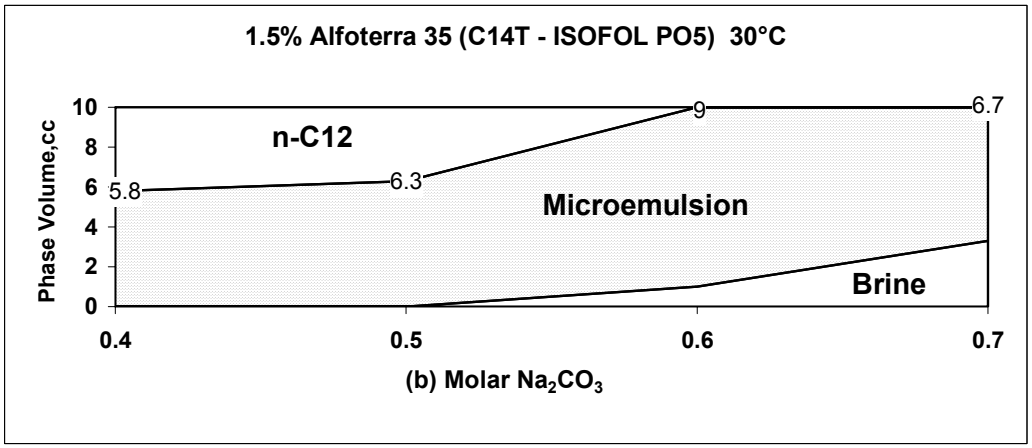

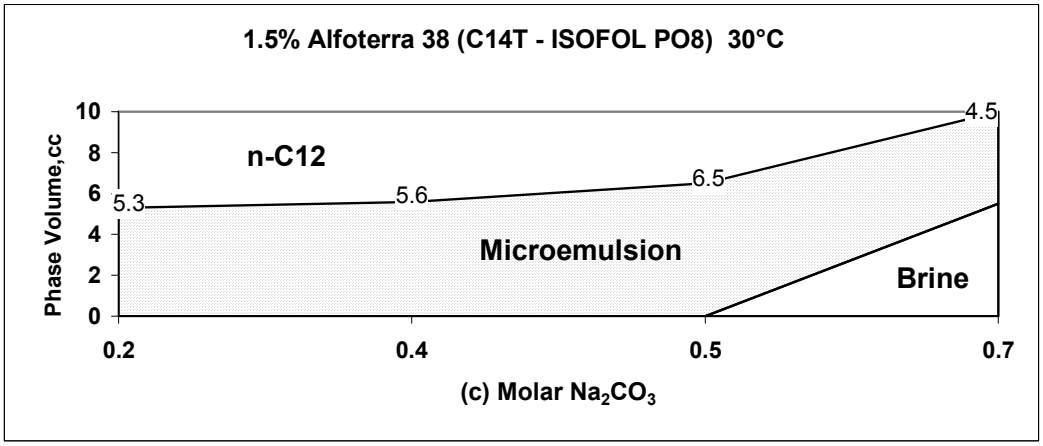

Fig. 10.- Phase-volume Diagram of 1.5 % ALFOTERRA® 33,35,38 Propoxylated & Sulfated C14T-Isofol :WOR=1, n-Dodecane and Na_2CO_3, 30°C

Addition of Propoxy Groups (PO) from 3 to 8 failed to induce more oil solubilization but appeared to promote emulsion in excess phases.

(a) PO = 3, (b) PO = 5, (c) PO = 8

Task 2 Phase behavior, adsorption, and composition changes during displacement

Subtask 2.3 Surfactant-enhanced spontaneous imbibition experiments

D. Leslie Zhang, Rice University

Introduction

The remaining oil saturation in water invaded regions of fractured, oil-wet, carbonate formations is often high. It may not be possible to apply a large pressure gradient across the matrix, and the oil is retained by capillarity. The recovery of the oil in the matrix thus depends on spontaneous imbibition, which can be enhanced by adding surfactant. The mechanisms involved in surfactant flooding of fractured, oil-wet formations are mainly wettability alteration and interfacial tension reduction.

Cationic surfactant has been used to alter wettability of carbonate formations to more water-wet conditions[1-5]. Standnes and Austad proposed the mechanism to be the formation of ion-pairs between surfactant monomers and the adsorbed carboxylates[1]. Their laboratory tests with chalk cores showed that oil recovery can reach 70%.

Xie et al[2] applied a cationic surfactant and a nonionic surfactant to over 50 cores from three dolomitic Class II reservoirs. The incremental oil recovery ranged from 5-10% OOIP. Wettability alteration was identified as the main factor. They also found that recovery rate with the nonionic surfactant was faster than that with the cationic surfactant because the former had higher interfacial tension.

Alkaline/anionic surfactant flooding has been extensively investigated, and both wettability alteration and interfacial tension reduction has been responsible for the increase in oil recovery[6-31]. The current work is dedicated to quantifying the effect of the important factors in alkaline/surfactant enhanced spontaneous imbibition in oil-wet carbonate formations.

Surfactant Formulations

Surfactant The surfactants evaluated are identified in Table 1. Ethoxylated (EO) and propoxylated (PO) sulfates were used because of their known tolerance to divalent ions. These surfactants are limited to reservoir temperatures where sulfate hydrolysis should not be a problem. For high temperature carbonate reservoirs, EO and PO sulfonates may be better choices.

CS-330 is similar to NEODOL 25-3S used previously[7], but is too hydrophilic to use by itself[27]. TDA-4PO is less hydrophilic, but its solutions at optimal sodium carbonate concentration are turbid and adsorption is anomalously high[27]. Thus the two surfactants are blended at equal weight ratio, and the resulting surfactant solution is abbreviated as “Blend”.

Electrolytes At the early stage of this research, sodium carbonate was used as the sole electrolyte. But a practical system should have only enough sodium carbonate to saponify the naphthenic acids present in the crude oil and propagate through the formation, and use inexpensive and non-scaling sodium chloride for the remainder of electrolyte strength. Here, sodium chloride is used along with 1% sodium carbonate to adjust the electrolyte strength. Two units for sodium carbonate concentration have been used, and their relationship is: 1% is equivalent to about 0.1M.

Surfactant / electrolyte solutions The appearance of surfactant solutions is very important, because turbid or two-phase solutions can cause a variety of problem, such as formation plugging, and surfactant retention. The appearance of y% Blend / 1% Na_2CO_3 / x% NaCl was plotted in Fig. 1.

Wettability Alteration on Calcite Plate

Carbonate surfaces are usually positively charged in neutral pH brine[27]. This attracts negatively charged compounds in crude oils, such as carboxylic acids. Therefore carbonate formations are usually intermediate-wet to oil-wet. According to Treiber et al.[32], 84% of carbonate formations are oil-wet, while 8% intermediate-wet, and 8% water-wet. Chillingar & Yen[33] reported similar results: 80% oil-wet, 12% intermediate-wet, and 8% water-wet.

The wettability of the crude oil MY3 was evaluated by measuring the water advancing contact angle on marble plates. The plates were solvent cleaned, polished on a diamond lap to remove the surface layer, pre-equilibrated with 0.1 M NaCl brine overnight, then aged in the crude oil for 24-48 hours at 80 °C. After cooling, the plate was immersed in an optical cell filled with 0.1 M NaCl brine. After all motion had stopped, an oil patch was left on the substrate, as shown in Fig. 2(a). It is clear that the plate is oil-wet since the water advancing contact angle is near 180°.

The effect of alkaline/surfactant solutions on wettability alteration is demonstrated in Fig. 2 and Fig. 3. The displacement of oil by reduction of the interfacial tension and the alteration of the wettability upon replacement of the brine with alkaline/surfactant solutions are shown as a function of time. The 0.05% Blend / 1% Na_2CO_3 / 0.5% NaCl system, Fig. 2(b), showed oil streaming off from the surface at early times as a result of the reduction in interfacial tension. Later, the oil left on the plate formed 1 mm oil drops, which were observed with higher magnification. Water **ADVANCING** contact angles were observed to decrease with time, Fig. 2(c)-(e). The final contact angles ranged from 80-140°

Low tension in 0.05% Blend / 1% Na_2CO_3 / 10% NaCl system lasted for a much longer time and only a few tiny drops around 0.05 mm were left on the plate at the end of the experiment, Fig. 3. The wettability of the marble plate was altered to intermediate-wet.

Similar observations were made for 0.05% Blend surfactant at other sodium carbonate and sodium chloride concentrations. The drop configurations after 50 hours are illustrated in Fig 4, and the measured Water **ADVANCING** contact angles and drop sizes are summarized in Fig. 5 and 6. When sodium carbonate concentration was increased from 0.45-1.2M, both contact angle and drop size decreased, Fig. 4(a)-(c) and Fig. 5. But for 1% Na_2CO_3 / NaCl system, when sodium chloride concentration was increased from 0.5-16%, contact angle changed little, Fig. 4(d)-(g), while the drop size reached a minimum around 10% NaCl (Or rather 12%, where at the end of the experiment, no drops could be observed with the maximum magnification), Fig. 6. The existence of minimum drop size indicates that at least transient interfacial tension experienced a minimum as sodium carbonate or sodium chloride concentration is increased. For dependence of hydrostatic configurations of axisymmetric oil drops on interfacial tension and contact angle, see the previous paper[27].

Similar to drop size, the amount of oil remaining on the marble plate in 0.05% Blend / 1% Na_2CO_3 / NaCl system also went through a minimum, at 10-12%, when sodium chloride concentration was increased from 0.5-16%, as shown in Fig. 7.

Wettability alteration with several anionic surfactants and sodium carbonate was examined by Seethepalli et al[28]. Most of the surfactants were shown to be able to alter wettability of calcite surfaces as well as or better than the cationic surfactant-dodecyltrimethylammonium bromide (DTAB). The best surfactant was Alfoterra 38, with a water RECEDING contact angle of about 32°. They reported only the receding contact angle because the drops were smaller than 0.1 mm, and it was difficult to measure an accurate contact angle, so a post-wettability test was performed.

Wettability alteration with 0.05% Alfoterra 38 / 0.3 M Na_2CO_3 was also performed in our laboratory, and results are shown in Fig. 8. The phenomena were observed to be similar to those of 0.05% Blend / 1% Na_2CO_3 / 10-12% NaCl. The remaining drop showed a water ADVANCING contact angle of about 90°. Yang et al.[34] showed that crude oil systems often have hysteresis or large difference between receding and advancing contact angle.

Phase Behavior

The objective of studying phase behavior is to determine the optimal salinity from visual observation of oil / water / surfactant tubes. The optimal salinity is usually determined from interfacial tension between microemulsion and excess phases[35]. But because the low surfactant concentration results in little microemulsion in the Type III region, measurements are usually either interfacial tension between excess phases, or non-equilibrium measurement at high water Water/Oil Ratio (WOR). The problems of both approaches are discussed below.

Problematic interfacial tension measurements between excess phases
Phase behavior and interfacial tension between excess phases were found to change with separation time. For example, interfacial tension of 0.05% Blend / Na_2CO_3 was first measured after 19 days of settling, with the minimum tension near 10^{-4} mN/m (dyne/cm), Fig. 9. The tension was measured again after 3 month and 20 days of settling. It was found that if the lower phase macroemulsion had not separated, interfacial tension was very close to the earlier measurement. But if the lower phase had separated, surfactant went to the middle layer. When sampling from the excess phases, there was little surfactant present to lower the interfacial tension.

Similar phenomena were observed for 0.05% TDA-4PO / Na_2CO_3 system, Fig. 10. Interfacial tension between excess phases was low after 7 days of settling, but went up significantly after 9 months. But when some of the middle layer was sampled along with excess phases after 9 months, the interfacial tension could be lowered again, especially in the case of 0.3 M Na_2CO_3, the tension was lowered almost to the earlier value. But this approach depends on where to sample the middle layer, the middle layer composition (the middle layer could consist of a few phases) and how much of the middle layer is sampled. Therefore the measurement is usually not reproducible.

Water/Oil Ratio Phase behavior was also found to change with WOR. Fig. 11 illustrates the phase behavior of 0.05% Blend / 1% Na_2CO_3 / NaCl at WOR of 1:1 and 10:1 after 7 weeks of settling. At WOR of 1:1, Fig. 11 (a), it is a lower phase emulsion system at 0.5% NaCl, and upper phase emulsion system at 1%, therefore the optimal sodium chloride concentration is in between. Similarly, at WOR of 10:1, Fig. 11 (b), optimal sodium chloride concentration is between 8-9%. Optimal salinities for other WOR values and surfactant concentrations were similarly determined, and are plotted in Fig. 12.

The non-equilibrium interfacial tension measurement by spinning drop method is at high WOR. In non-equilibrium measurements, low tension is often only a transient phenomenon. The soap is extracted from the oil and is solubilized by the micelles in the surfactant solution. Interfacial tension at different WOR may differ by orders of magnitude [27].

The dependence of optimal salinity on WOR also explains why the drop size in wettability alteration experiments depends on electrolyte strength. In wettability alteration experiment, a small patch of oil is surrounded by a large amount of aqueous solution, so the WOR is very high. When electrolyte concentration is increased, phase behavior gradually changes from under-optimum to optimum to over-optimum. Since IFT is the lowest at optimum, the maximum stable drop size determined by Bond number experiences a minimum at optimal salinity.

Dependence of optimal salinity on surfactant concentration and WOR can be correlated with natural soap / surfactant mole ratio, Fig. 13. The amount of soap was calculated based on the acid number of the crude oil - 0.2 mg potassium hydroxide / gram oil. Lower ratios correspond to dominance by the synthetic surfactant. The curve plateaus at around 13% NaCl, which is close to the optimal salinity of the Blend surfactant.

Spontaneous Imbibition

Spontaneous imbibition in capillary gap between vertical parallel plates

The schematic set up of the experiment is shown in Fig. 14. A marble plate pre-equilibrated with 0.1 M NaCl brine overnight, then aged in crude oil MY3 at 80 °C for 48 hrs, is placed in an optical cell with a plastic film as a spacer to create a 13 μm gap between the plate and the front wall of the cell. A bevel is ground at the bottom of the plate to allow the aqueous phase to be present without flow resistance. The glass of the front of the cell has been treated with a dilute solution of hexadecyltrimethylammonium bromide (CTAB) to make it preferentially oil-wet.

Oil in the gap is not displaced when the cell is filled with 0.1 M NaCl brine and left for 20 hrs, Fig. 15(a). The buoyancy forces cannot overcome the capillary entry pressure to displace the oil from the gap. However, when the brine is replaced with 0.05% Blend / 1% Na_2CO_3 / 1%NaCl, spontaneous imbibition of the aqueous phase occurs, Fig. 15(b). The fraction of oil displaced is plotted against dimensionless time for gravity drainage for a range of electrolyte strengths in Fig. 16. Here, the flow is assumed to be plane Poiseuille flow between parallel plates.

$$t_{D,g} = \frac{k\Delta\rho g t}{\mu_o L} \quad \text{..... (1)}$$

$$k = \frac{h^2}{12} \quad \text{..... (2)}$$

where *h* is the gap width between the parallel plates.

Compared with the analytical solution for gravity drainage of linear relative permeability (n=1) and assuming zero capillary pressure, the displacement rate is about an order of magnitude slower. This can be caused by two reasons: 1) the accumulation of a large amount of oil (compared with that in the gap) in the bevel at the time surfactant solution was added; and 2) the plate surface's being not perfectly flat, and the gap width being less than that of the spacers.

The system with 4.5% Na_2CO_3 and 0% NaCl was the system with second best displacement in Fig. 16. Fig. 9 shows this to be the system with WOR of 1:1 that had the lowest IFT when measured after 19 days. The high WOR observation of a drop on a plate, Fig. 4, would suggest that the system with 1.2 M or 12% Na_2CO_3 would have been the optimum.

The systems with 0.05% Blend / 1% Na_2CO_3 / x% NaCl had the maximum oil displacement with 3% NaCl, which is close to the optimal salinity at WOR of 3:1 (Fig. 12). At 6% NaCl, the least oil was displaced. It may be because of the phase separation of the surfactant solution (Fig. 1), after which the denser surfactant rich phase stayed at the bottom of the cell.

The contrast in displacement efficiency between the different systems was not large because the parallel plate geometry has little opportunity for trapping compared to porous media. However, it does illustrate that the optimal salinity for displacement may not be the same as that observed for very large WOR such as the drop on a flat plate, Fig. 4. Thus the design of an optimal system should consider the multi-component, multi-phase chromatographic displacement in porous media.[36]

Spontaneous imbibition with dolomite cores Spontaneous imbibition experiments were conducted with formation brine, stock-tank oil, MY3, and core samples of the dolomite formation of the reservoir of interest. The properties of the dolomite core samples and experimental conditions are listed in Table 2. There was no further extraction or cleaning of the cores. The composition of the formation brine is in Table 3. The initial oil saturation was established by flowing oil with the indicated pressure drop. Some samples were aged 24 hours at 80°C. Oil recovery by spontaneous imbibition was measured by placing the oil-saturated cores in imbibition cells filled with either formation brine or alkaline surfactant solution (Fig. 17). Not a single drop of oil was recovered by spontaneous imbibition in formation brine during one to two weeks (Fig 17a). The formation brine was replaced with alkaline surfactant solution, and the enhanced oil recovery by spontaneous imbibition was measured. Small drops of oil on the top end face of the core could be observed accumulating, detaching, and being collected in the imbibition cell (Fig. 17b). The appearance of oil on the top face rather than the sides of the core suggests that the displacement was dominated by buoyancy rather than countercurrent capillary imbibition. The oil recovery as a function of time is shown in Fig 18.

Possible factors affecting the difference in oil recovery in Fig. 18 include permeability, initial oil saturation, surfactant formulation, and condition of aging. The surfactant formulation and aging conditions are not the dominant parameters because systems with the greatest and least recovery have the same surfactant formulation, and the system aged at 80°C has greater recovery than the system aged at room temperature. The effect of difference in permeability can be evaluated by plotting the oil recovery as a function of dimensionless time for gravity-dominated recovery.

$$t_{Dg} = \frac{k\, k_{ro}^{o} \Delta\rho\, g\, t}{\left(S_{oi} - S_{or}\right) \phi\, \mu_o\, L} \quad \text{..... (3)}$$

The fractional recovery is expressed as a fraction of recoverable oil, assuming that the remaining oil saturation at the last measured point in Fig. 18 is the residual oil saturation. The experimental results are compared to the 1D, gravity-drainage analytical solution[37,38] assuming zero capillary pressure and a relativity permeability exponent of n = 3. The analytical solution is as follows.

$$E_R \equiv \frac{S_{oi} - \bar{S}_o}{S_{oi} - S_{or}} \quad \text{..... (4)}$$

$$E_R = \begin{cases} t_{Dg}, & t < t_{BT} \\ 1 - \dfrac{(1-1/n)}{(nt_{Dg})^{\frac{1}{n-1}}}, & t > t_{BT} \end{cases} \quad \text{..... (5)}$$

$$t_{Dg,BT} = 1/n \quad \text{..... (6)}$$

The fractional recovery is plotted as a function of dimensionless time for gravity drainage and compared with the analytical solution in Fig. 19. The recovery expressed in this way accounts for the difference in permeability. The fractional recovery appears to scale as if the rate of recovery of the mobile oil is caused by gravity drainage. However, the remaining oil saturation (ROS) appears to be a function of permeability or initial oil saturation (Table 2). More investigation is needed to determine if permeability or initial oil saturation is indeed the responsible parameter, and if so, why. The surfactant and alkali system needs to be optimized to minimize the remaining oil saturation.

The hypothesis that the recovery was dominated by capillary imbibition was examined by plotting the oil recovery as a function of dimensionless time for recovery by spontaneous capillary imbibition[39] in Fig. 20.

$$t_{D,P_c} = t\sqrt{\frac{k}{\phi}}\frac{\sigma}{\sqrt{\mu_o \mu_w}}\frac{1}{L_c^2} \quad \text{..... (7)}$$

The IFT in the dimensionless time is a value of 10^{-3} mN/m, which was a typical value for the three systems[27]. The measured oil recovery occurred faster than that for the very strongly water-wet correlation. This observation implies that either some other mechanism, such as gravity, was contributing to recovery, or capillary imbibition was contributing but the IFTs are different from the assumed value.

If the oil recovery is dominated by buoyancy and each matrix block acts independently, the analytical solution, Eq. 5, can be used to scale up to different permeability and matrix-block size. The time to a given level of recovery will be proportional to the height of the matrix block, L, and inversely proportional to

permeability, *k*. However, the assumption that the matrix blocks act independently is challenged by the possibility of capillary contact between matrix blocks. Capillary contact between matrix blocks and re-entry of oil into matrix blocks will lengthen the time for oil recovery.

Conclusions

1. The system of crude oil MY3, brine and marble plate is strongly oil-wet.
2. With alkali / anionic surfactant system, water-advancing contact angle ranged from intermediate-wet to preferentially water-wet.
3. Advancing contact angle and drop size of MY3 crude oil on a marble plate are dependent on electrolyte type and concentration. Drop size experiences a minimum with electrolyte strength. Contact angle decreases with increasing sodium carbonate concentration to the maximum concentration investigated. When sodium carbonate concentration is fixed at 1%, sodium chloride concentration does not seem to affect wettability alteration.
4. IFT measurements are problematic for alkali / anionic surfactant systems. At low surfactant concentration, IFT is measured between excess phases, which changes with settling time because of the separation of surfactant from the excess brine phase.
5. Alkali/surfactant phase behavior is dependent on salinity, surfactant concentration, and WOR. Dependence of optimal salinity on surfactant concentration and WOR can be correlated with natural soap / surfactant mole ratio.
6. Oil recovery from oil-wet dolomite cores has been demonstrated by spontaneous imbibition with an alkaline anionic surfactant solution. Recovery is apparently governed by gravity.

Acknowledgements

We thank U.S. DOE (DE-FC26-03NT15406) and the Rice Consortium on Processes in Porous Media for financial support; Marathon Oil Company, esp. Dr. Hung-Lung Chen for providing crude oil, core samples and imbibition cells; Larry Britton of University of Texas and Upali Weerasooriya of Harcros for surfactant samples; Gary Pope of University of Texas, Varadarajan Dwarakanath and Richard Jackson of Intera for suggestions.

References

1. Standnes, D. C. and Austad, T.: “Wettability Alteration in Chalk 2. Mechanism for Wettability Alteration from Oil-Wet to Water-Wet Using Surfactants”, *JPSE*, **28**, 123-143, 2000.
2. Xie, X., Weiss, W.W., Tong, Z., and Morrow, N.R., “Improved Oil Recovery from Carbonate Reservoirs by Chemical Stimulation”, presented at the 2004 SPE/DOE Fourteenth Symposium on Improved Oil Recovery, Tulsa, OK, Apr., 2004.
3. Austad, T. and Milter, J., “Spontaneous Imbibition of Water into Low Permeable Chalk at Different Wettabilities Using Surfactants”, SPE 37236

presented at the International Symposium on Oilfield Chemistry, Houston, TX, Feb. 1997.
4. Austad, T., Matre, B., Milter, J., Sævareid, A., and Øyno, L., "Chemical Flooding of Oil Reservoirs 8. Spontaneous Oil Expulsion from Oil- and Water-Wet Low Permeable Chalk Material by Imbibition of Aqueous Surfactant Solutions", *Colloids and Surfaces A.*, **137**, 117-129, 1998.
5. Standnes, D. C., Nogaret, L. A. D., Chen, H. L., and Austad, T., "An Evaluation of Spontaneous Imbibition of Water into Oil-Wet Carbonate Reservoir Cores Using a Nonionic and a Cationic Surfactant", *Energy & Fuels*, **16**, 1557-1564, 2002.
6. Olsen, D. K., Hicks, M. D., Hurd, B. G., Sinnokrot, A. A., and Sweigart, C. N., "Design of a Novel Flooding System for an Oil-Wet Central Texas Carbonate Reservoir", SPE20224 presented at the SPE Seventh Symposium on Enhanced Oil Recovery, Tulsa, OK, 1990.
7. Nelson, R. C., Lawson, J. B., Thigpen, D. R., and Stegemeier, G. L., "Cosurfactant-Enhanced Alkaline Flooding", SPE/DOE 12672 presented at the SPE/DOE Fourth Symposium on Enhanced Oil Recovery, Tulsa, OK, Apr. 1984.
8. Martin, F. D., and Oxley, J. C., and Lim, H., "Enhanced Recovery of a "J" Sand Crude Oil with a Combination of Surfactant and Alkaline Chemicals", SPE 14293 presented at the 60th Annual Technical Conference and Exhibition of SPE, Las Vegas, NV, Sep. 1985.
9. Shuler, P. J., Kuehne, D. L., and Lerner, R. M., "Improving Chemical Flood Efficiency with Micellar/Alkaline/Polymer Processes", 80-88, *JPT*, Jan. 1989.
10. French, T. R., and Burchfield, T. E., " Design and Optimization of Alkaline Flooding Formulations", SPE 20238 presented at the SPE/DOE Seventh Symposium on Enhanced Oil Recovery, Tulsa, OK, 1990.
11. Falls, A. H., Thigpen, D. R., Nelson, R. C., et al., "A Field Test of Cosurfactant-Enhanced Alkaline Flooding", SPE 24117 presented at the SPE/DOE Eighth Symposium on Enhanced Oil Recovery, Tulsa, OK, 1992.
12. Baviere, M., Glenat, P., Plazanet, V., and Labrid, J., "Improvement of the Efficiency/Cost Ratio of Chemical EOR Processes by Using Surfactants, Polymers, and Alkalis in Combination", SPE 27821 presented at the SPE/DOE Ninth Symposium on Improved Oil Recovery, Tulsa, OK, Apr. 1994.
13. Baviere, M., Glenat, P., Plazanet, V., and Labrid, J., "Improved EOR by Use of Chemicals in Combination", *SPERE*, 187-193, Aug. 1995.
14. Gao, S., Li, H., and Li, H., "Laboratory Investigation of Combination of Alkali/Surfactant/Polymer Technology for Daqing EOR", *SPERE*, 194-197, Aug. 1995.
15. Song, W., Yang, C., Han, D., Qu, Z., Wang, B., and Jia, W., "Alkaline-Surfactant-Polymer Combination Flooding for Improving Recovery of the Oil with High Acid Value", SPE 29905 presented at the International Meeting on Petroleum Engineering, Beijing, China, Nov. 1995.
16. Al-Hashim, H. S., Obiora, V., Al-Yousef, H. Y., Fernandez, F., and Nofal, W., "Alkaline Surfactant Polymer Formulation for Saudi Arabian Carbonate

Reservoirs", SPE 35353 presented at the Tenth Symposium on Improved Oil Recovery, Tulsa, OK, Apr. 1996.
17. French, T. R., "A Method for Simplifying Field Application of ASP Flooding", SPE 35354 presented at the Tenth Symposium on Improved Oil Recovery, Tulsa, OK, Apr. 1996.
18. Gao, S., Li, H., Yang, Z., Pitts, M. J., Surkalo, H., and Wyatt, K., "Alkaline/Surfactant/Polymer Pilot Performance of the West Central Saertu, Daqing Oil Field", *SPERE*, 181-188, Aug. 1996.
19. Wang, C., Wang, B., Cao, X., and Li, H., "Application and Design of Alkaline-Surfactant-Polymer System to Close Well Spacing Pilot Gudong Oilfield", SPE 38321 presented at the SPE Regional Meeting held in Long Beach, CA, Jun. 1997.
20. Wang, D., Zhang, Z., Cheng, J., Yang, J., Gao, S., and Li., L., "Pilot Tests of Alkaline/Surfactant/Polymer Flooding in Daqing Oil Field", SPERE, 229-233, Nov., 1997.
21. Qu, Z., Zhang, Y., Zhang, X., and Dai, J., "A Successful ASP Flooding Pilot in Gudong Oil Field", SPE 39613 presented at the SPE/DOE Improved Oil Recovery Symposium, Tulsa, OK, Apr., 1998.
22. Tong, Z., Yang, C., Wu, G., Yuan, H., Yu, L., and Tian, G., "A Study of Microscopic Flooding Mechanism of Surfactant/Alkali/Polymer", SPE 39662 presented at the SPE/DOE Improved Oil Recovery Symposium, Tulsa, OK, Apr., 1998.
23. Wang, D., Cheng, J., Wu, J., Wang, F., Li, H., and Gong, X., "An Alkaline/Surfactant/Polymer Field Test in a Reservoir with a Long-Term 100% Water Cut", SPE 49018 presented at the SPE Annual Technical Conference and Exhibition, New Orleans, LA, Sep. 1998.
24. Arihara, N., Yoneyama, Akita, Y., and Lu, X., "Oil Recovery Mechanisms of Alkali-Surfactant-Polymer Flooding", SPE 54330 presented at the 1999 SPE Asia Pacific Oil and Gas Conference and Exhibition, Jakarta, Indonesia, Apr. 1999.
25. Wang, D., Cheng, J., Wu, J., Yang, Z., Yao, Y., and Li, H., "Summary of ASP Pilots in Daqing Oil Field", SPE 57288 presented at the SPE Asia Pacific Improved Oil Recovery Conference, Kuala Lumpur, Malaysia, Oct., 1999.
26. Qiao, Q., Gu, H., Li, D., and Dong, L., "The Pilot Test of ASP Combination Flooding in Karamay Oil Field", SPE 64726 presented at the International Oil and Gas Conference and Exhibition in China, Beijing, China, Nov. 2000.
27. Hirasaki, G.J. and Zhang, D.L., "Surface Chemistry of Oil Recovery from Fractured, Oil-Wet, Carbonate Formations", SPEJ, Jun, 2004, 151-162.
28. Seethepalli, A., Adibhatla, B., and Mohanty, K.K., "Wettability Alteration during Surfactant Flooding of Carbonate Reservoirs", SPE 89423 presented at the SPE/DOE Fourteenth Symposium on Improved Oil Recovery, Tulsa, OK, Apr. 2004.
29. Vargo, J., Turner, J., Vergnani, B., Pitts, M. J., Wyatt, K., Surkalo, H., and Patterson, D., "Alkaline-Surfactant-Polymer Flooding of the Cambridge Minnelusa Field", *SPERE&E*, **3** (6), 552-557, Dec. 2000.

30. Manrique, E. J., de Carvajal, G. G., Anselmi, L., Romero, C., and Chacon, L. J., “Alkali/Surfactant/Polymer Use at VLA 6/9/21 Field in Maracaibo Lake”, SPE 59363 presented at the SPE/DOE Improved Oil Recovery Symposium, Tulsa, OK, Apr. 2000.
31. Hernandez, C., Chacon, L. J., Anselmi, L., Baldonedo, A., Qi, J., Dowling, P. C., and Pitts, M. J., “ASP System Design for an Offshore Application in the La Salina Field, Lake Maracaibo”, SPE 69544 presented at the SPE Latin American and Caribbean Petroleum Engineering Conference, Buenos Aires, Argentina, Mar. 2001.
32. Treiber, L. E., Archer, D. L., and Owens, W. W., “A Laboratory Evaluation of the Wettability of Fifty Oil-Producing Reservoirs”, *SPEJ*, 531-540, Dec. 1972.
33. Chilingar, G. V., and Yen, T. F., “Some Notes on Wettability and Relative Permeabilities of Carbonate Reservoir Rocks II”, *Energy Sources*, **7,** 67-75, 1983.
34. Yang, S.-Y., Hirasaki, G.J., Basu, S., and Vaidya, R., “Mechanisms for Contact Angle Hysteresis and Advancing Contact Angles”, *JPSE*, **24**, 63-73, 1999.
35. Healy, R. N., Reed, R. L., and Stenmark, D. G., “ Multiphase Microemulsion Systems”, *SPEJ*, 147-160, 1976.
36. Hirasaki, G. J., "Application of the Theory of Multicomponent, Multiphase Displacement to Three-Component, Two-Phase Surfactant Flooding", *SPEJ*, 191-204, Apr. 1981.
37. Richardson, J.G. and Blackwell, R.J.: “Use of Simple Mathematical Models for Predicting Reservoir Behavior,” *JPT*, 1145, Sep. 1971**.**
38. Hagoort, J.: “Oil Recovery by Gravity Drainage,” *SPEJ*, 139, Jun. 1980.
39. Xie, X. and Morrow, N.R.: “Oil Recovery by Spontaneous Imbibition From Weakly Water-Wet Rocks,” *Petrophysics*, **42**(4), 313, 2001.

TABLE 1 SURFACTANT IDENTIFICATION

Trade Name	Structure Name
CS-330	Sodium dodecyl 3EO sulfate
TDA-4PO	Ammonium iso-tridecyl 4PO sulfate
Alfoterra 38	Sodium tetradecyl 8PO sulfate
Blend	Blend of equal weight amount of CS-330 and TDA-4PO

TABLE 2—CORE PROPERTIES AND RECOVERY

Property	Core A	Core B	Core C
Diameter (in.)	1.5	1.5	1.5
Length (in.)	3.5	3	3
Porosity (%)	20	24	24
Permeability (md)	90	122	40
Brine	Brine 1	Brine 2	Brine 2
Crude oil	MY3	MY3	MY3
Pressure drop (psi)	250	130	550
Initial oil saturation	0.71	0.68	0.82
Aging	80 ºC, 24 hr	80 ºC, 24 hr	None
Time in brine (days)	9	8	14
Recovery in brine (%OOIP)	0	0	0
Surfactant	TDA-4PO	CS-330+ TDA-4PO	CS-330+ TDA-4PO
Surf. conc. (wt%)	0.05	0.025+0.025	0.025+0.025
Na_2CO_3 (M)	0.3	0.3	0.3
Time in surf. (days)	381	138	132
Recovery in surf (%OOIP)	28	44	14
ROS	0.51	0.38	0.70

TABLE 3—FORMATION BRINE COMPOSITION

Salts	Brine 1 (g/L)	Brine 2 (g/L)
NaCl	24.497	5.815
KCl	0.275	0.000
$CaCl_2.2H_2O$	5.502	2.942
$MgCl_2.6H_2O$	7.984	2.032
Na_2SO_4	0.606	0.237
$Fe(NH_4)_2(SO_4)_2.6H_2O$	0.000	0.007

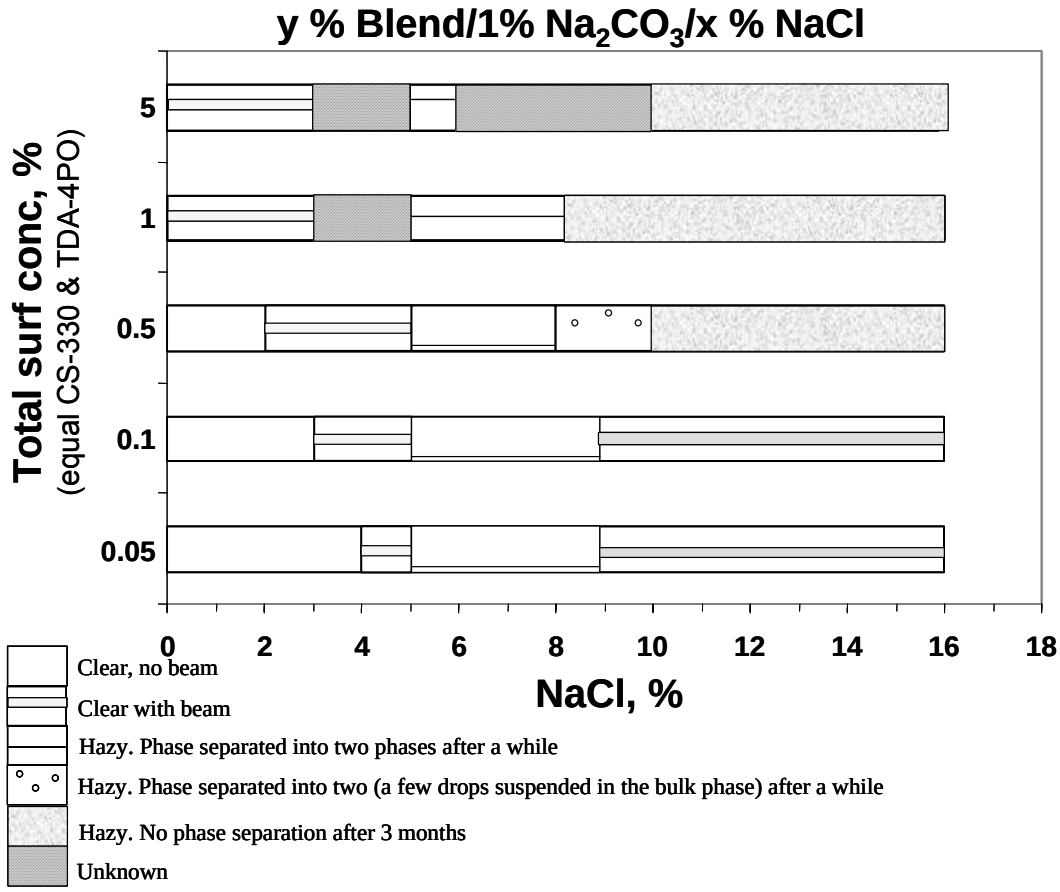

Fig. 1 The appearance of y % Blend / 1% Na_2CO_3 / x% NaCl.

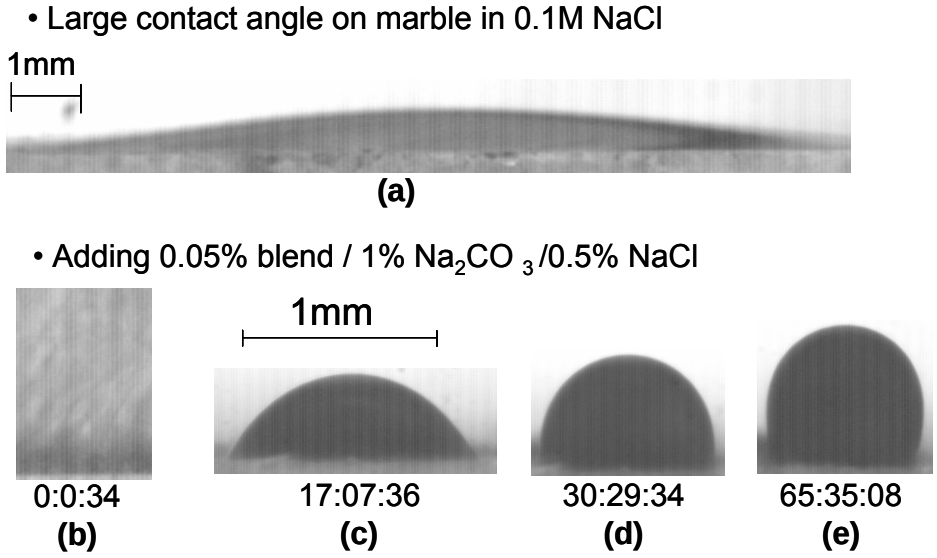

Fig. 2 Wettability alteration of a marble plate with 0.05% Blend / 1% Na_2CO_3 / 0.5% NaCl.

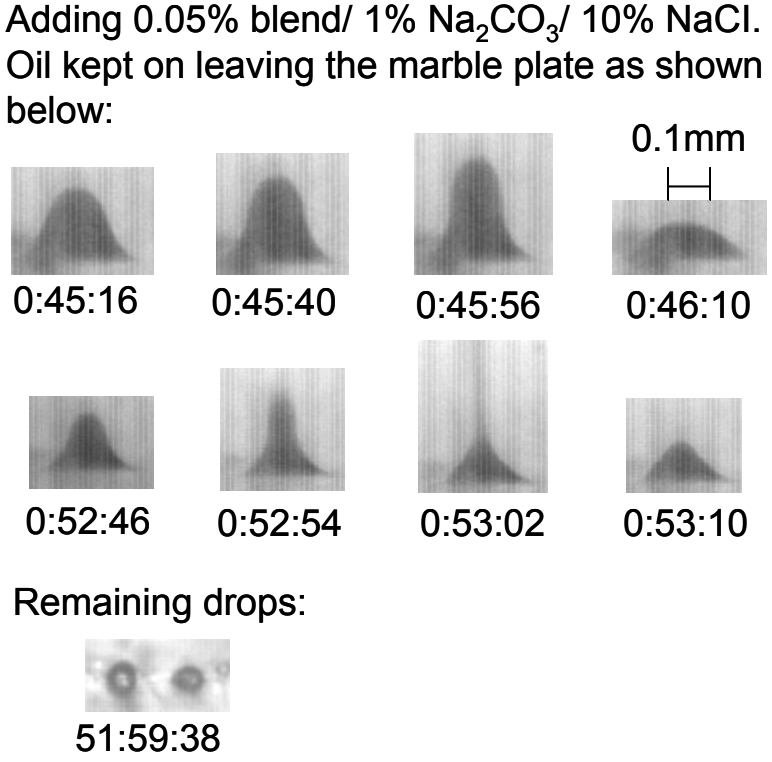

Fig. 3 Wettability alteration of calcite plate with 0.05% Blend / 1% Na_2CO_3 / 10% NaCl

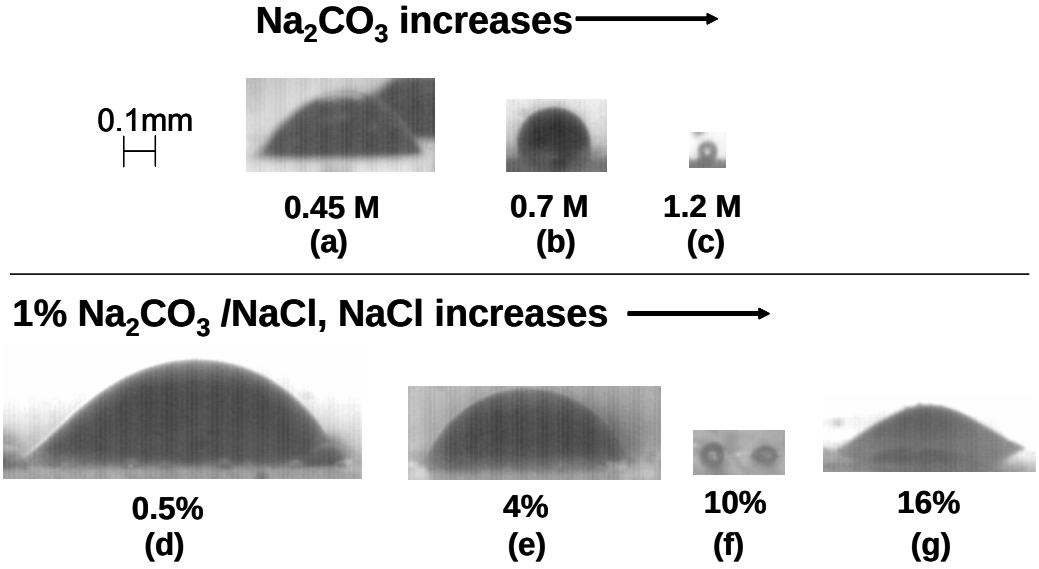

Fig. 4 Final drop configuration after wettability alteration with 0.05% Blend surfactant. Time : greater than 50 hours

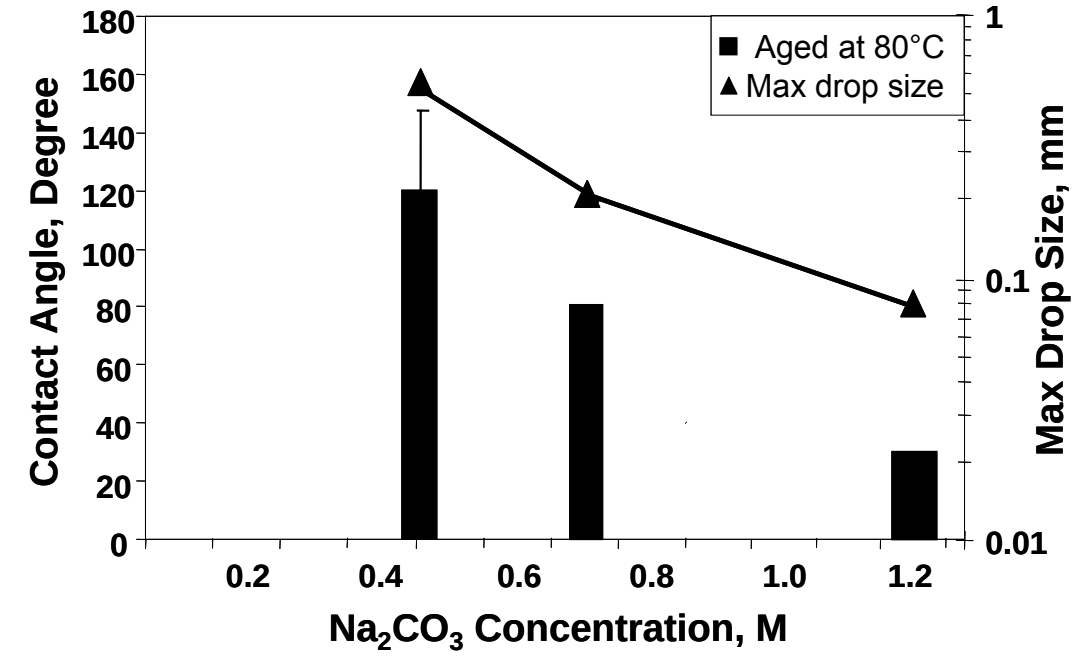

Fig. 5 Wettability alteration with 0.05% Blend/Na_2CO_3

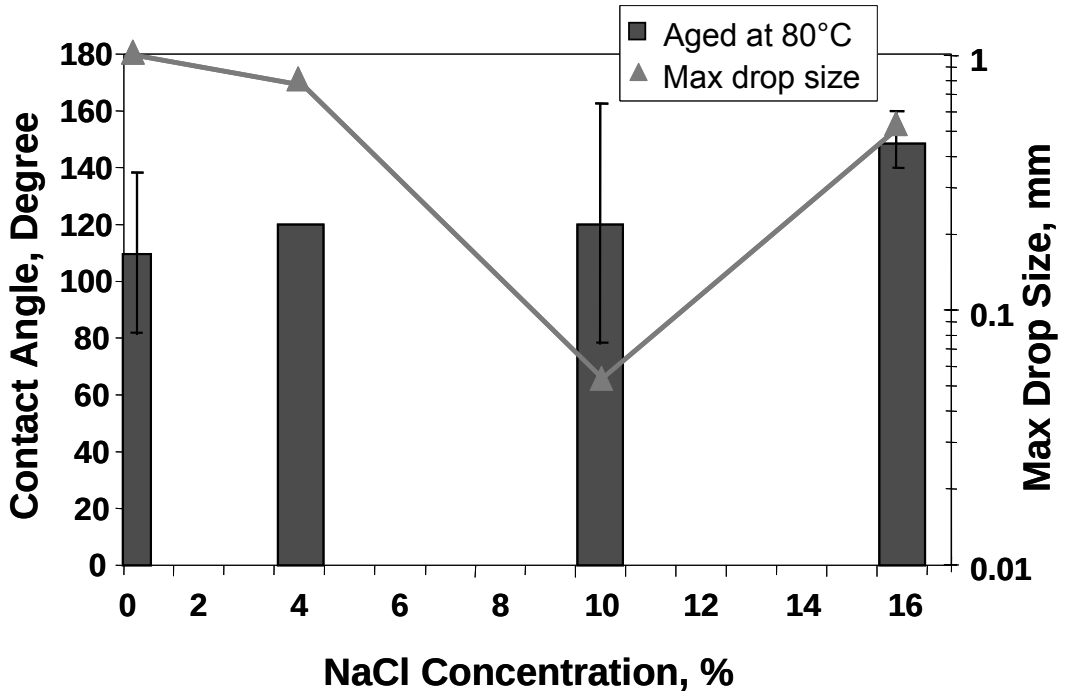

Fig. 6 Wettability alteration with 0.05% Blend/1% Na_2CO_3/NaCl

Surf: 0.05% blend / 1% Na_2CO_3 / NaCl

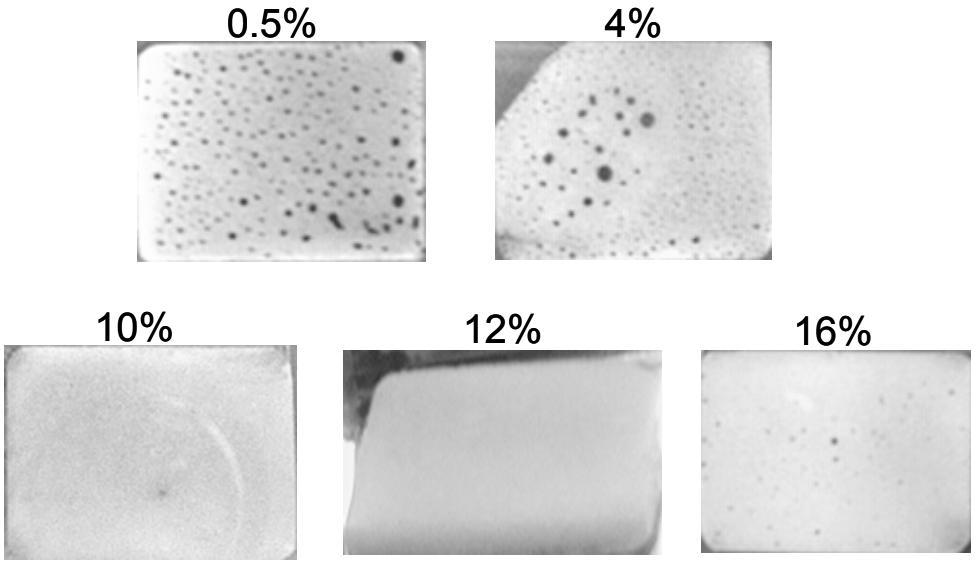

Fig. 7 Effect of salinity on oil remaining on the marble plate

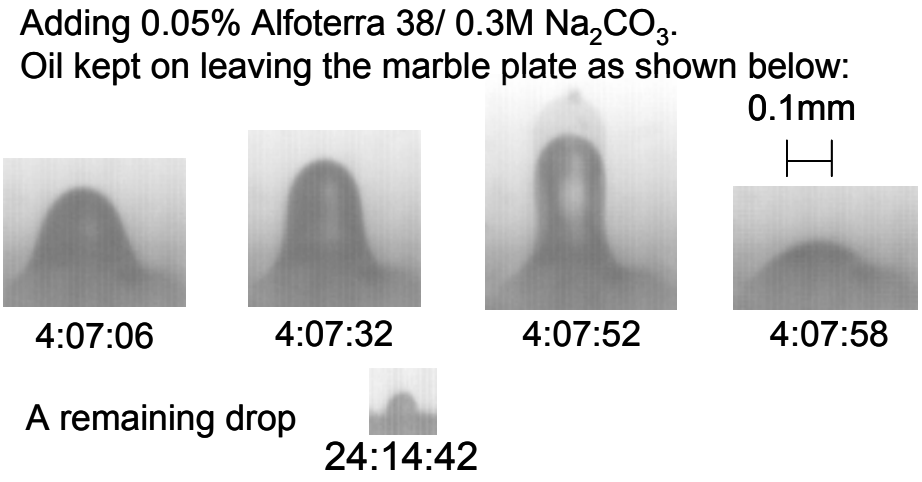

Fig. 8 Wettability alteration of calcite plate with 0.05% Alfoterra 38 / 0.3M Na_2CO_3.

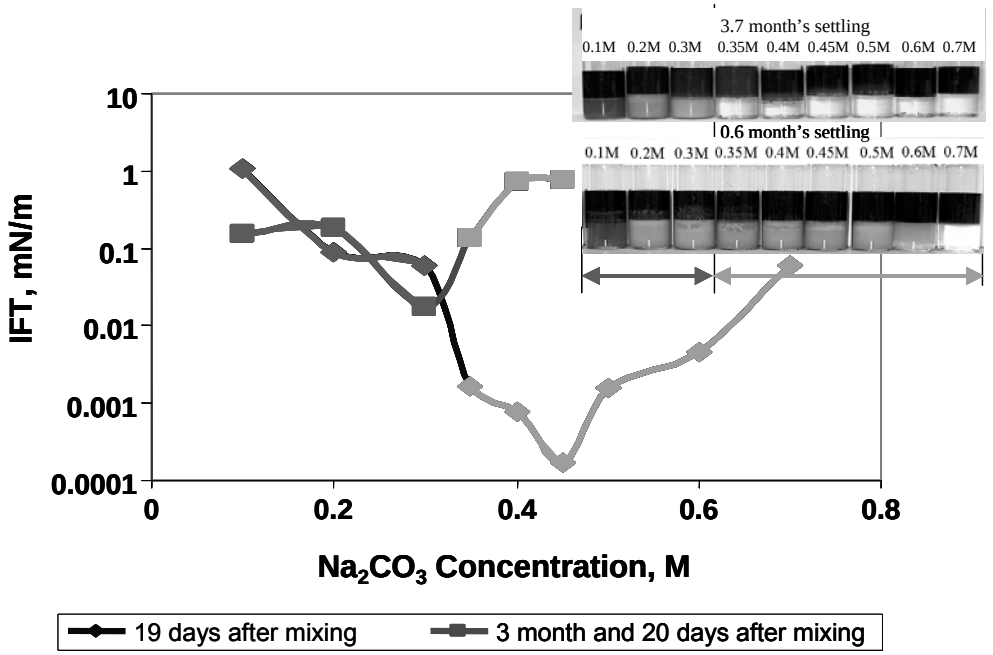

Fig. 9 Phase behavior and IFT of 0.05% Blend surfactant / Na_2CO_3 change with separation time.

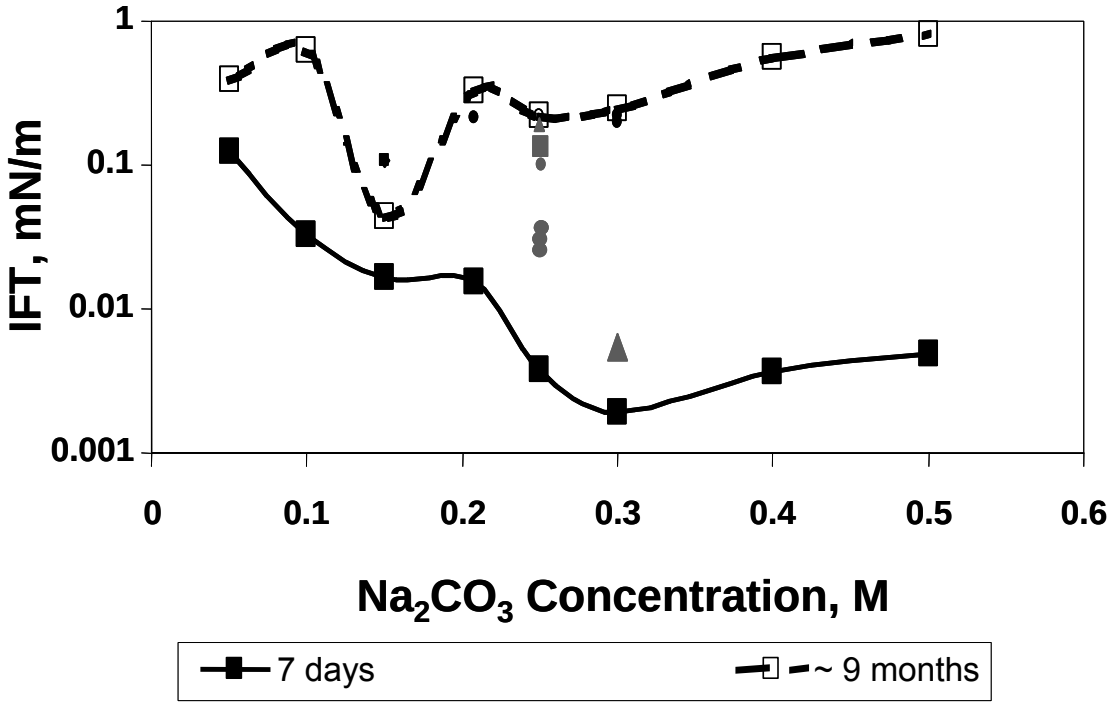

Fig. 10 IFT of 0.05% TDA-4PO / Na_2CO_3 change with separation time. After long time of settling, the addition of middle layer lowers the interfacial tension again (represented by circles and triangles).

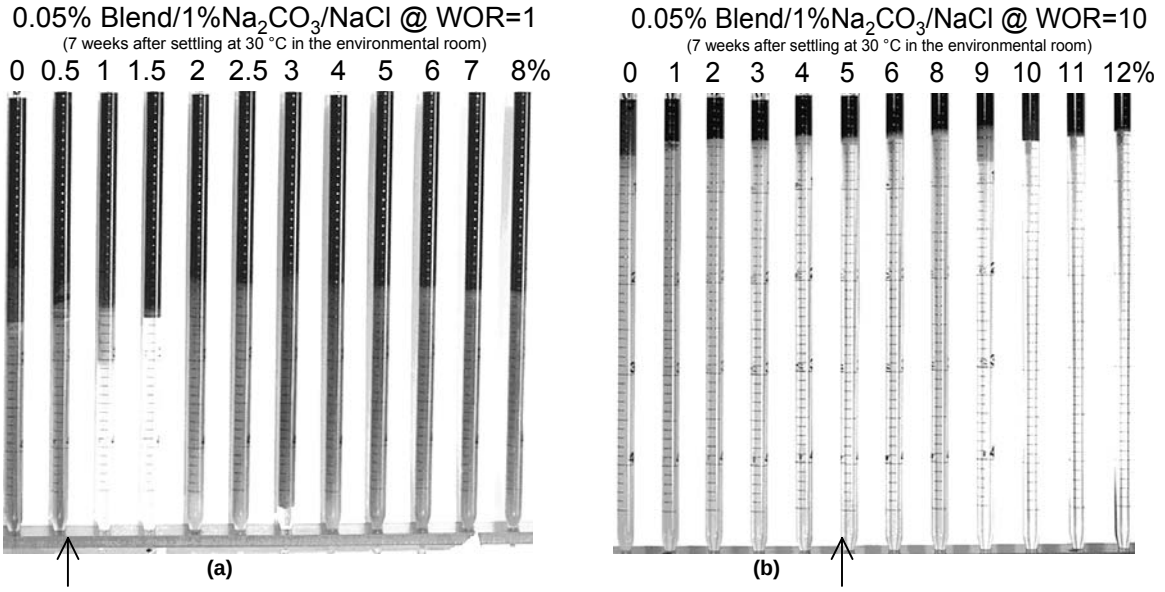

Fig 11 Phase behavior is a function of WOR. Arrows indicate the optimal NaCl concentration.

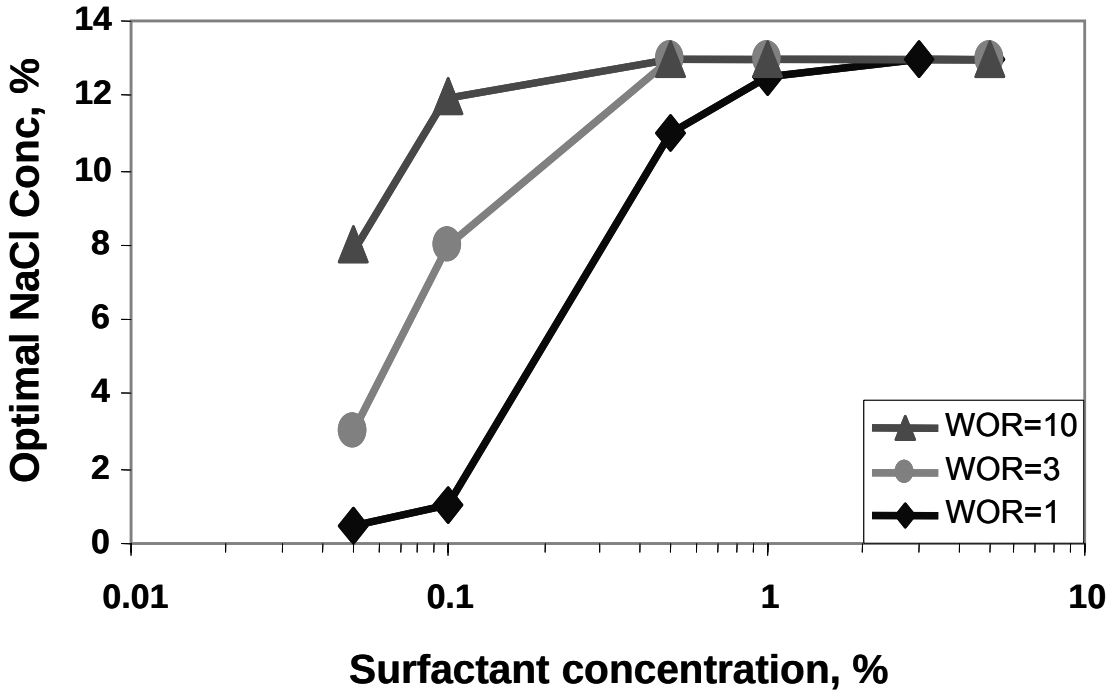

Fig. 12 Optimal sodium chloride concentration as a function of WOR and surfactant concentration for crude oil MY3 and the blend of equal weight amount of CS-330 and TDA-4PO.

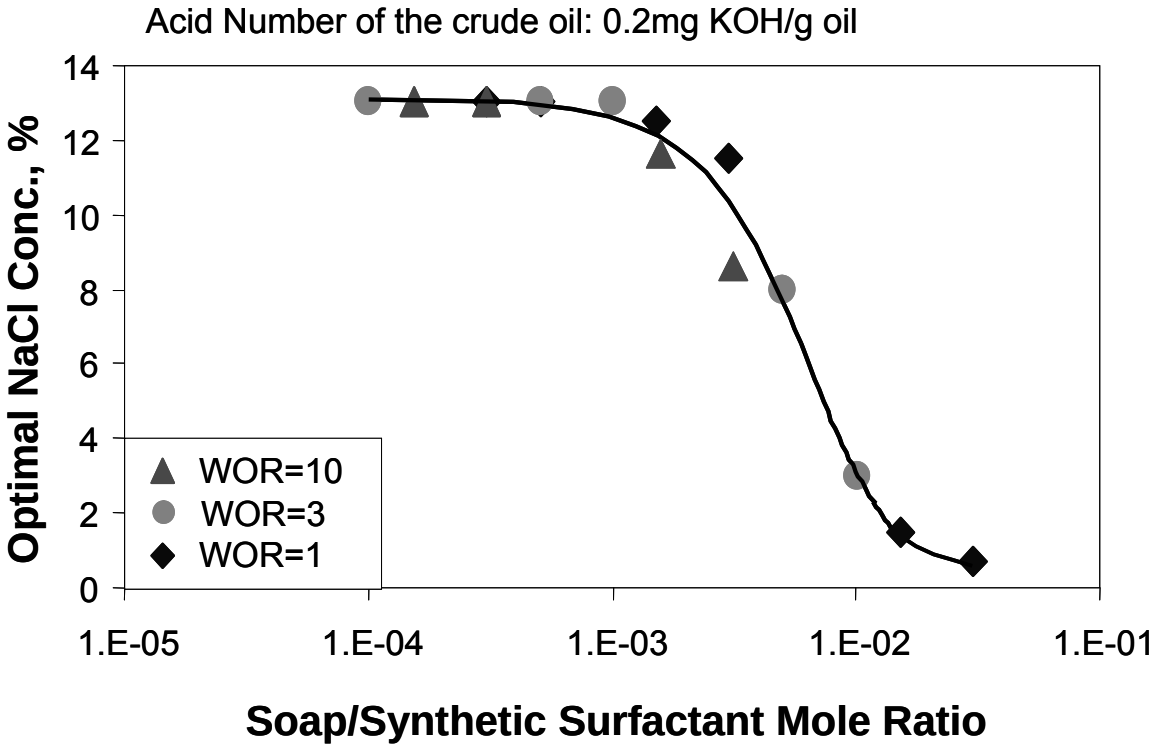

Fig. 13 Optimal sodium chloride concentration as a function of natural soap/synthetic surfactant mole ratio for crude oil MY3 and the Blend of equal weight amount of CS-330 and TDA-4PO.

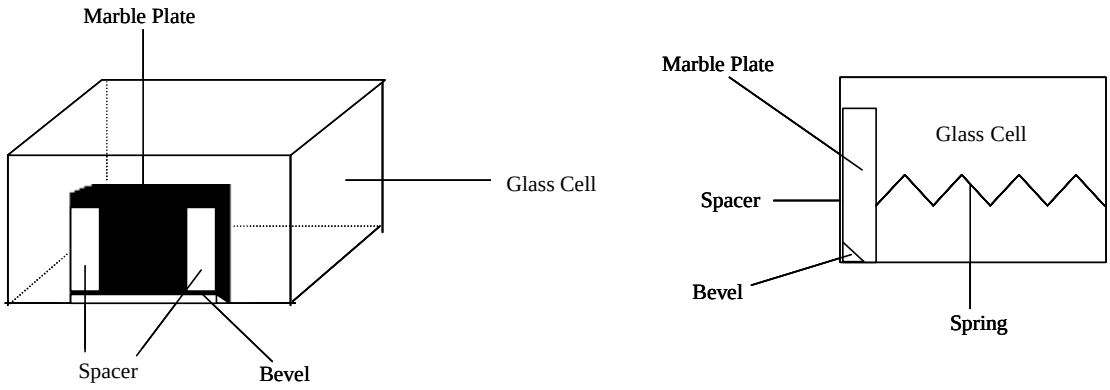

Fig. 14 A calcite (marble) plate has two plastic films to create a 13 μm gap between the plate and the front of an optical cell.

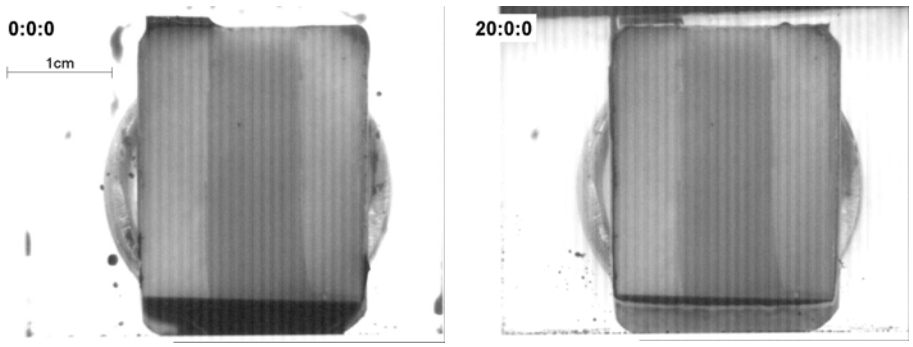

(a) With brine

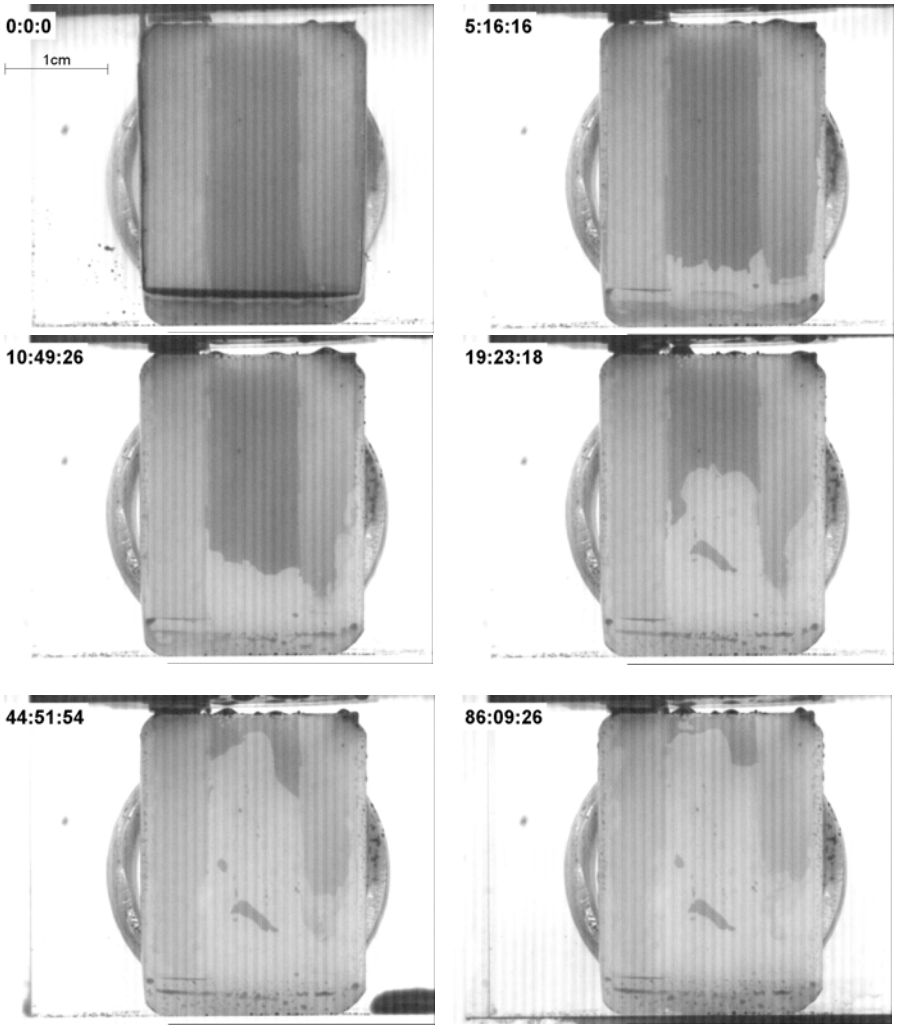

(b) With .05% Blend/1% Na_2CO_3/1% NaCl

Fig. 15 Displacement of crude oil in a narrow gap with brine (a) or with 0.05% Blend/1% Na_2CO_3/1% NaCl

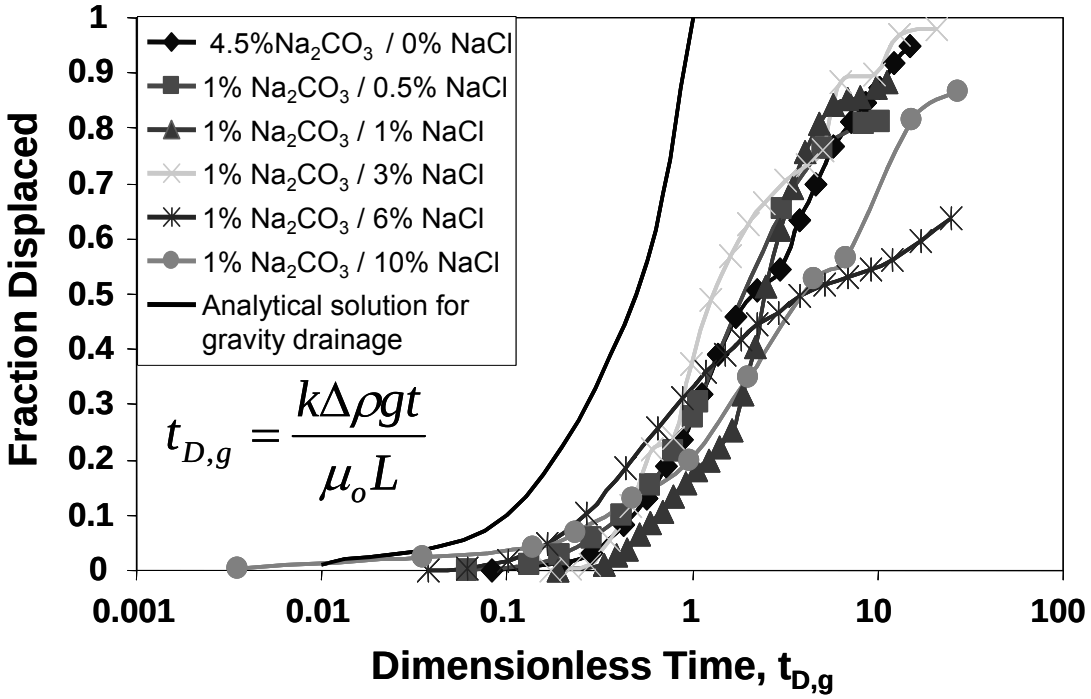

Fig. 16 Spontaneous imbibition in a capillary gap between vertical parallel plates as a function of dimensionless time for gravity drainage.

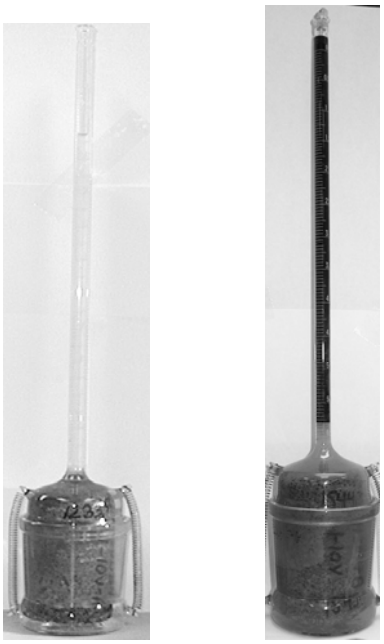

(a) (b)

Fig. 17 Spontaneous imbibition with (a) brine, or (b) alkaline surfactant solution.

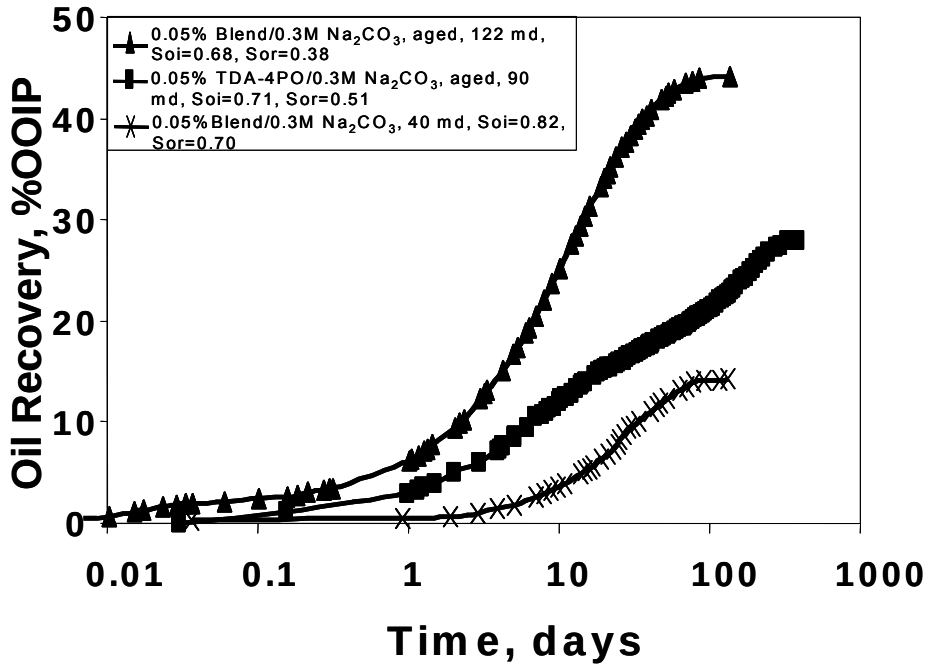

Fig. 18 Oil recovery by spontaneous imbibition.

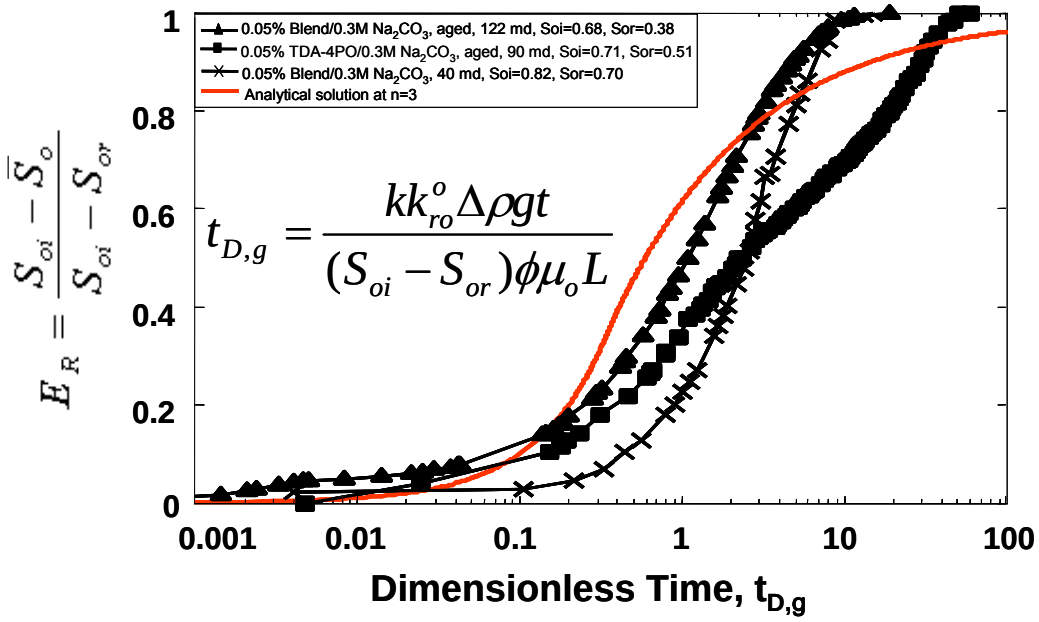

Fig. 19 Oil recovery by spontaneous imbibition as function of dimensionless time for gravity drainage.

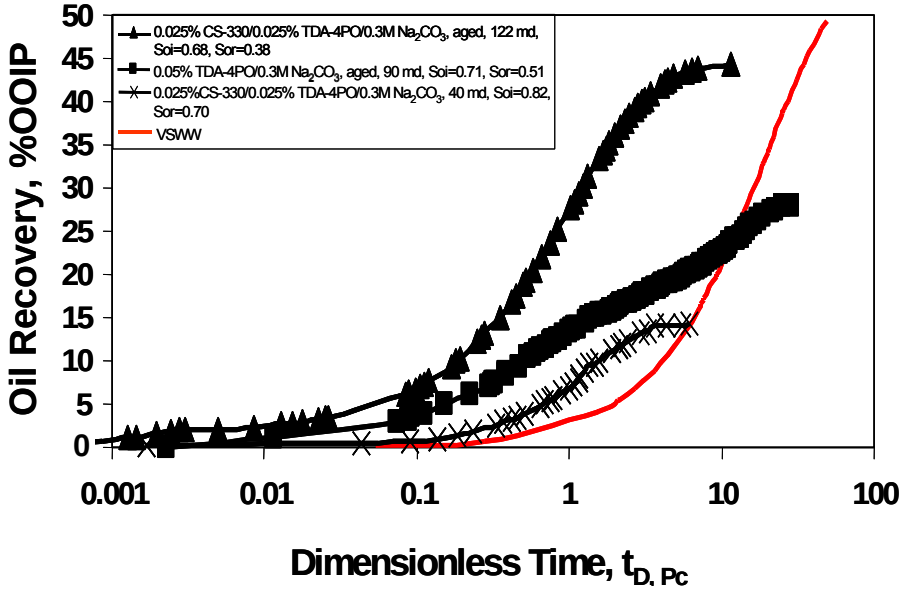

Fig. 20 Oil recovery by spontaneous imbibition as function of dimensionless time for capillary imbibition, assuming IFT of 10^{-3} mN/m

Task 2 Phase behavior, adsorption, and composition changes during displacement

Subtask 2.5 Adsorption

Adsorption of ionic surfactant on silica and dolomite media

Shunhua Liu

Abstract

The adsorption of surfactants is one of the key problems in the alkali-surfactant flooding process. Both static and dynamic experiments are performed to evaluate the adsorption of surfactant on the dolomite. The surfactant concentrations are determined by potentiometric titration with Benzethonium Chloride (hyamine 1622). Also the adsorption on silica sand is measured by the dynamic experiments. The non-adsorption tracers, chloride ions, were determined by the conductivity measurement.

1 Static Adsorption Experiment

The surfactant we used is the blend surfactant (1:1 weight ratio CS-330 and TDA-4PO). The structures of these two surfactants are illustrated as Figure 1. Such ethoxylated and propoxylated sulfates and their mixtures have high tolerance to divalent cations typically present in reservoir brines and are among surfactants being actively considered for surfactant and alkaline-surfactant oil recovery processes.

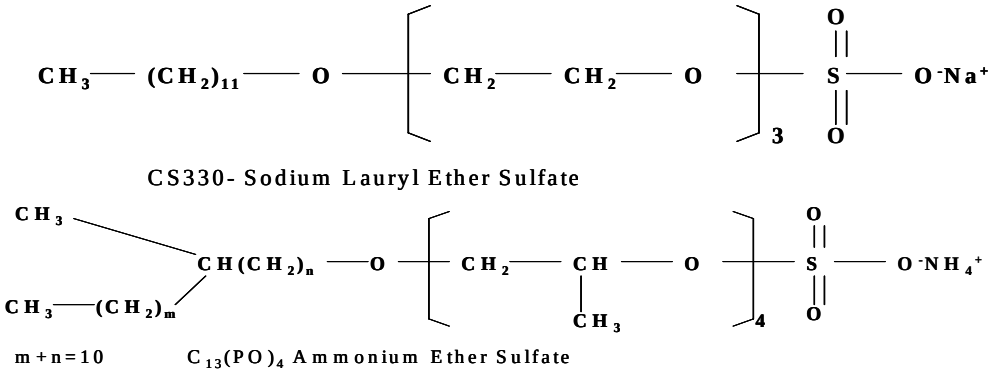

Figure1 Surfactants Structure

The initial surfactant concentration was fixed at either 0.05% or 0.1% (active material). The surfactant solutions were mixed with the dolomite powders at varied weight ratios. The equilibrium surfactant concentration, which was obtained after 24 hours mixing, was determined by titration. The surface area of dolomite powder that was determined by the BET adsorption is 1.7m^2/gram dolomite powder.

The adsorption of the blended surfactant without or with sodium carbonate is shown in Figure 2. The adsorption isotherm in the absence of sodium

carbonate is similar to a Langmuir adsorption isotherm with a plateau adsorption of about 0.002 mmol/m^2 or 1.7mg(surfactant)/gram(dolomite). Addition of 0.2 – 0.4 M sodium carbonate reduced the adsorption by a factor of 10 and the saturation plateau is about 2×10^{-4} mmol/m^2 or 0.17 mg(surfactant)/gram(dolomite).

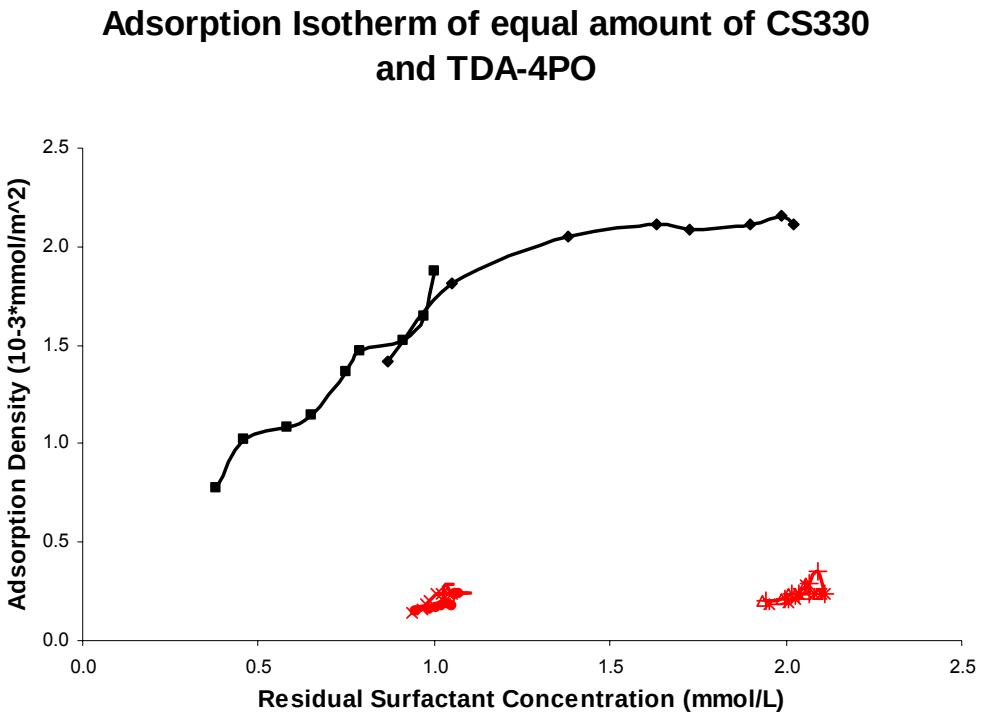

Figure 2 Adsorption on powdered dolomite of blended surfactant with/without Na_2CO_3

From the static adsorption experiments, we find that the addition of sodium carbonate can significantly reduce anionic surfactant adsorption on the dolomite powder. The reduction of adsorption can be attributed to change surface charge to negative charge by the addition of CO_3^{2-}, the potential determining ions. (Hirasaki and Zhang, 2004)

2 Dynamic Adsorption Experiments

2.1 Dynamic Experimental Procedures

Dynamic adsorption experiments on the silica sand and dolomite sand were performed in a one-foot column packed with sand. The experimental apparatus diagram is shown in figure 3. The experimental procedure is:

1.Fill the column with de-ionized water

2.Inject the surfactant solution into the column by the pump; the solution also contains NaCl as a nonabsorbent tracer.

3.Collect the effluent at different times and measure the concentration of the surfactant and NaCl to obtain the break- through curves of the two components

4.For the silica sand, we use isobutyl alcohol and water to wash the column for the next experiment. For dolomite sand, we repack the column with fresh dolomite sand because the adsorbed surfactant could not be totally removed by the washing process.

Experiments on dolomite core were also performed with similar experimental procedures.

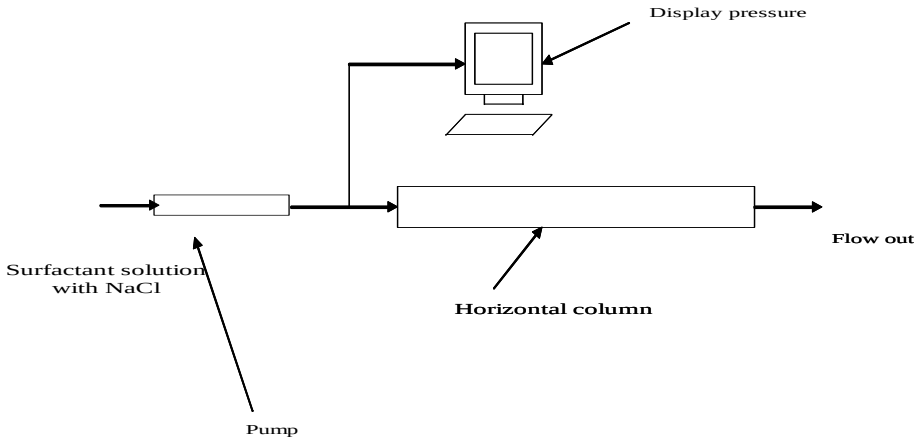

Figure 3 Experimental Apparatus Diagram

In the experiment, the conductivity of the solution was used to measure the NaCl concentration, and potentiometric titration was used to measure the surfactant concentration. Because the ionic surfactant affects the conductivity of the water, an auxiliary experiment was performed to determine whether this effect would introduce error in measuring the NaCl. The results showed that there was not a significant error induced by the ionic surfactants. Furthermore, the following equations were obtained for the calculation:

[Conductivity]= 16905*[NaCl %]+ 30±140.
or **[NaCl %]= 5.92*10^{-5}*[Conductivity]- 2*10^{-3}±8*10^{-3}** (1)

2.2 One Dimensional adsorption model

Below is a brief description of the one dimensional adsorption model that we used for the dynamic adsorption experiments. The major assumptions of the model are:

1.No velocity in the r and θ directions, i.e., one-dimensional flow

2.The adsorption isotherm can be approximated with a constant slope over the range of concentration studied, i.e., the adsorption is linear with the local concentration

3.The physical properties, such as viscosities and densities, do not change with the concentration of the solute.

4.The dispersion coefficient K_l is assumed to be proportional to velocity and the velocity is constant.

5.The medium is homogeneous.

With these assumptions, the mass conservation equation with adsorption is as follows:

$$\phi(1+\beta)\frac{\partial c}{\partial t}+u\frac{\partial c}{\partial x}=\phi K_l\frac{\partial^2 c}{\partial x^2} \qquad x>0,\ t>0 \qquad (2)$$

where ϕ is the porosity.

K_l is the dispersion coefficient.

The slope of the adsorption isotherm with respect to the reduced concentration is denoted by β. The concentration is transformed to a reduced concentration that has a range between 0 and 1. Hereafter, the concentration used here is the dimensionless concentration. Thus the Boundary Conditions and the Initial Conditions are:

C (x, 0) =C_{IC}=0, x>0

C (0, t) =C_{BC}=1, t>0

By using the interstitial velocity v=u/ϕ, the differential equation reduces to:

$$\frac{\partial c}{\partial t}+\frac{v}{(1+\beta)}\frac{\partial c}{\partial x}=\frac{K_l}{(1+\beta)}\frac{\partial^2 c}{\partial x^2} \qquad (3)$$

In the absence of dispersion, the solution to this differential equation is an indifferent step wave with a velocity equal to $v/(1+\beta)$. Thus the slope of the adsorption isotherm describes the retardation of the concentration wave. By transforming the variables, the PDE can be translated into an ODE

$$\frac{d^2C}{d\eta^2} + 2\eta\frac{dC}{d\eta} = 0 \qquad \text{where} \qquad \eta = \frac{x - \frac{vt}{1+\beta}}{\sqrt{\frac{4K_l t}{1+\beta}}} \tag{4}$$

By integrating the ODE with the boundary conditions, the solution obtained is:

$$C = \frac{1}{2}\left[1 - \frac{2}{\sqrt{\pi}}\int_0^{\eta} e^{-\eta^2}\, d\eta\right] = \frac{1}{2}\operatorname{erfc}(\eta) \tag{5}$$

With the characteristic system length L, the distance variable will be made dimensionless with respect to L. Thus the non-dimensional variable η is:

$$\eta = \frac{x_D - \frac{t_D}{(1+\beta)}}{2\sqrt{\frac{t_D}{Pe(1+\beta)}}} \tag{6}$$

where $x_D = x/L$, $t_D = uAt/\phi AL$ and $Pe = Lv/K_l$.

Therefore, with the break-through curve, i.e., x_D=1, the concentration history can be obtained. And the retardation of the break-through curve can be expressed as β. If the nonabsorbent tracer and adsorbing solute break-through curves coincide, then β=0, that is no adsorption occurred for the component measured.

Since the data obtained are the effluent history, we can calculate the value of β and Pe by following manipulation. From the relation of the complementary error function to the cumulative Gaussian probability distribution, the slope of adsorption isotherm and the Peclet number can be estimated by the mean and standard deviation of a Gaussian distribution. The cumulative Gaussian probability distribution is given by the following formula:

$$P\{y\} = \frac{1}{2}\left[1 + \operatorname{erf}\left(\frac{u}{\sqrt{2}}\right)\right] \tag{7}$$

$$u = \frac{y - \mu}{\sigma} \tag{8}$$

$$y = \mu + \sigma u \tag{9}$$

where μ and σ are the mean and standard deviation of the Gaussian distribution.

Recall that the effluent concentration is given by equation (5) as.

$$C = \frac{1}{2}\operatorname{erfc}(\eta) = \frac{1}{2}\left[1 - \operatorname{erf}(\eta)\right] \qquad \text{where} \qquad \eta = \frac{1 - \frac{t_D}{(1+\beta)}}{2\sqrt{\frac{t_D}{Pe(1+\beta)}}} \tag{10}$$

Next we transform the variables such that the transformed variables are a cumulative Gaussian distribution. First, transform C such that it has the same dependence on the error function as the Gaussian distribution.

$$\frac{1}{2}\left[1 + erf(\eta)\right] = 1 - C \Rightarrow P \tag{11}$$

The argument of the error function should map the independent variables.

$$\eta(x_D = 1) = \frac{1 - \frac{t_D}{(1+\beta)}}{2\sqrt{\frac{t_D}{Pe(1+\beta)}}} = \frac{1 + \beta - t_D}{2\sqrt{\frac{t_D(1+\beta)}{Pe}}} \Rightarrow \frac{u}{\sqrt{2}}$$

$$\frac{1 - t_D}{\sqrt{t_D}} \Rightarrow y$$

Finally, the expression for μ and σ are:

$$\mu = -\beta \qquad \text{and} \qquad \sigma \approx \sqrt{2}\sqrt{\frac{1+\beta}{Pe}}$$

From the experimental data C and the t_D, P, y and η can be calculated. With y and η, μ and σ can be calculated by linear regression. Then β and Pe are obtained.

Since the exact porosities of the sand column and the dolomite are unknown, they should be determined first. The fact that there is no adsorption for NaCl in the sand or the dolomite can be used to estimate the porosity. For the NaCl data, a pore volume is guessed at first, and then the μ and σ are calculated based on the guessed pore volume. Because β equals zero for no adsorption case, the porosity for which β=0 would be the true porosity. The porosity calculated by this method is similar to the porosity that comes from the weight method. With the calculated porosity, we can obtain the β and Peclet Number by using the linear regression for the surfactant data. The simulation curve also can be plotted with the calculated β and Peclet Number.

2.3 Adsorption on silica sand

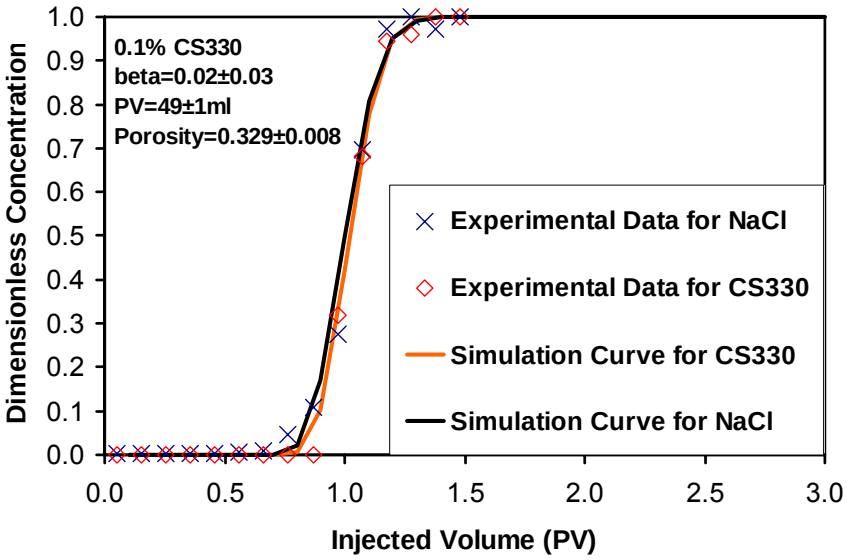

Figure 4 Adsorption of CS330 in silica sand column

Figures 4, 5 and 6 show the break-through curves and simulation curves of the CS330, TPA-4PO and their blend in the silica sand column respectively. From these three plots, no significant adsorption for the surfactant is found in the silica sand packed column because the break-through curves of the two components (NaCl and surfactant) superpose each other. And we find that the one-dimensional model can simulate this kind of displacement experiment very well.

The reason that the adsorption of anionic surfactant is negligible on the silica surface is due to the negatively charged interface of brine/silica, which repels the negatively charged surfactant by electrostatic forces.

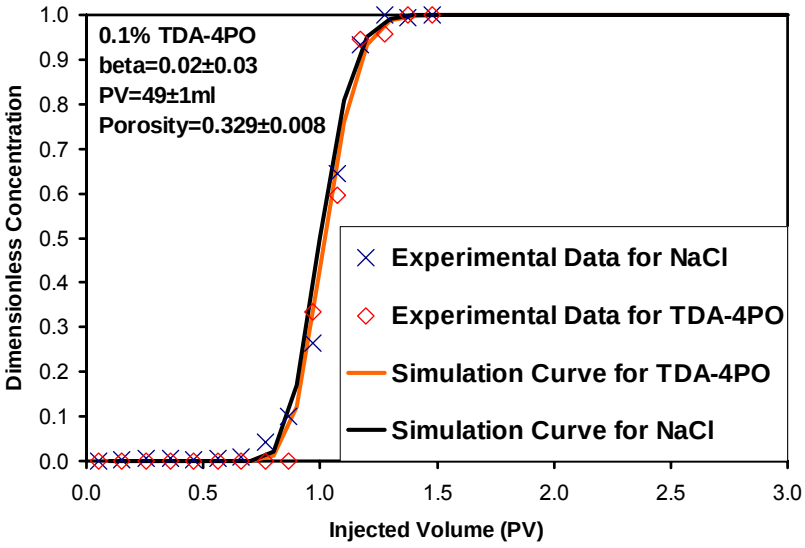

Figure 5 Adsorption of TDA-4PO in silica sand column

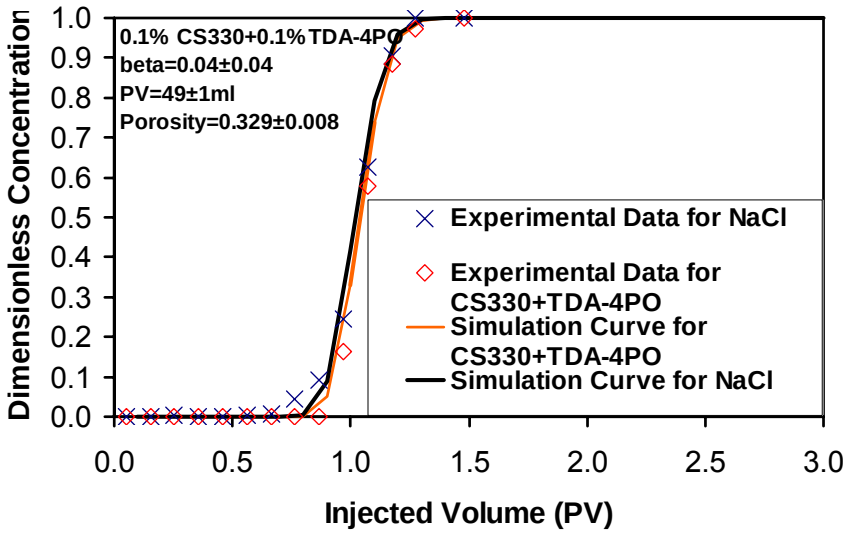

Figure 6 Adsorption of blend surfactants in silica sand column

2.4 Adsorption on dolomite

Figure 7 shows the break-through curve and the simulation curve of the CS330 and NaCl in the dolomite core (permeability is 122~284 md; porosity is 0.171±0.003). The break-through curve for CS330 has some lag compared with the NaCl. That means the dolomite adsorbs some surfactant. From the

simulation result, β is estimated as β=0.27±0.04, which is much larger than β in the silica sand.

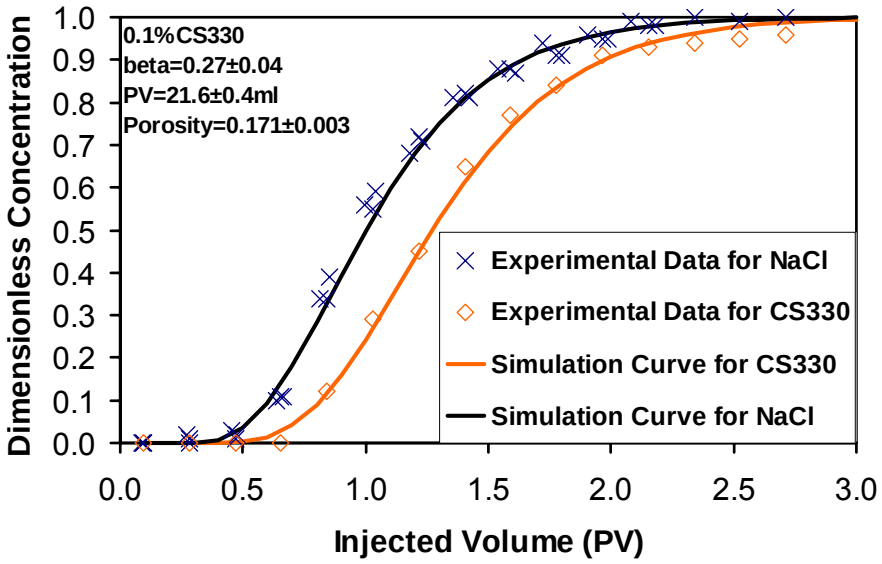

Figure 7 Adsorption of CS-330 in dolomite core

Because we do not have the cores with nearly identical properties and we cannot measure the BET surface of cores, we use the dolomite sand as an alternative porous medium for the adsorption experiments. The surface area of dolomite sand and dolomite powder were determined by the BET adsorption to be 0.3 m^2/gram and 1.7 m^2/gram, respectively. We assumed the adsorption density, i.e., the adsorption amount per active surface area is not changed from dolomite powder to dolomite sand. We can calculate the β from the static adsorption isotherm by using the equation (12).

$$\beta = \frac{c_s}{c} = \frac{(1-\phi)}{\phi}\rho_{dolomite} S\, k_{iso} \qquad (12)$$

where ϕ is the porosity of the column

$\rho_{dolomite}$ is the density of the dolomite

S is the BET surface area of the medium

k_{iso} is the slope in the isotherm plot from Figure 2

The break-through curve and the simulation curve of the mixture surfactant and NaCl for dolomite sand pack column (porosity is 0.33~0.34) are plotted in Figure 8. Figure 8 indicates that the adsorption of surfactant on dolomite sand is significant. Figure 8 also demonstrates that the adsorption of surfactants is not an instantaneous process and depends on the flow rate. At a high interstitial velocity of 12 feet/day (β=0.22), the retardation is much smaller than that at 1.2 feet/day. Even at the lower flow rate (β=0.34 at 1.2feed/day), β is less than that calculated from the static adsorption isotherm (β=0.40).

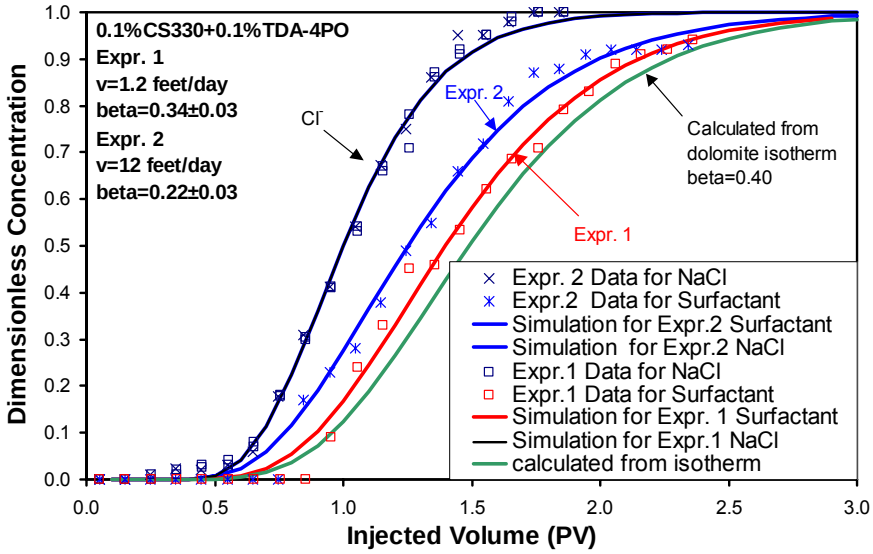

Figure 8 Adsorption of blend surfactants in dolomite sand column

The addition of sodium carbonate can significantly reduce surfactant adsorption, as shown in Figure 9. At the same flow rate, β is reduced from 0.34 to 0.07.

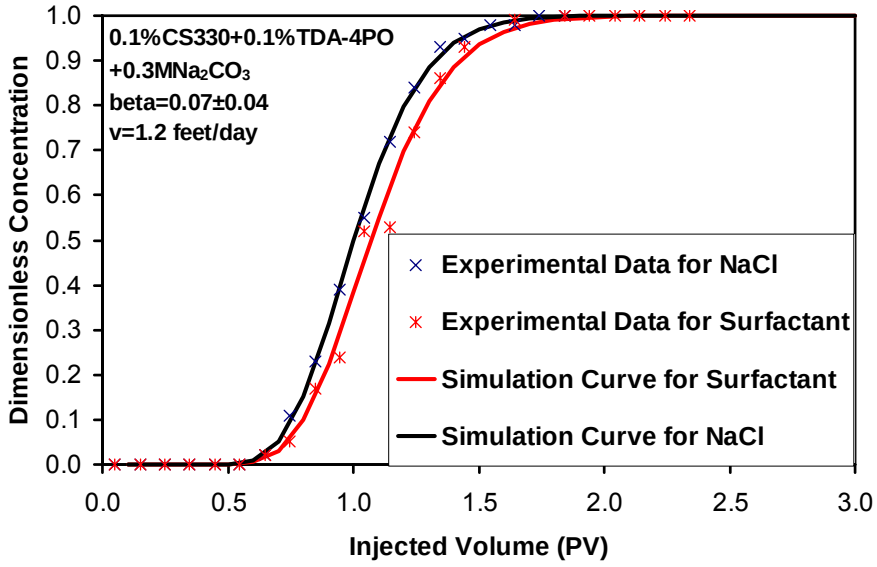

Figure 9 Adsorption of blend surfactants with alkali in dolomite sand

Table 1 Summary of experimental conditions and results.

Porous Media	From	Permeability	Porosity	Pore volume	Inject Surfactant Concentration	Flow rate	Retardation β
Silica sand	US Silica Ottawa Foundry	~120 darcy	0.329±0.008	49±1ml	CS330 (0.1%)	8feet/day	0.02±0.03
Silica sand	US Silica Ottawa Foundry	~120 darcy	0.329±0.008	49±1ml	TDA-4PO (0.1%)	8feet/day	0.02±0.03
Silica sand	US Silica Ottawa Foundry	~120 darcy	0.329±0.008	49±1ml	CS330 (0.1%) TDA-4PO (0.1%)	8feet/day	0.04±0.04
Dolomite core	Marathon Oil Company	122~284 md	0.171±0.003	21.6±0.4ml	CS330 (0.1%)	5feet/day	0.27±0.03
Dolomite sand	Unimin corporation		0.335±0.008	50±1ml	CS330 (0.1%) TDA-4PO (0.1%)	1.2feet/day	0.34±0.03
Dolomite sand	Unimin corporation		0.338±0.008	50±1ml	CS330 (0.1%) TDA-4PO (0.1%)	12feet/day	0.22±0.03
Dolomite sand	Unimin corporation		0.337±0.008	50±1ml	CS330 (0.1%) TDA-4PO (0.1%) Na2CO3 (0.3M)	1.2feet/day	0.07±0.04

3 Conclusion

1.For silica sand, there is no significant adsorption of these two surfactants (CS330, TDA-4PO) or their mixture.

2.For dolomite core or sand, the adsorption of the surfactant cannot be neglected.

3. Flow rate affects dynamic surfactant adsorption. A relatively low rate is required for the adsorption to reach equilibrium.

4.Adding alkali to the surfactant solution reduces the adsorption amount significantly.

Task 3 Foam for Mobility Control

3.1 Foam diversion in fracture network model

The main purpose of this research is to investigate the foam flow in fracture system and foam diversion effect in heterogeneous fracture system. Hirasaki and Lawson [1985] investigated the foam flow rheology in capillary tubes. We modified their equations to apply to foam flow in fractures and did experiments to verify our theory.

Experimental technique

The fracture model has been established as in the figure 1.

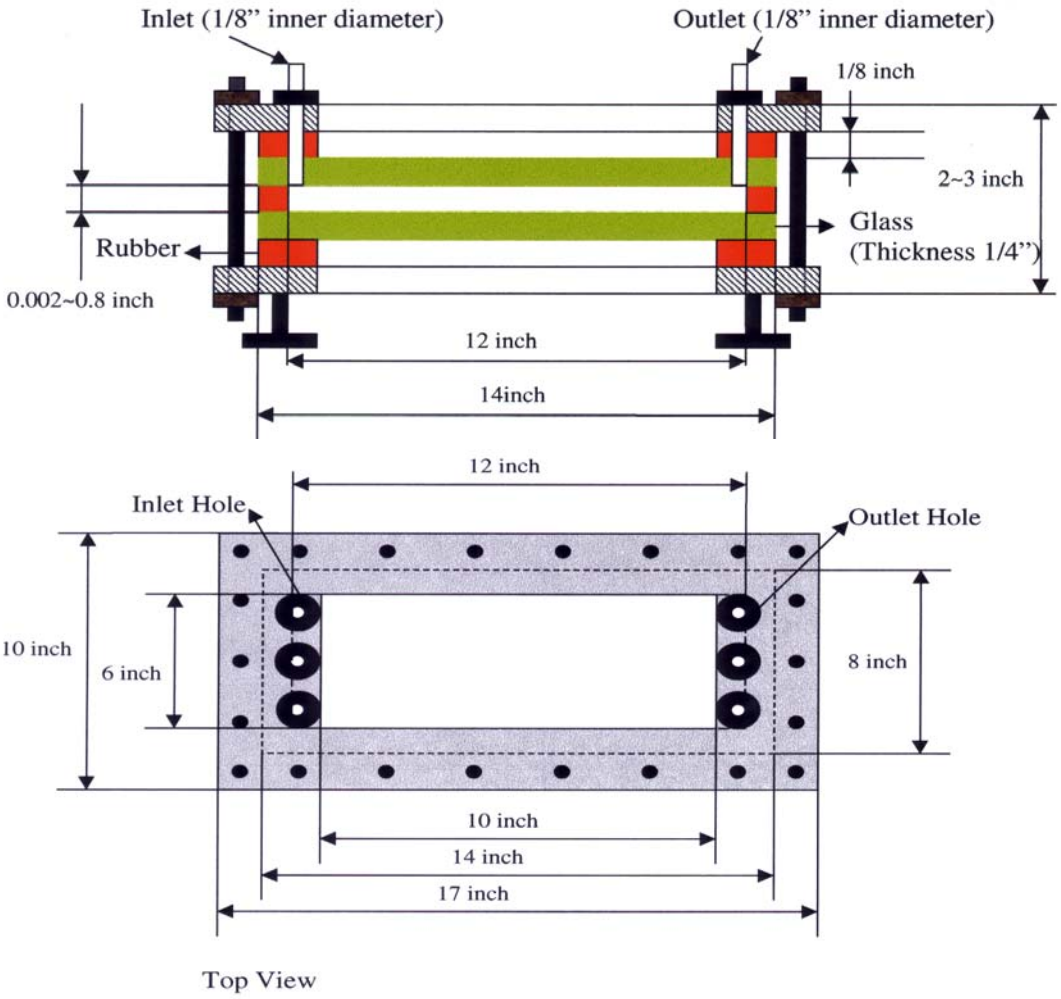

Figure 1. Detailed diagram of fracture model

The fracture model mainly consists of two parallel plates. Changing the gasket thickness between the two parallel plates can change the thickness of the fracture. The foam is pre-generated in a foam generator and then injected into the fracture model.

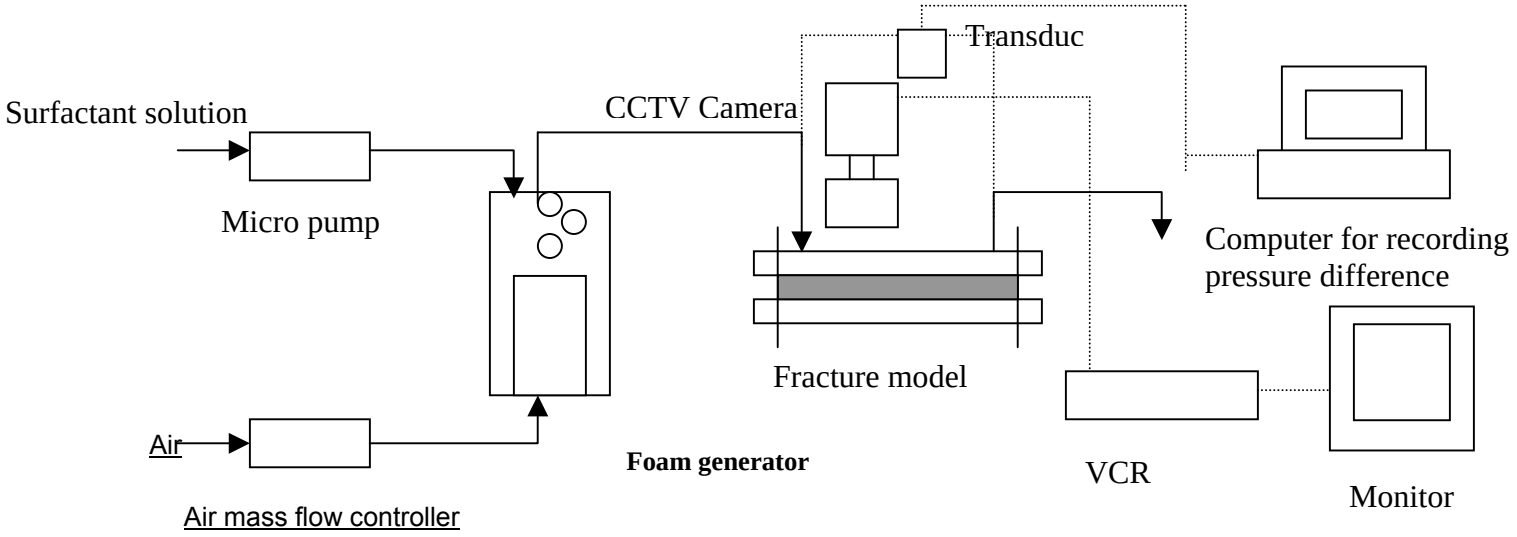

Fig. 2. Set –up diagram for foam mobility control experiment in fracture model

The set-up diagram of the equipment for the foam experiments is shown in figure 2. A Micro pump is used to inject surfactant solution and a mass flow controller is used to inject air into the foam generator. Relatively uniformed size bubbles can be generated only when the air and surfactant solution are introduced on opposite sides of the frit in the foam generator. Choosing frits with different pore size can generate different sizes of bubbles. Also by changing fractional flow, flow-rate, bubble size and gap width, we can investigate these factors' influence on the apparent viscosity.

Two methods were used to determine the bubble size, image analysis and capillary tube experiment. Image analysis takes pictures of foam bubbles in the facture directly and uses Photoshop software to analyze the mean bubble size and bubble size distribution. Capillary tube experiment connects a capillary tube with known size to the outlet of foam generator and the mean bubble size is determined by counting the number of lamellae in the capillary tube. This can verify the mean bubble size obtained from image analysis and determine if the bubble size changes in the fracture.

The surfactant solution in the experiments was 0.5% C13-4PO (TDA-4PO) and 0.5% CS330. The salinity was 0.23% NaCl, 0.07% $CaCl_2$ and 0.04% $MgCl_2$. The bubble sizes used in the experiment were 0.4, 0.6, 0.8 and 1.0mm in diameter for fracture thickness of 0.2mm and 0.4 and 0.6mm in diameter for

fracture thickness of 0.1mm. The fractional flows were 0.0, 0.2, 0.33, 0.5 and 0.67. The values used for the viscosity of solution and surface tension were 1.0 mPa·s and 28 mN/m.

Theory

From Hirasaki and Lawson [1985], the most important variable affecting foam apparent viscosity in uniform, smooth capillaries is foam texture. The principal factors affecting apparent viscosity of foam in uniform capillaries are dynamic changes at gas/liquid interfaces. The apparent viscosity is the sum of three contributions as in figure 3:

1. Slugs of liquid between gas bubbles resist flow.
2. Viscous and capillary forces result in interface deformation against the restoring force of surface tension.
3. The surfactant is swept to accumulate at the back and be depleted at the front of bubble, which causes a surface tension gradient that resists flow.

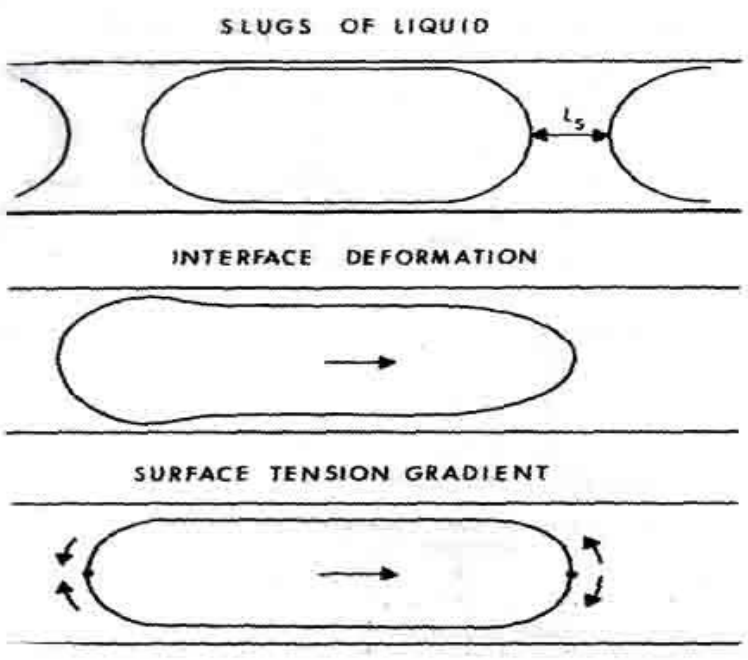

Fig. 3. Mechanisms affecting apparent viscosity in capillary tube

The contribution of deformation of the foam bubble to apparent viscosity in uniform fracture can be predicted by comparing with that from foam flow in

capillary tube. In a capillary tube, the equation for the net dynamic pressure drop across a single bubble is:

$$\Delta p_{dynamic} = 2.26(\sigma / r_c)(3\mu U / \sigma)^{2/3}[(r_c / R)^2 + 1]$$

Where U is the velocity of bubble, σ is the surface tension, r_c is the radius of curvature of gas-liquid interface and R is the capillary radius.

Correspondingly, the equation for the total dynamic pressure drop across a single bubble in parallel plates is:

$$\Delta p_{dynamic} = 2.26(\sigma / r_c)(3\mu U / \sigma)^{2/3}$$

The apparent viscosity from the contribution of foam bubble deformation in uniform fracture can be predicted from the Plane-Poiseuille flow:

$$\mu_{app}^{shape} = \frac{n_L \Delta p_{dynamic} h^2}{12U} = 0.57 \frac{(\mu n_L h)}{(r_c / h)} (3\mu U / \sigma)^{-1/3}$$

Where n_L is the number of equivalent lamellae per unit length and h is the thickness of the fracture.

n_L and r_c are important parameters in determining the value of apparent viscosity. By assuming that individual bubbles are distributed uniformly in the fracture, the number of lamellae per unit length can be expressed in terms of the fracture thickness and the equivalent bubble radius:

$$n_L = \left(\frac{f_g h}{\frac{4}{3}\pi r_B^3} \right)^{\frac{1}{2}}$$

Where f_g is fractional flow, h is the fracture thickness and r_B is the equivalent bubble radius. In all the experiments, the highest fractional flow is 0.67. The foam bubbles are normally separated and the equivalent bubble diameter is bigger than the fracture thickness. The radius of curvature, r_c, is equal to the half thickness of the fracture.

The contribution to apparent viscosity from liquid slugs in uniform fracture can be predicted from the contribution of liquid viscosity in the total fluid. That is:

$$\mu_{app}^{liq} = (1 - f_g)\mu^{liq}$$

Where μ^{liq} is the viscosity of pure liquid and f_g is the gas fractional flow.

The total apparent viscosity can be obtained from measuring the pressure difference across the model. That is from Plane-Poiseuille law:

$$\mu_{app} = \frac{h^2}{12U}\nabla p$$

Where ∇p is the pressure gradient.

By comparing the sum of μ_{app}^{shape} and μ_{app}^{liq} with the value of μ_{app}, the contribution from surface tension gradient was found to be insignificant in our system.

Experimental results

The mean bubble sizes obtained from image analysis and capillary tube experiment are quite close as shown in figure 4. The bubble size is shown as an equivalent spherical diameter. The standard deviation of bubble size distribution is about 20%. From figure 4, the mean bubble size and standard deviation remains constant at different flow rate and different fractional flow as long as the bubble equivalent diameter was less than 5 times the fracture thickness.

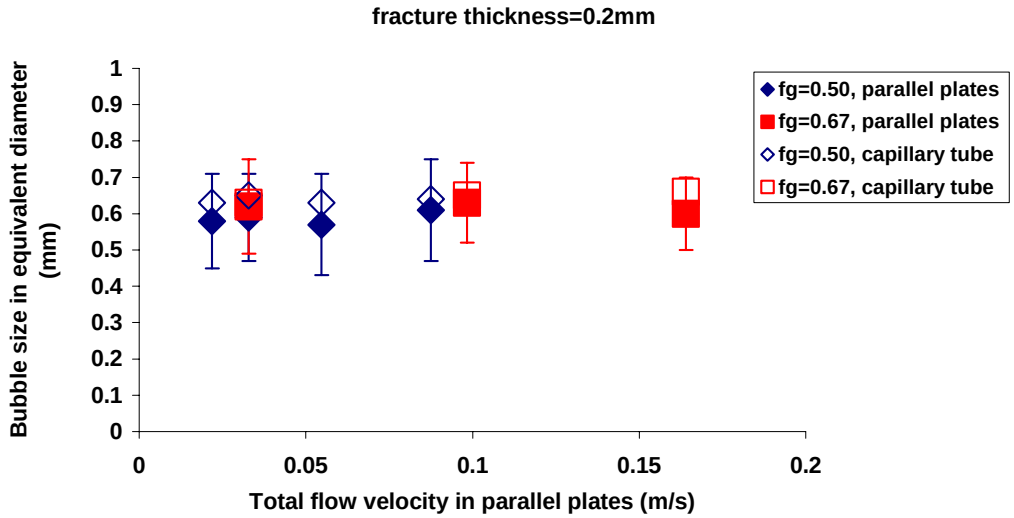

Fig. 4. Bubble size distribution

Experiments were done to investigate the effects of different flow rate, bubble size, fractional flow, and fracture thickness on the apparent viscosity of foam flow in uniform fracture. From the experiments, the most important variable affecting foam viscosity in homogeneous fracture system is foam texture. Foam of finer texture has more lamellae per unit length, and as a result, greater resistance to flow. The foam bubbles in our experiments are individual bubbles because the fracture thickness is small compared to the equivalent diameter of the bubbles.

Some experimental results are shown as in figure 5. From figure 5, the data from the experiment fit the theory value (apparent viscosity contribution from liquid slug and bubble deformation without contribution from surface tension gradient) quite well at low flow rate. Because our theory is based on the Hele-Shaw flow, which is valid for creeping flow at Reynolds number less than one, the data begin to deviate from the theory value at higher Reynolds number. The Reynolds numbers at which the data begin to deviate from theory are shown in figure 6 & 7. Deviation occur above Reynolds number of about 2-15. Also, we found when the ratio of the diameter of bubble to fracture thickness is above 5~8, the bubble size in the fracture is different from that out of the foam generator. Because our theory is based on the assumption of relatively uniform bubble size during flow, this may cause the deviation from the theory.

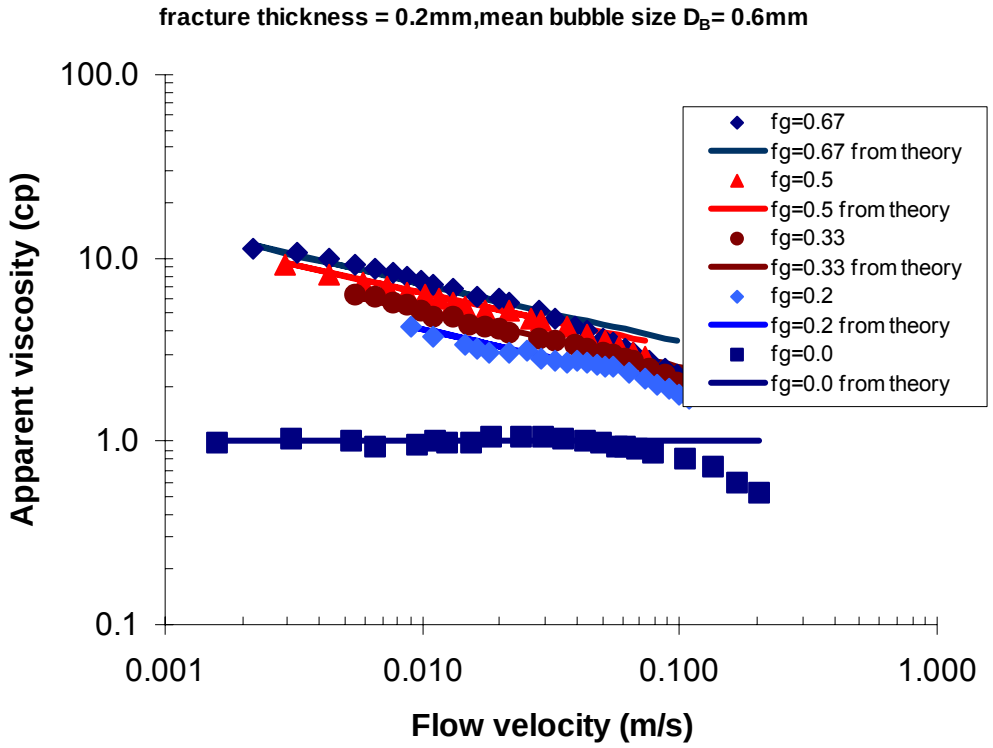

Fig. 5. Effect of flow rate and fractional flow on apparent viscosity

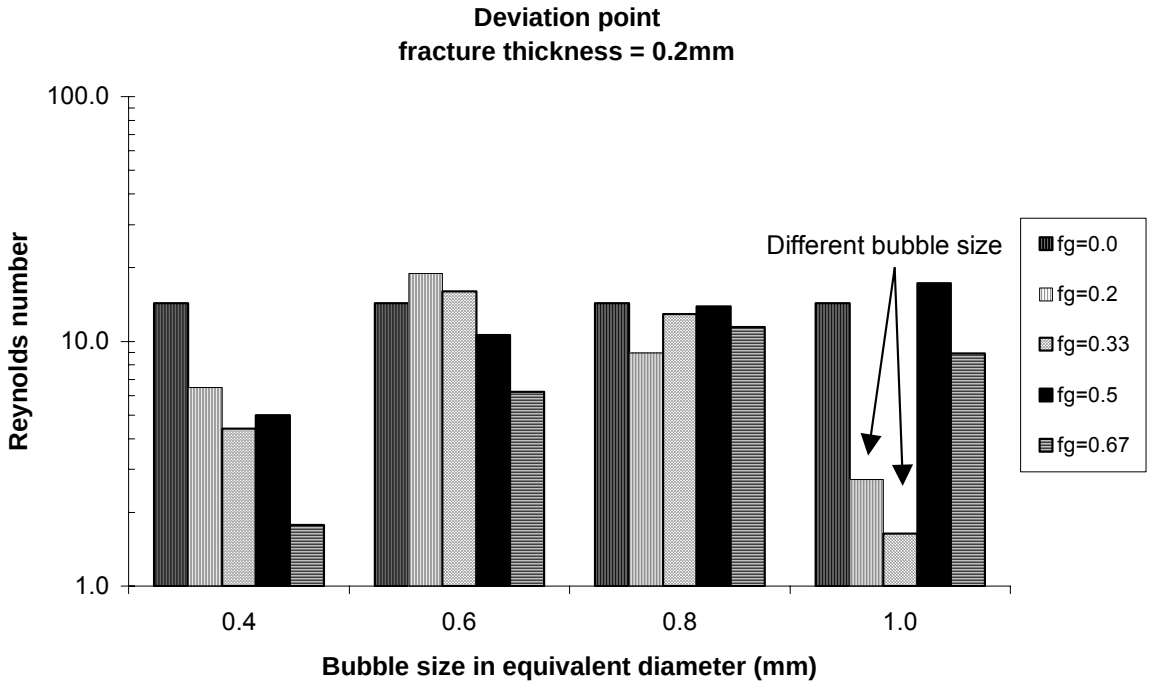

Fig. 6. Deviation point for fracture thickness=0.2mm

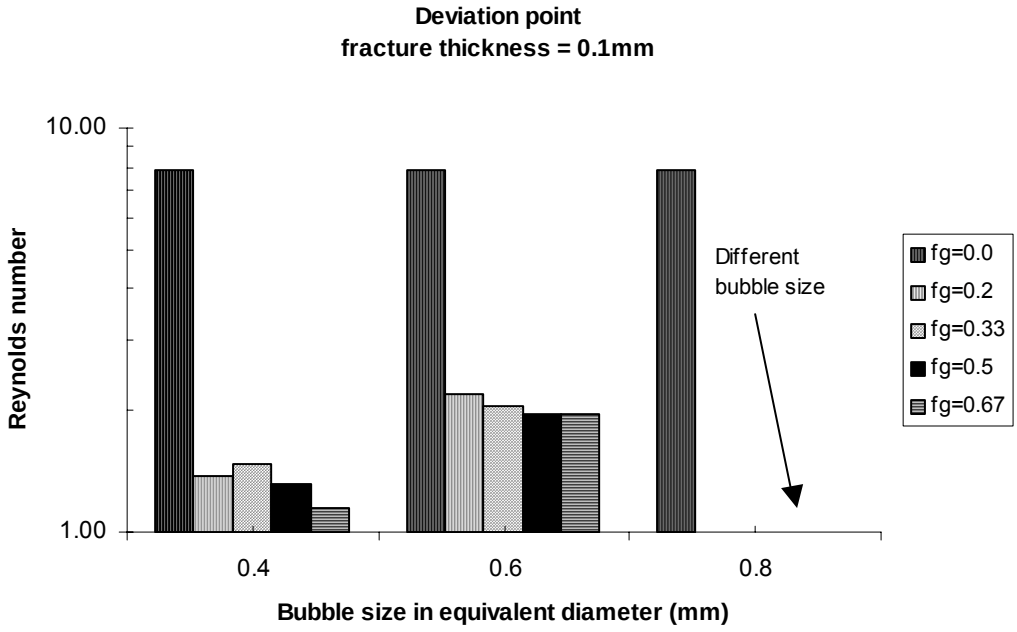

Fig. 7. Deviation point for fracture thickness=0.1mm

Figure 8 shows the effect of fractional flow on apparent viscosity. With the increase of gas fractional flow or foam quality, the number of lamellae per unit length increases, which causes the increase of apparent viscosity.

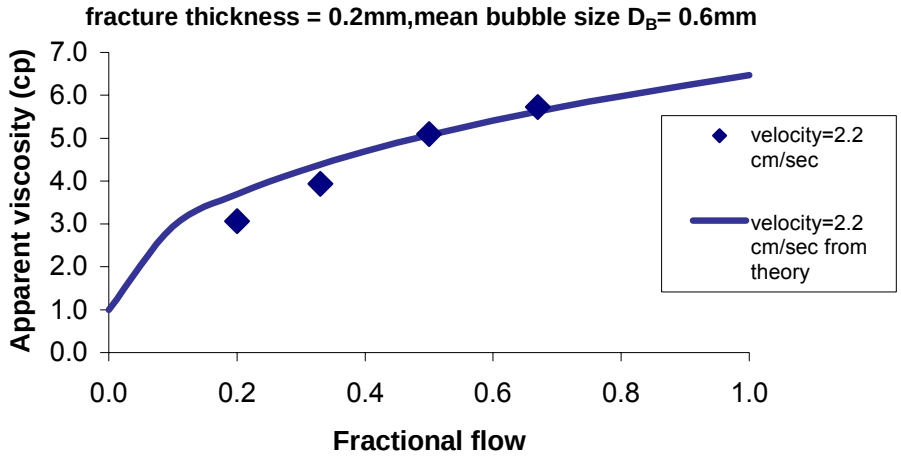

Fig. 8. Effect of fractional flow on apparent viscosity

The lamellae per unit length decrease with the increase of bubble size. So the apparent viscosity decreases when the bubble size increases as in figure 9.

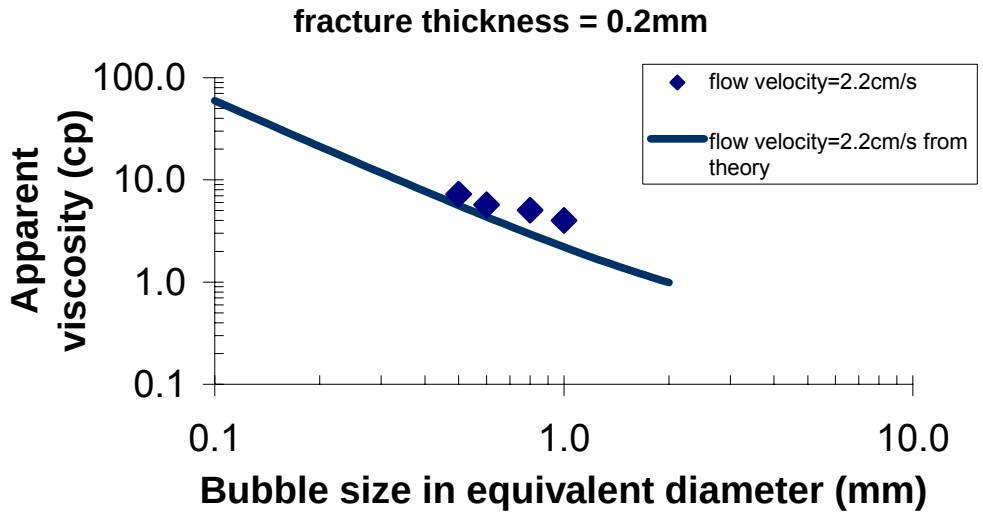

Fig 9. Effect of bubble size on apparent viscosity

Figure 10 shows the effect of fracture thickness on the apparent viscosity. Because the lamellae per unit length increase with fracture thickness, the apparent viscosity is larger with bigger fracture thickness. This feature is important in the foam application. Because the apparent viscosity in high permeability region (bigger fracture thickness) is larger than in the low

permeability region (smaller fracture thickness), foam can block the fluids flow in high permeability region and divert it into low permeability region.

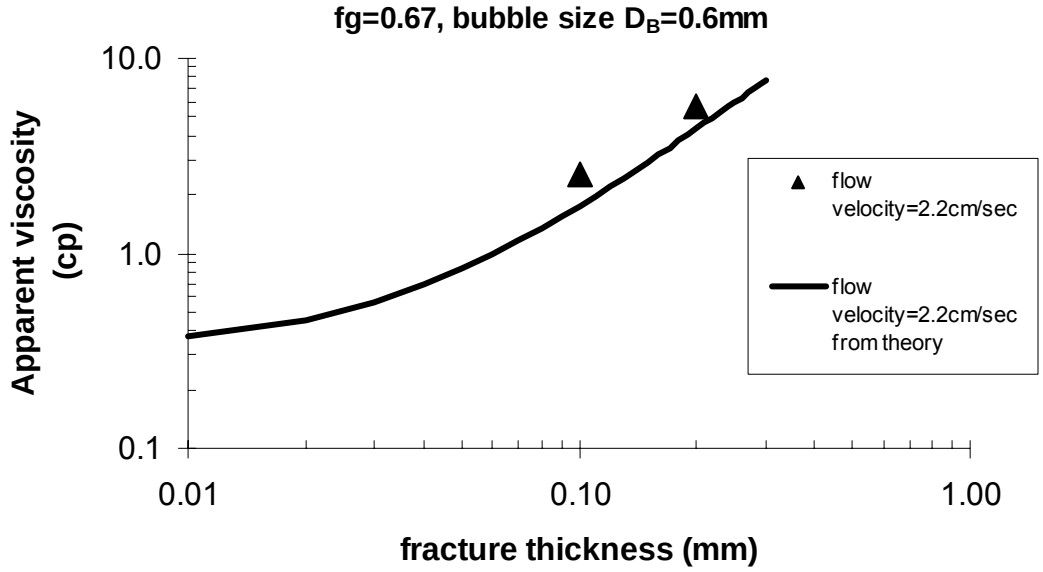

Fig. 10. Effect of fracture thickness on apparent viscosity

Conclusions

At the experimental conditions stated above, when Reynolds number is less than the deviation value and mean bubble sizes stay the same as that generated in the foam generator, the following conclusions can be made for the foam flow through a smooth, uniform fracture:

1. The foam texture (a measure of the bubble volume) is a key parameter in determining the number of lamellae per unit length, which is the main factor affecting the foam viscosity in smooth uniform fractures.
2. The apparent viscosity is the sum of two contributions: that resulting from slugs of liquid between bubbles and the resistance to deforming the interface when a bubble passes through a fracture. The surface tension gradient contribution does not appear to be significant in our experiments.

Future work

In the next step, we will change our model from homogeneous parallel plates to heterogeneous facture to investigate the diversion effect of foam. From the above theory and experimental results, it is expected that the distribution will be improved over liquid only injection because the apparent viscosity of foam is greater in thicker fractures.

Task 4: Simulation of Field-Scale Processes

Discovery and development of naturally fractured reservoirs has increased dramatically during the past 15 years. Many oil reservoirs in the United States are naturally fractured. More than 20 billion barrels of oil remain in large Texas fields such as the Spraberry, Yates, and Ellenberger fields yet relatively little research has been done on the use and modeling of EOR methods for these large fields and very little success has been achieved to date in increasing the oil production from these complex reservoirs.

Oil production from naturally fractured reservoirs sometimes occurs by spontaneous water imbibition and oil expulsion from the matrix rock into the fracture network. Unfortunately many fractured reservoirs exhibit a matrix wettability state that is not sufficiently water wet to favor water imbibition. There have been some recent attempts to alter the matrix wettability by using either chemicals (Spinler *et al.*, 2000; Chen *et al*, 2000; Yang and Waldleigh, 2000; Babadagli, 2001) or steam (Snell *et al.* 1999; Al-Hadhrami *et al*., 2000; Graue *et al*., 2001; Tang and Kovscek, 2002). Some laboratory experiments have been done to investigate the use of surfactants in fractured chalk.

The objective of this task was to adapt the existing chemical reservoir simulator UTCHEM to model wettability alteration in oil reservoirs due to surfactant injection.

Wettability is a very important parameter controlling the capillary pressure. However, the wettability is not an explicit parameter in the flow equations but its effects should be reflected by the changes in capillary pressure and relative permeability curves. Using table look up option UTCHEM can now read multiple tables for relative permeability and capillary pressure to represent different wetting conditions. At the initial condition, the reservoir may be taken as oil-wet or mixed-wet and input tables of saturation and relative permeability and capillary pressure for these conditions are used. The alteration of wettability with time is modeled by injecting surfactant solution. Once the surfactant concentration in each gridblock reaches a specified input value, corresponding to the laboratory value at which wettability changes, the relative permeabilities and capillary pressure for water-wet conditions are used.

The implementation in UTCHEM involved the modification of existing subroutines and addition of new routine. For instance, in the main program (AAMAIN), a new conditional cycle was included to allow the user to choose whether changes in capillary pressure and relative permeabilities after the surfactant injection should be taken into account or not. The user decides to use the new utility by including a new variable in the input data called ITAB. When the value of ITAB is equal to 1 then the changes in capillary pressure and relative permeabilities, due to variations in wettability, are simulated. A new subroutine called KRPC was created and called from the main program. This subroutine reads the data points of relative permeabilities and capillary pressures versus water saturation and interpolates the data for other saturation values. Surfactant concentration in each gridblock is compared to the input value of WETI. The

WETI parameter represents the value at which a change from either oil-wet or mixed-wet to more water-wet happens in each gridblock. When the surfactant concentration is greater than WETI, the tables of capillary pressure and relative permeabilities for a water-wet system are used. In the remaining cases with surfactant concentrations lower or equal to WETI, the tables representing the initial wetting state of oil-wet or mixed-wet are used.

Modifications were also made in subroutine INOUT by calling two new subroutines: IUTIL and TABLE. The first routine is used just for initialization of some variables; the second one calls some other utility routines (LOOKUP, NUMBER, SPLINE, PRTTAB, PRTSPL, ETC). These subroutines allow interpolating and extrapolating the relative permeability and capillary pressure data in each table. Multiple tables can be read for each property. The switching data of relative permeability and capillary pressure tables between two conditions, water-wet and mixed-wet, are performed by giving two sets of tables for each property representing different wetting states. The user provides the tabular data as the input data.

The subroutine RPERM0 is called from subroutine TIME0 in the main program and its purpose is to calculate relative permeabilities and capillary pressure at the start of the simulation (at time zero). A new section was included in subroutine RPERM0 to initialize these properties assuming mixed-wet or oil-wet conditions. The initialization is done by reading the tables corresponding to the initial condition of either mixed-wet or oil-wet through the table lookup subroutine.

Several two-dimensional dual porosity/dual permeability simulations were set up to validate the implementation of the table look up option in a naturally fractured reservoir model. Very small gridblock with high permeability and porosity are representing the fracture and large gridblocks with low permeability and high porosity representing the matrix blocks. Injection and production wells are located and perforated in the fracture gridblock. Also, sensitivities to some parameters were tested. These simulations show that UTCHEM is now capable of handling changes in wettability. The results were consistent with the observation that additional oil can be recovered from oil-wet cores when surfactant solution changes the wettability and imbibes into the cores.

Simulation Results

Two-dimensional dual permeability/dual porosity fracture simulations were performed to validate the implementation of the relative permeability and capillary pressure for multiple wetting conditions and wettability alteration due to surfactant injection. The first series of simulations were performed with the injected surfactant modeled as an agent to alter the wettability without reducing the interfacial tension or mobilizing oil. The second series of the simulations were performed with the injected surfactant modeled as an agent to reduce interfacial tension and mobilize the oil with no effect on wettability.

Simulation Results of Series I

Base case simulation

The base case simulation was set up to verify the implementation of the table look up routine. Only one set of tabular data for relative permeability and capillary pressure was used. The relative permeability and capillary pressure data are shown in Figs. 4.1 and 4.2. These data correspond to an oil wet reservoir condition. An aqueous solution with 1 vol% surfactant concentration was injected at a rate of 50 ft^3/day for a period of 400 days that corresponds to about 0.6 pore volumes. In this simulation, the mechanism for oil recovery is due to wettability alteration and capillary imbibition. The effects of surfactant phase behavior and interfacial tension reduction were not modeled.

Core experiments using Yates reservoir core indicated that the injection of dilute surfactants resulted in an improved oil recovery compared to injection of brine (Yang and Waldleigh, 2000). As part of Task 2 of this project numerous wettability alteration experiments were done with surfactant solutions and Yates crude oil at Rice University. The simulations described here are also based on the properties of Yates reservoir. The Yates field was discovered in 1926 and is a massive naturally fractured carbonate reservoir located at the southern tip of the Central Basin platform in Permian Basin of west Texas (Chen *et al*., 2001). The matrix permeability ranged from 50 to 250 md and average fracture permeability is 1000 md. The matrix porosity ranged from 15% to 22%.

Oil saturation and surfactant concentration distributions after 400 days of surfactant injection are shown in Figs. 4.3 and 4.4. The cumulative oil recovery as a function of time is shown in Fig. 4.8 with about 4% oil recovered at the end of the simulation.

Base case simulation with wettability alteration

In this simulation, the capability of taking into the account the change in wettability by using a different set of relative permeability and capillary pressure data is tested. The simulation data are the same as those used in the base case discussed above with the exception that two sets of relative permeabilities and two sets of capillary pressure tables were used. One set corresponds to the initial oil wet state of the reservoir and the second set corresponds to a strongly water-wet condition. Figures 4.1 and 4.5 show the relative permeabilities for the two wetting conditions. The capillary pressure for the water-wet case was assumed to be zero and the capillary pressure for the oil-wet case is plotted in Figure 4.2. Figures 4.1 and 4.5 illustrate one traditional indicator of wettability, the crossover saturation, where $k_{ro} = k_{rw}$. For the water-wet condition, the crossover is located at water saturation higher than 50 percent while for the oil-wet condition it is located at water saturation less than 50 percent.

The injection well was set to inject 50 ft^3/day of water containing 1 vol% surfactant solution for a period of 400 days. A surfactant concentration of 0.1 percent was used as the criterion to change the wettability to water-wet and thus use water-wet relative permeability and capillary pressure data. Oil saturation

and surfactant concentration distributions were monitored with time to see how the changes in wettability affect the swept volume and the oil recovery. The areal distributions of oil saturation and surfactant concentration at the end of the simulation (400 days) are plotted in Figs. 4.6 and 4.7. The oil saturation distribution in the case with wettability alteration shown in Fig. 4.6 reveals that a better sweep was achieved compared to the case with no wettability changes. This happened when changes in wettability, from an oil-wet condition to a water-wet condition, occurred and the simulator adjusted the relative permeability and the capillary pressure by table look up. For the case of no changes in wettability, the oil saturation was reduced only in the cells near the injector whereas high oil saturations remained everywhere else.

The surfactant concentration distribution was also compatible with the oil saturation distribution. The surfactant concentration is high for several gridblocks when the changes in wettability are considered as shown in Fig. 4.7 but remained low for the most of the gridblocks in the case without the change in wettability (Fig. 4.4).

Cumulative oil recovery is shown in Fig. 4.8. The oil recovery is higher in the case where changes in wettability took place compared to the base case simulation where the wettability remained unchanged. This is congruent with the improved swept volume as observed in the oil saturation distribution.

A series of sensitivity simulations were made to explore the effect of parameters such as initial oil saturation in the matrix blocks, relative permeability curves, capillary pressure, and initial wetting state on oil recovery.

Initial oil saturation

To investigate the effect of initial oil saturation in the rock matrix when the wettability is altered, several simulations were performed with different initial oil saturations. The initial oil saturation was 0.7 in the simulation discussed in the previous section. Three cases were compared corresponding to initial oil saturations of 0.3, 0.5, and 0.7. Figure 4.9 compares the oil recovery for these cases. As would be expected, the oil recovery is higher where the initial oil volume is higher.

Relative permeability

To see the effect of relative permeability data on the oil recovery, different relative permeability data were used for both oil and water phases for the initial wetting conditions of oil wet. With the exception of the relative permeability tables for the initial wetting state, the rest of the input was the same as the base case with wettability modifications. The water-wet relative permeabilities were the same as those in the base case. The relative permeabilities are compared with those used in the base case labeled as original in Fig 4.10. Figure 4.11 compares the cumulative oil recovery for these simulations. The oil recovery is

consistent with the relative permeability data since the higher the oil relative permeability the higher the oil recovery.

Capillary pressure

Another input parameter that was investigated was the capillary pressure for the water-wet condition. The water-wet capillary pressure was zero for the base case simulation with wettability changes. Simulations were performed with different capillary pressure data for the water-wet condition. Capillary pressure data are plotted in Fig. 4.12. Figure 4.13 compares the cumulative oil recovery for the simulations with different capillary pressure data. The oil recovery was fairly insensitive to the capillary pressure data used after the wettability alteration from originally oil wet to water-wet conditions.

Mixed-wet relative permeability and capillary pressure

The purpose here was to investigate the effect of original wettability distinguished by petrophysical properties such as relative permeability and capillary pressure on the oil recovery. Both relative permeability and capillary pressure data were modified from those used in the base case from the oil wet to mixed wet. Figure 4.14 compares the relative permeabilities for this case and those used in the base case simulation. It can be seen that as the wettability becomes more oil-wet, the relative permeability of this phase decreases. The same happens with the water. Capillary pressures for the mixed-wet condition are shown in Fig 4.15.

Figure 4.16 shows the oil recovery is about 20% at the end of 400 days. For the purpose of comparison, another simulation was performed assuming the same initial wettability of mixed wet, but no alteration in wetting state. Figure 4.16 compares the oil recoveries and once again oil recovery is increased when the wettability was altered from initially mixed-wet to water-wet.

Simulation Results of Series II

Base case simulation

Two-dimensional dual porosity/dual permeability simulations were performed to investigate the role of surfactant in reducing interfacial tension and mobilizing oil and the role of gravity in a naturally fractured reservoir. The simulation domain is 504 ft long and 120 ft thick (vertical dimension). Gridblocks with a width of 1 ft, a permeability of 1000 md and a porosity of 2% were used to represent the fractures between matrix blocks. Matrix blocks are 100 ft square with a permeability of 50 md and a porosity of 30%. Each matrix block was subgridded to 20 ft blocks.

The bottom of the reservoir represents the original oil water contact (OOWC) where layers 7 through 12 are saturated with both oil and water. Layer

6 represents the oil water contact (OWC) where layers 1 through 6 are saturated with oil at residual water saturation (Fig. 4.17). The reservoir and fluid properties are given in Table 4.2. The relative permeability used represents an oil wet/mixed-wet condition. A 3 vol% surfactant slug was injected for a period of 300 days followed by water injection for another 2700 days. The initial and injected salinity is 0.174 meq/ml. Injection well is located in fracture gridblock of 6 and completed in layers 8 through 11. The Production well is located in the fracture gridblock of 24 and is completed in the oil zone in layers 2 through 5. Both injection and production wells are under constant rate of 50 ft^3/d.

The effluent concentration is given in Fig. 4.18 with a peak concentration of about one half of the injected value of 0.03 volume fraction. Figure 4.19 shows the cumulative oil recovery as a fraction of original oil in place (OOIP) with about 38% recovery at the end of the flood. The oil saturation distributions at several times during the flood are given in Figs. 4.20 through 4.23. The combination of viscous forces due to the water injection and reduced capillary forces due to the lower interfacial tension resulting from the injection of surfactant pushes the oil towards the producer. Oil is initially produced from the oil zone on the top (Fig. 4.20). At 900 days the oil saturation is reduced from 0.7 to nearly 0.45 in the gridblocks between the wells (Fig. 4.22). The oil saturation nearly at the end of the flood at 2700 days is given in Fig. 4.23. The oil saturation is close to 30% in all the layers with the exception of the top layer that was not swept with the injected fluid.

The distributions of total surfactant concentration at several times during the flood are given in Figs. 4.24 through 4.28. The concentration of surfactant is at the injected value of 3% near the injection well (Figs. 4.23 and 4.24) and becomes diluted due to the water injection following the chemical slug (Figs. 4.26 and 4.27). Very little surfactant is left in the reservoir at the end of the flood (Fig. 4.28).

For the purpose of comparison, a waterflood simulation of the same case was performed where water was injected at the same rate of 50 ft^3/day for a period of 3000 days. Figure 4.29 gives the oil recovery of about 35% at the end of the waterflood compared to the value of 38% for the surfactant flood. The distributions of oil saturation at different waterflooding times are given in Figs. 4.30 through 4.32. Oil initially migrated upward due to the buoyancy and gets produced. The oil saturation in the gridblocks between the wells is about 33% with the exception of those in the top layer.

Several sensitivity simulations were performed to investigate the significant of parameters such as matrix gridblock size, matrix permeability, initial water saturation in matrix blocks, vertical to horizontal permeability ratio, injection/production rate, and the amount of surfactant injected (slug size). Table 4.3 lists the sensitivity parameters for each case. A comparison of cumulative oil recovery is given in Fig. 4.33. The cumulative oil recovery increased from 38% to about 44% by reducing the gridblock size in the horizontal direction from 20 ft to 10 ft. Additional oil recovery was obtained when the vertical to horizontal permeability was reduced to reduce the cross flow. The combination of the

reduced gridblock size (less reservoir volume and more throughput of surfactant), reduced cross flow, and higher initial oil saturation of the simulation run grav-6 caused an increase of about 12% in cumulative oil recovery compared to the base case value of 38%.

Summary and Conclusions

A new capability has been added to UTCHEM oil reservoir simulator to model and simulate the different wetting conditions and wettability alteration as a result of the surfactant injection in naturally fractured reservoirs. Using table look up option UTCHEM can now read multiple tables for relative permeability and capillary pressure to represent different wetting conditions. At the initial condition, the reservoir may be taken as oil-wet or mixed-wet and input tables of saturation and relative permeability and capillary pressure for these conditions are used. The alteration of wettability with time is modeled by injecting surfactant solution. Once the surfactant concentration in each gridblock reaches a specified input value, corresponding to the laboratory value at which wettability changes, the relative permeabilities and capillary pressure for water-wet conditions are used.

Several simulations were performed to validate the implementation of the table look up option for the relative permeability and capillary pressure data and the wettability alteration routines and to investigate the significance of parameters such relative permeabilities, capillary pressures, matrix permeability, initial oil saturation, vertical to horizontal permeability ratio on the performance of surfactant floods in naturally fractured reservoir.

REFERENCES-TASK 4

Al-Hadhrami, and Blunt, M.J (2000)," Thermally Induced Wettability Alteration to Improve Oil Recovery in Fractured Reservoirs," SPE paper 59289 presented at the SPE/DOE Improved Oil recovery Symposium, Tulsa, Oklahoma, April 3-5.

Babadagli, T. (2001) “Scaling of Cocurrent and Countercurrent Capillary Imbibition for Surfactant and Polymer Injection in Naturally Fractured Reservoirs,” *SPE J*, Dec., 465-478.

Chen, H.L., Lucas, L.R., Nogaret, L.A.D., Yang, H.D., and Kenyon, D.E. (2000) “Laboratory Monitoring of Surfactant Imbibition Using Computerized Tomography,” SPE 59006 presented at the SPE/DOE IOR Symp., April 2-5, Tulsa, OK.

Graue A., Bogno T., Baldwin, B.A., and Spinler, E.A. (2001). "Wettability Effects on Capillary Oil-Recovery Mechanisms in Fractured Reservoirs," SPE Reservoir Evaluation & Engineering, Dec. 2001, 455-466.

Spinler, E.A. and Baldwin, B.A. (2000) “Surfactant Induced Wettability Alteration in Porous Media,” in *Surfactants, Fundamentals and Applications in the*

Petroleum Industry, Schramm, L.L., ed, Cambridge University Press, Cambridge, 159-202.

Tang, G., and Kovscek, A.R. (2002) "Experimental Study of Heavy Oil Production from Diatomite by Water Imbibition at Elevated Temperature," SPE 75132 presented at the SPE/DOE IOR Symposium, Tulsa, Oklahoma., April 13-17.

Yang, H.D. and E.E. Wadleigh (2000). "Dilute Surfactant IOR-Design Improvement for Massive, Fractured Carbonate Applications," SPE 59009 presented at the SPE International Petroleum Conference and Exhibition in Mexico, Villahermosa, Mexico, Feb. 1-3.

Table 4.1 Summary of Input Data for Series I Simulation

Parameter	**Matrix**	**Fracture**
Permeability (md)	50	1000
Porosity	0.3	0.02
Initial water saturation	0.3	1.0
Water viscosity (cp)	0.82	
Oil viscosity (cp)	6.73	
Water injection rate (ft^3/d)	50	
Production well flowing BHP (psia)	300	

Table 4.2 Reservoir and Fluid Properties (Simulation Series II)

Parameter	**Matrix**	**Fracture**
Permeability	50 md	1000 md
Porosity	0.3	0.02
Initial water saturation in layers 1-6	0.3	0.0
Initial water saturation in layers 7-12	0.6	1.0
Number of gridblocks	29 x 1 x 12	
Vertical to Horizontal permeability	1	
Water viscosity	0.5 cp	
Oil viscosity	2 cp	
Water injection rate in layers 8-11	50 ft^3/d	
Production rate in layers 2-5	50 ft^3/d	
Residual water saturation	0.3	
Residual oil saturation	0.30	
Initial and injected Salt concentration	0.174 meq/ml	
Injected surfactant concentration	3 vol%	
Surfactant slug size	300 days	

Table 4.3 Variables for Sensitivity Simulations

Variable	**Grav-5 (Base Case)**	**Grav-6**	**Grav-7**	**Grav-8**	**Grav-9**
Gridblock size, ft	x = 20 z = 10	**x =10** **z = 5**	x =10 z = 5	x =10 z = 5	x =10 z = 5
K_v/K_h	1	**0.1**	0.1	0.1	0.1
S_{wi} in layers 6-12	0.6	**0.5**	0.5	0.5	0.5
Inj./prod. rate, ft_3/d	50	50	**25**	**25**	50
Matrix perm., md	50	50	50	**10**	50
Surf. slug size, days	300	300	300	300	**150**

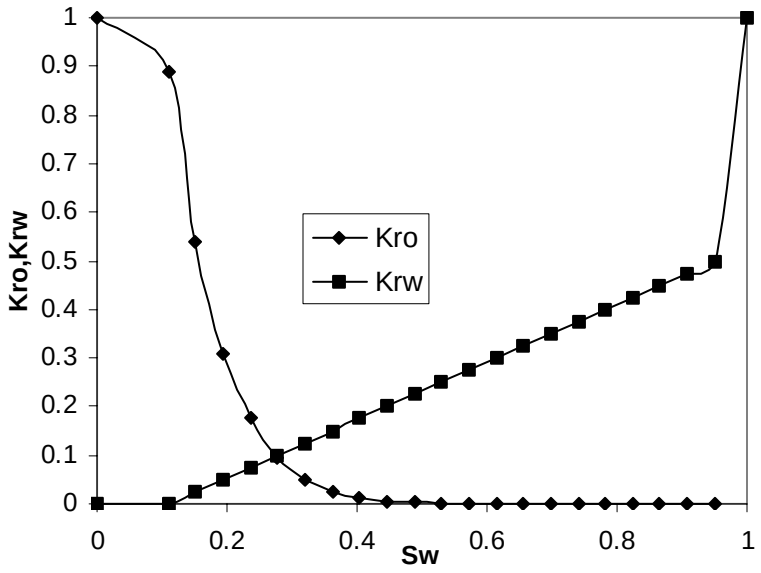

Figure 4.1 Relative permeability for the oil-wet condition

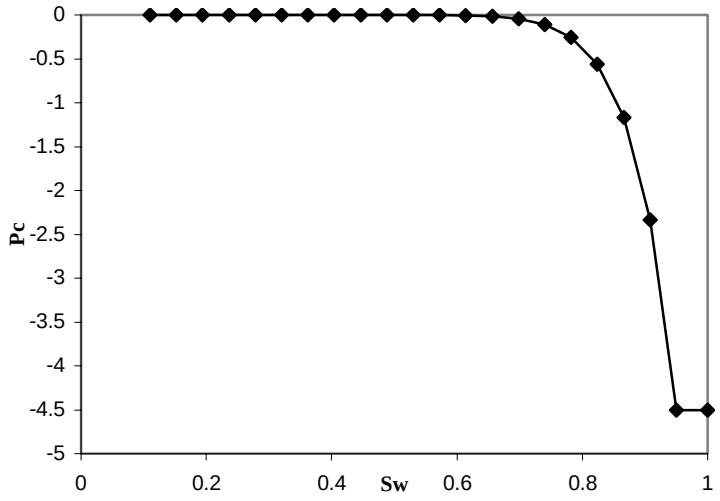

Figure 4.2 Capillary pressure for the oil-wet condition

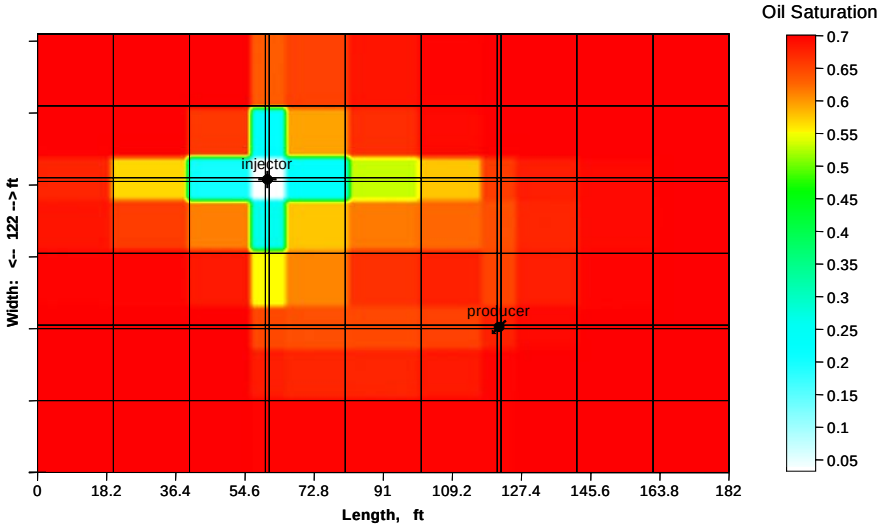

Figure 4.3 Oil saturation at 400 days for the base simulation case

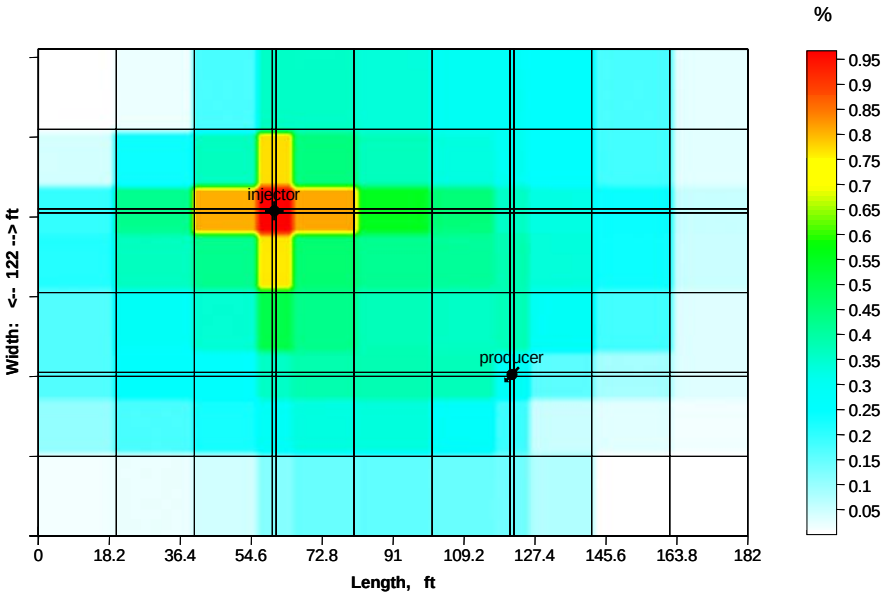

Figure 4.4 Surfactant concentration at 400 days for the base simulation case

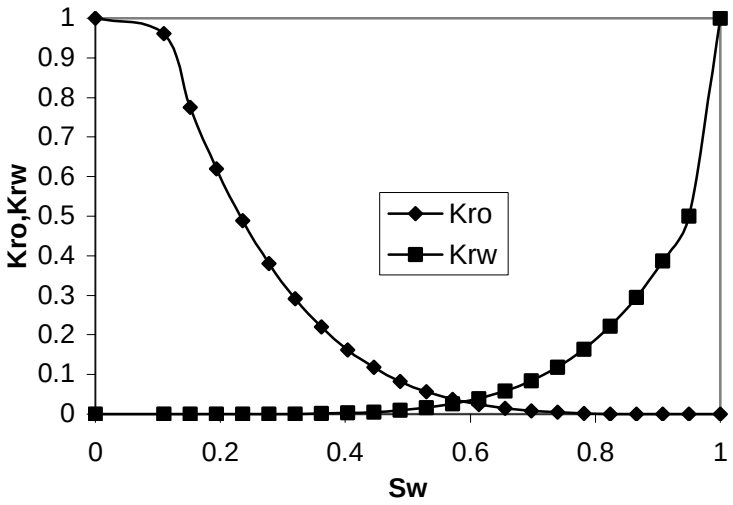

Figure 4.5 Relative permeability curves for the water wet condition

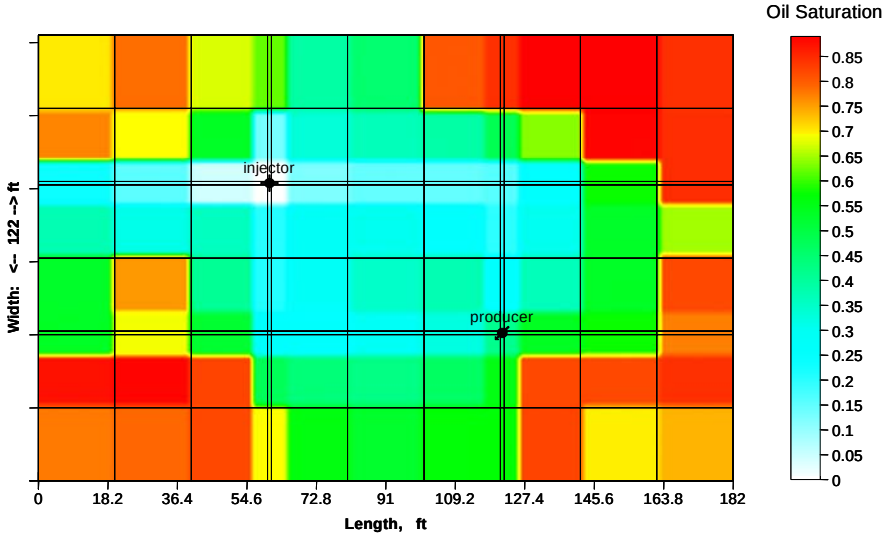

Figure 4.6 Oil saturation at 400 days for the base case simulation with changes in wettability

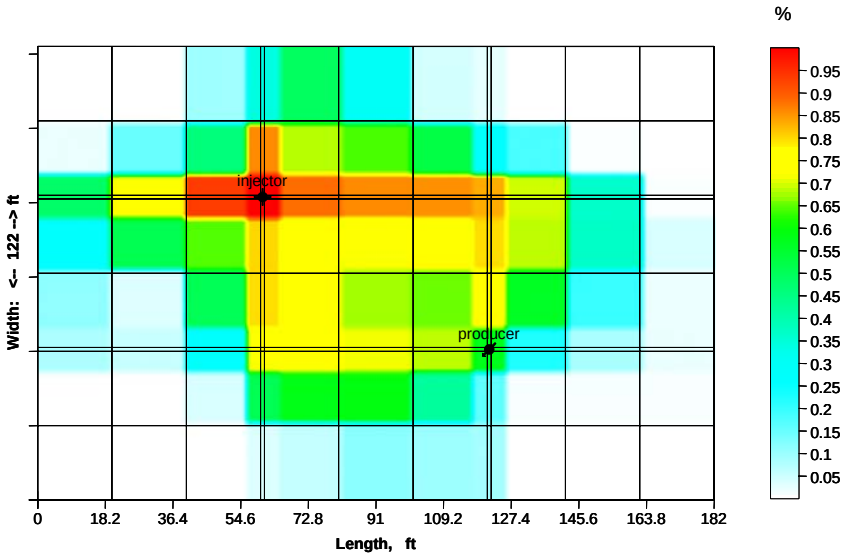

Fig. 4.7 Surfactant concentration at 400 days for the base case with changes in wettability

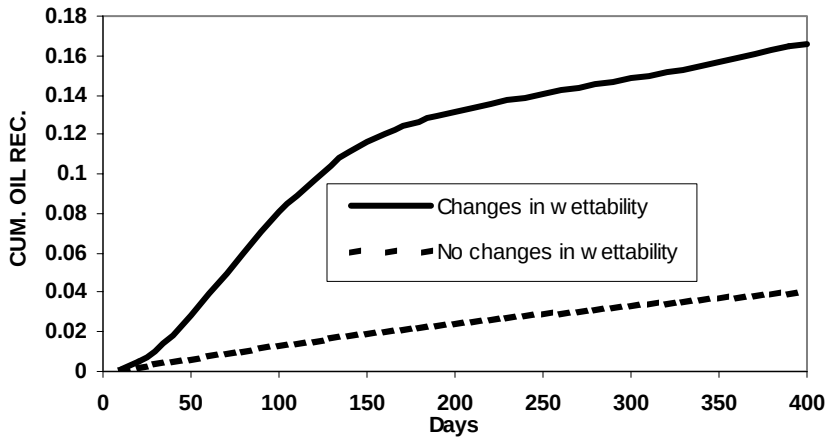

Figure 4.8 Effect of wettability alteration on oil recovery

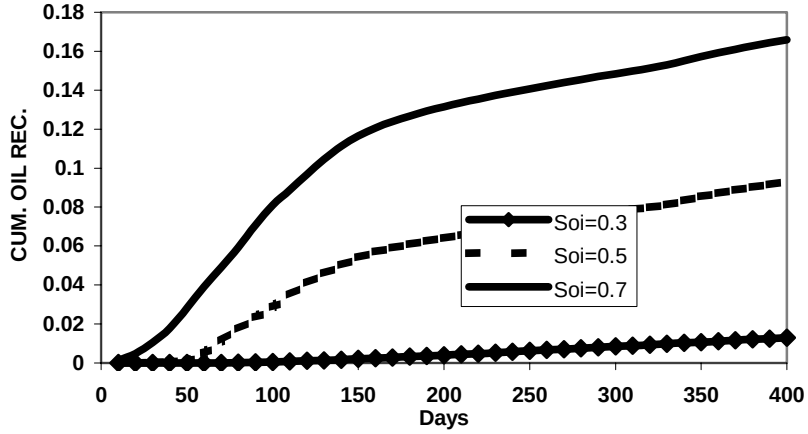

Figure 4.9 Oil recovery sensitivity to initial oil saturation in the matrix blocks

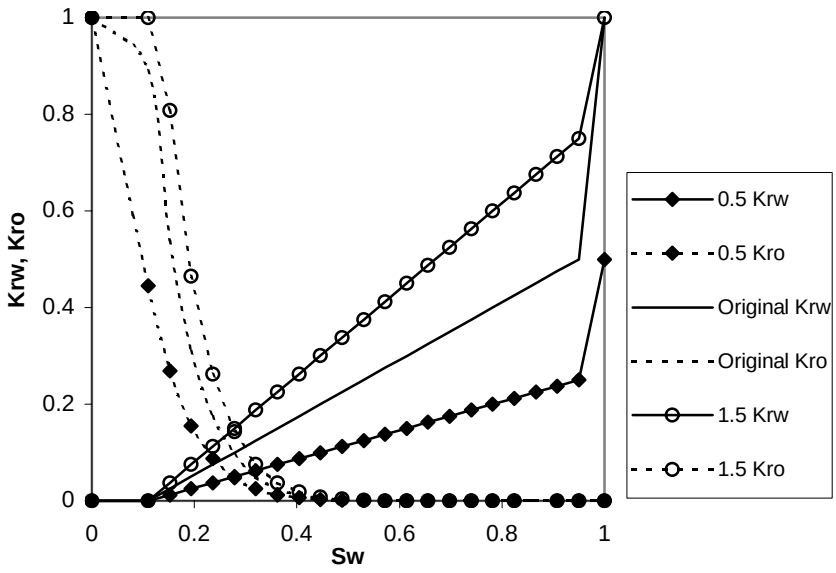

Figure 4.10 Original and modified relative permeabilities of the oil-wet condition

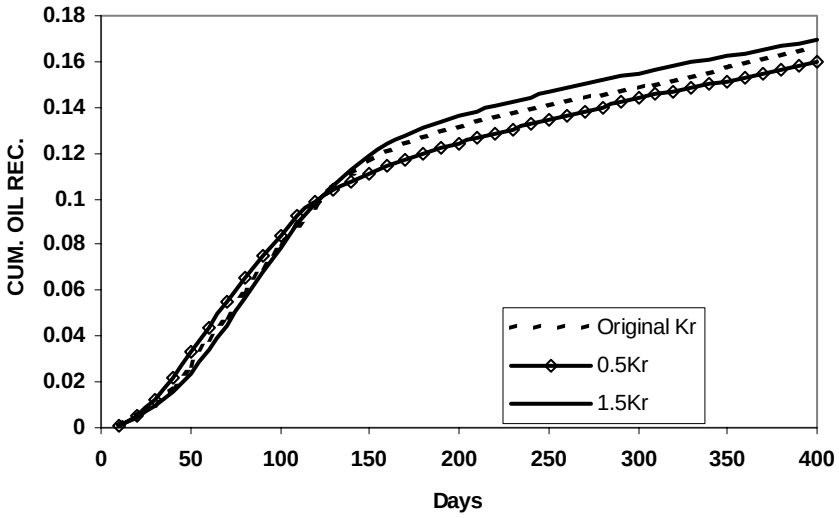

Figure 4.11 Oil recovery sensitivity to oil-wet relative permeabilities

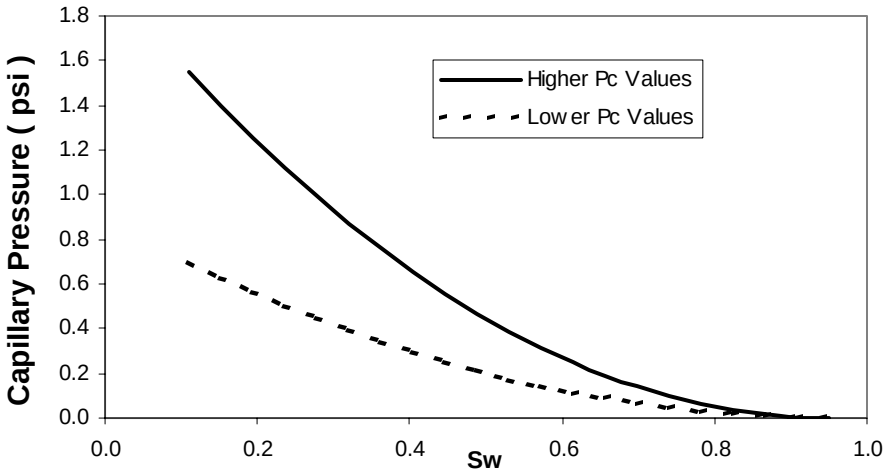

Figure 4.12 Modified water-wet capillary pressures

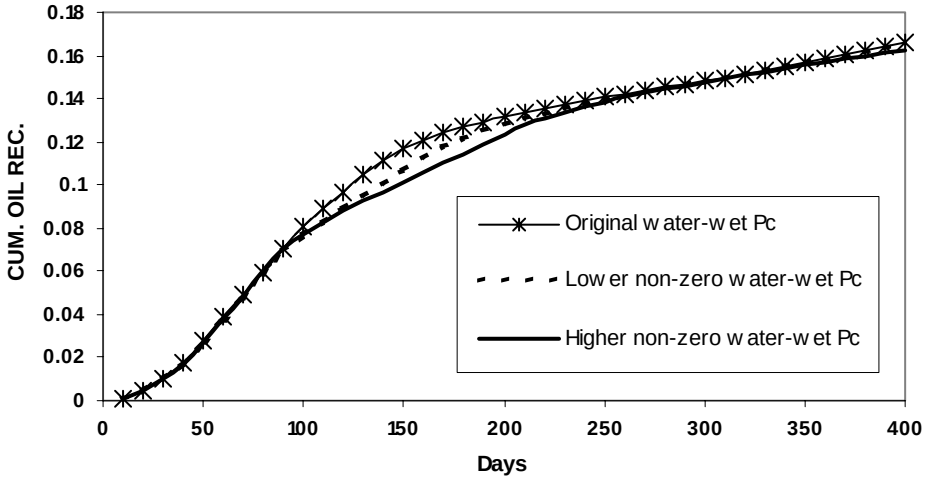

Figure 4.13 Oil recovery sensitivity to changes in the water wet capillary pressure

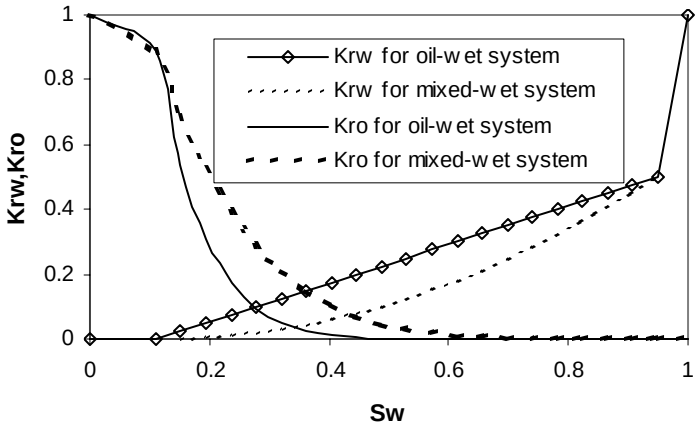

Figure 4.14 Relative permeability for the oil-wet system and the mixed-wet system

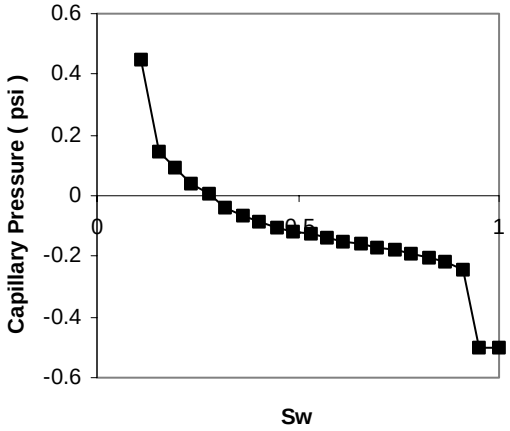

Figure 4.15 Capillary pressure for the mixed-wet system

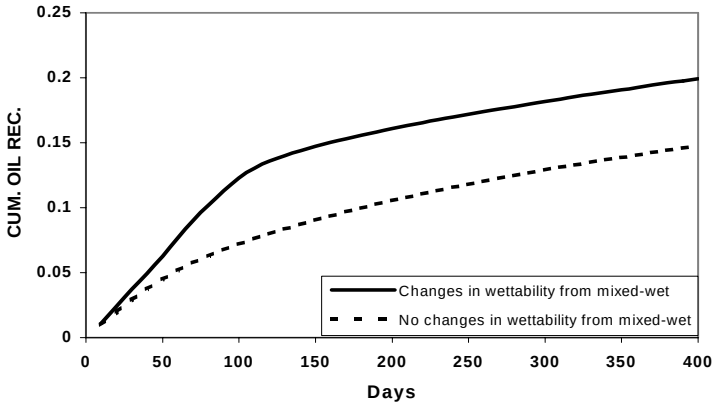

Figure 4.16 Oil recovery for an initially mixed-wet system

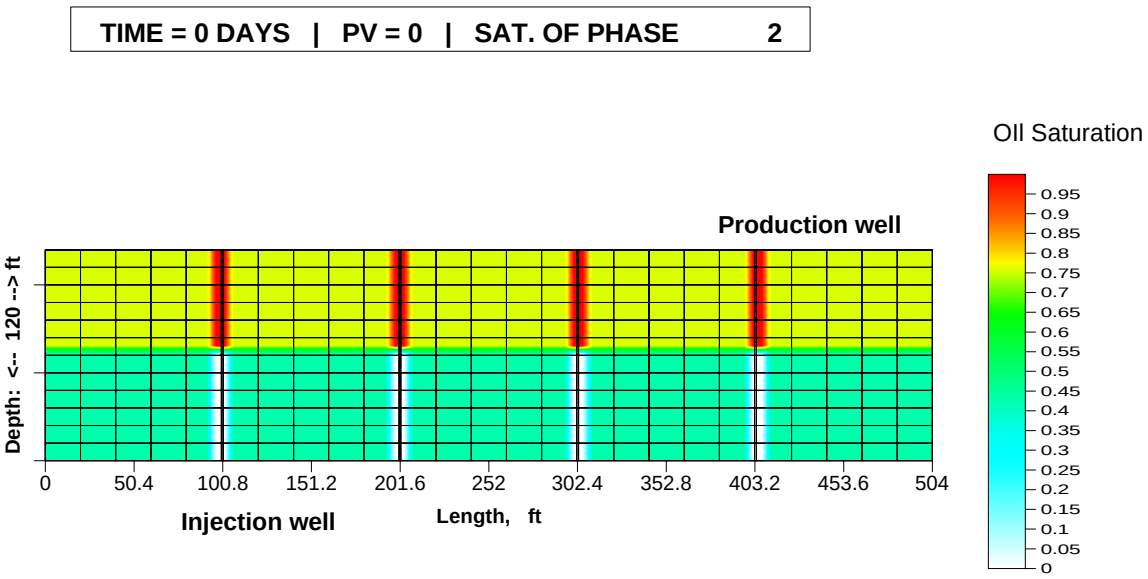

Fig. 4.17 Initial oil saturation in matrix and fracture gridblocks for the Base Case surfactant simulation

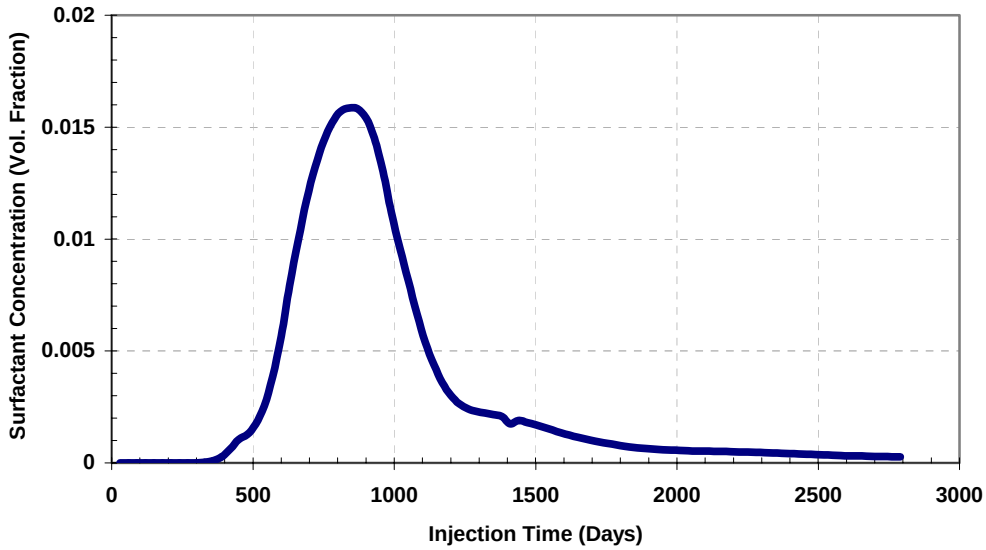

Fig. 4.18 Surfactant concentration at the production well

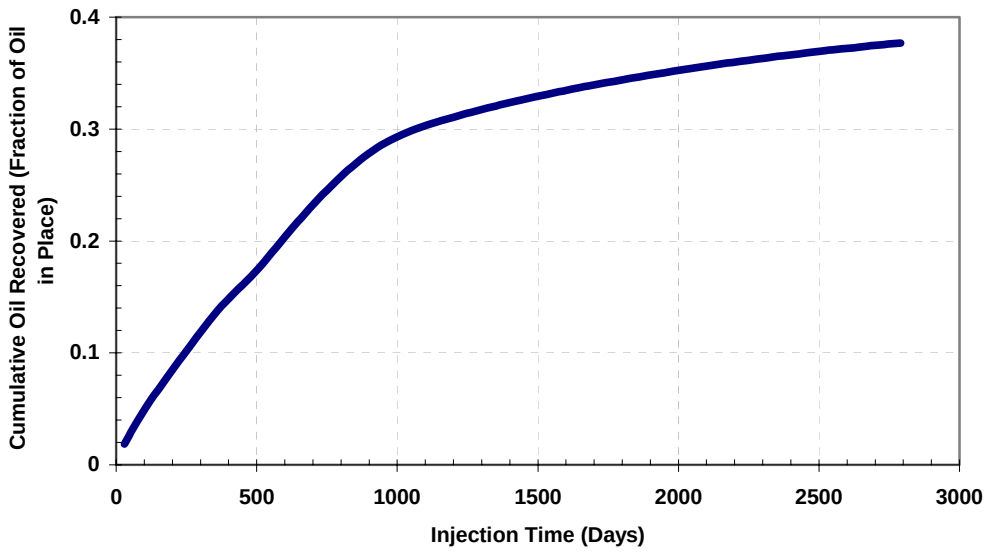

Fig.4.19 Cumulative oil recovered during the surfactant flood of the Base Case

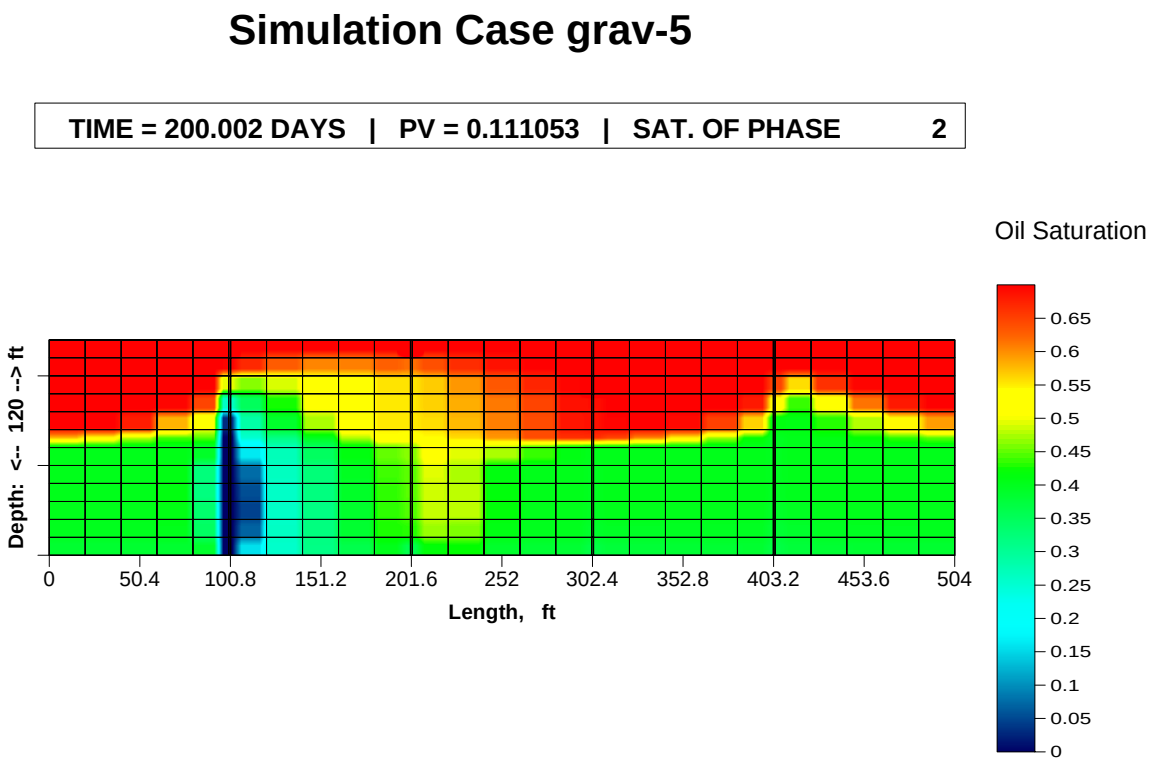

Fig. 4.20 Oil saturation distribution at 200 days of surfactant injection

Simulation Case grav-5

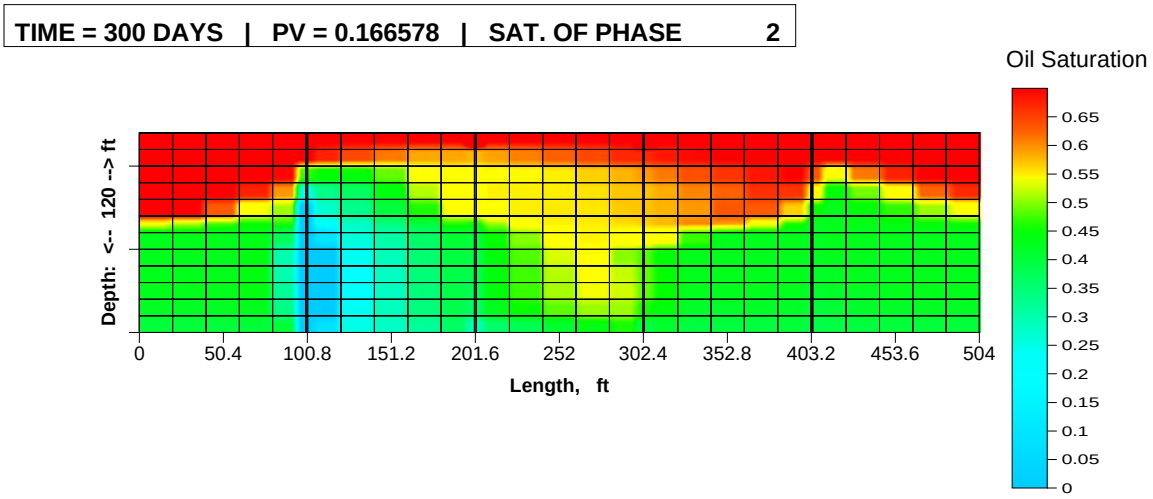

Fig. 4.21 Oil saturation distribution at the end of surfactant injection of 300 days

Simulation Case grav-5

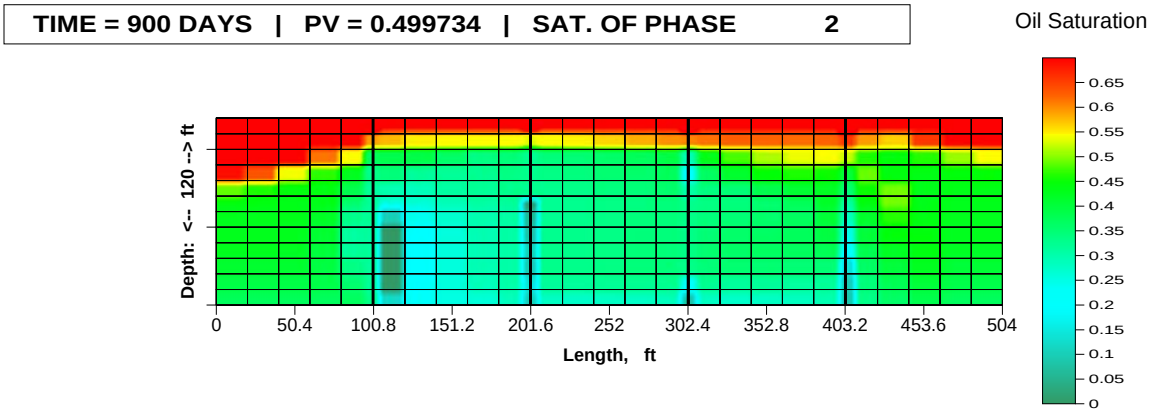

Fig. 4.22 Oil saturation distribution during water injection at time 900 days

Simulation Case grav-5

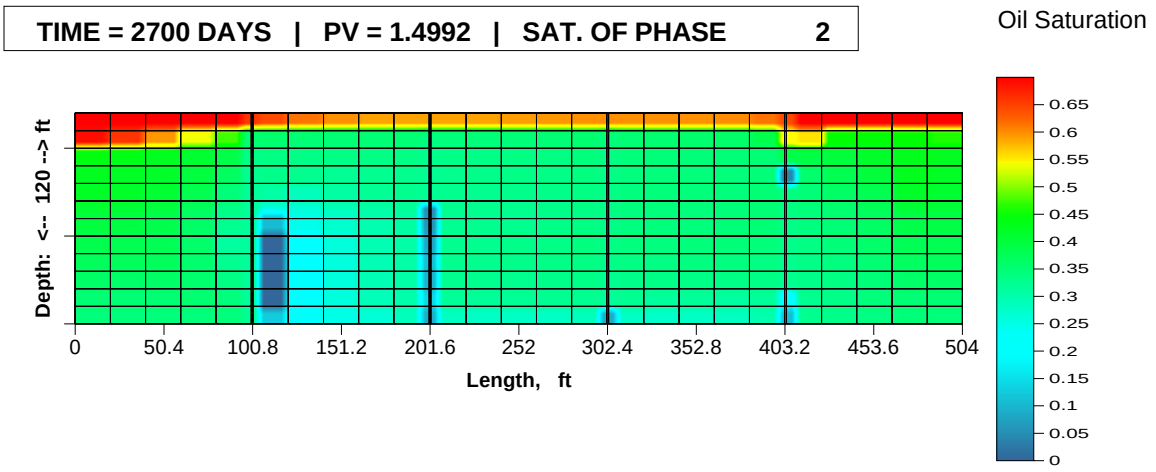

Fig. 4.23 Oil saturation distribution at the end of the flood

Simulation Case grav-5

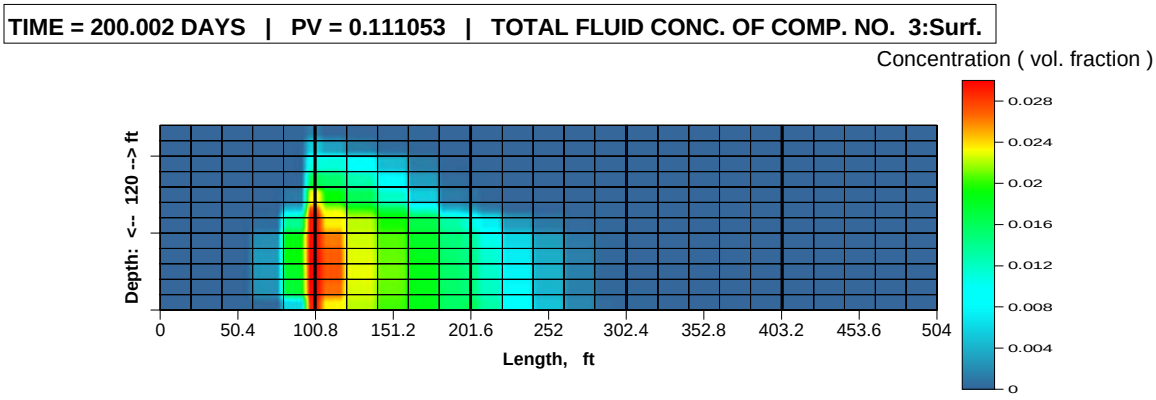

Fig. 4.24 Surfactant concentration distribution during surfactant injection

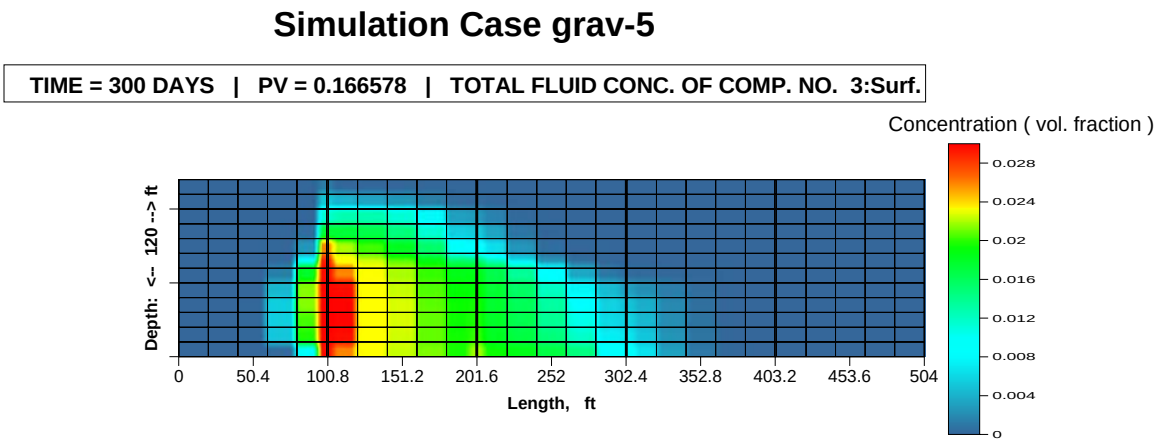

Fig. 4.25 Distribution of surfactant concentration at the end of surfactant injection

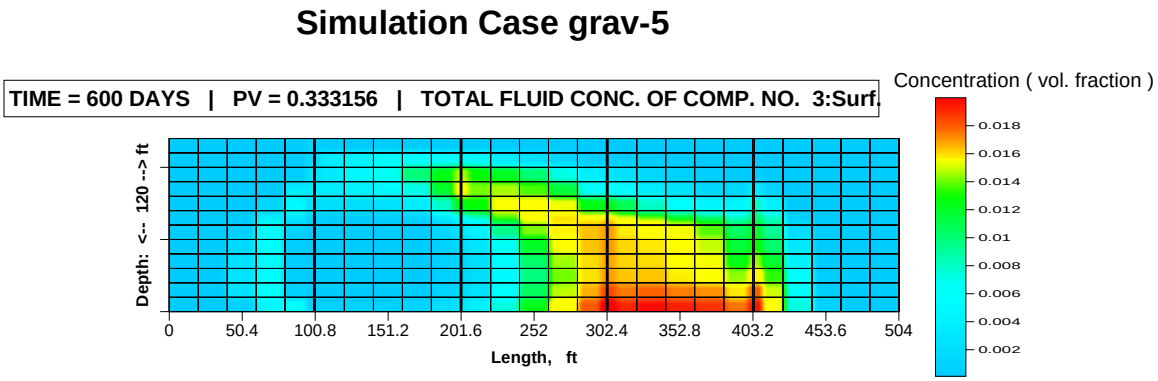

Fig. 4.26 Distribution of surfactant concentration during water injection at 600 days

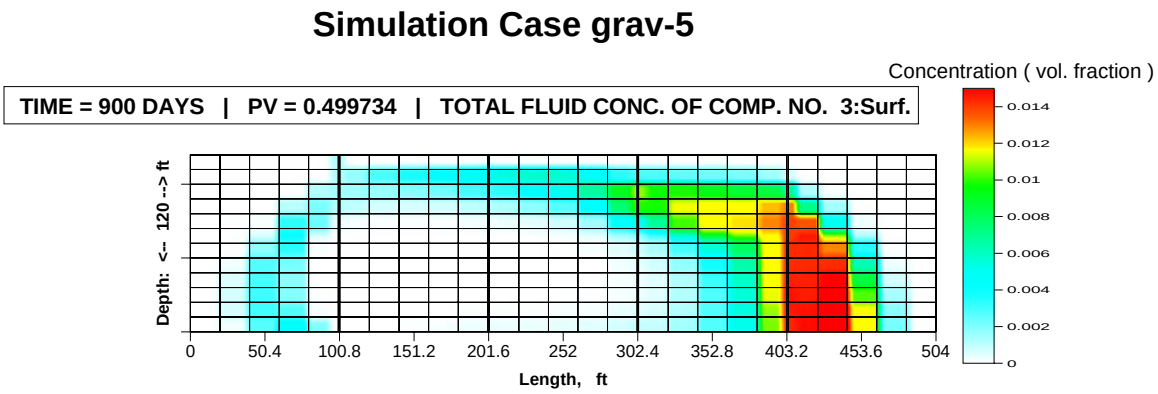

Fig. 4.27 Distribution of surfactant concentration during water injection at 900 days

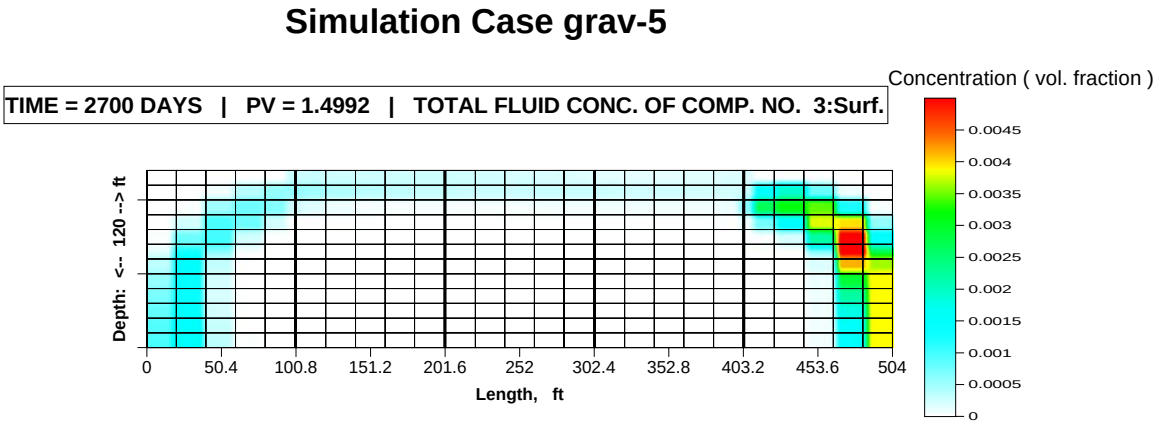

Fig. 4.28 Distribution of surfactant concentration at the end of the flood

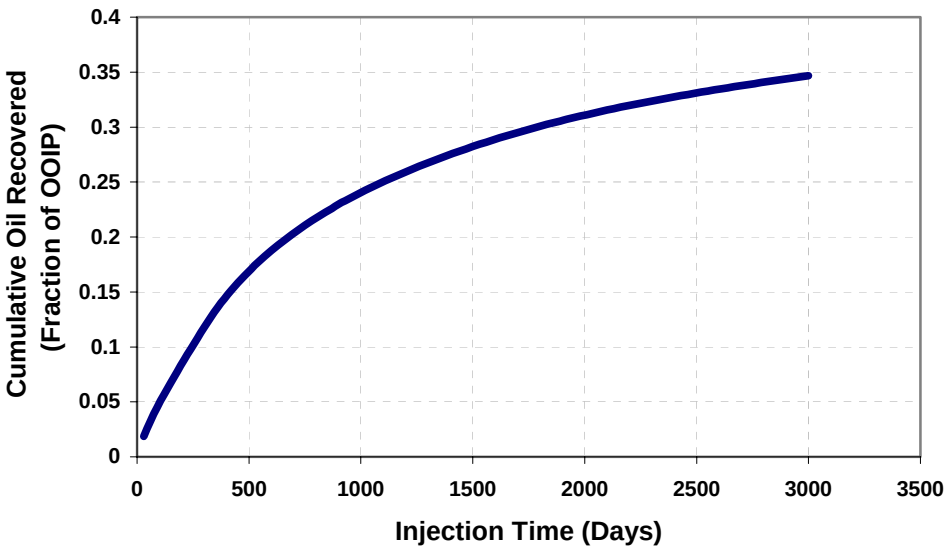

Fig. 4.29 Cumulative oil recovery for waterflood

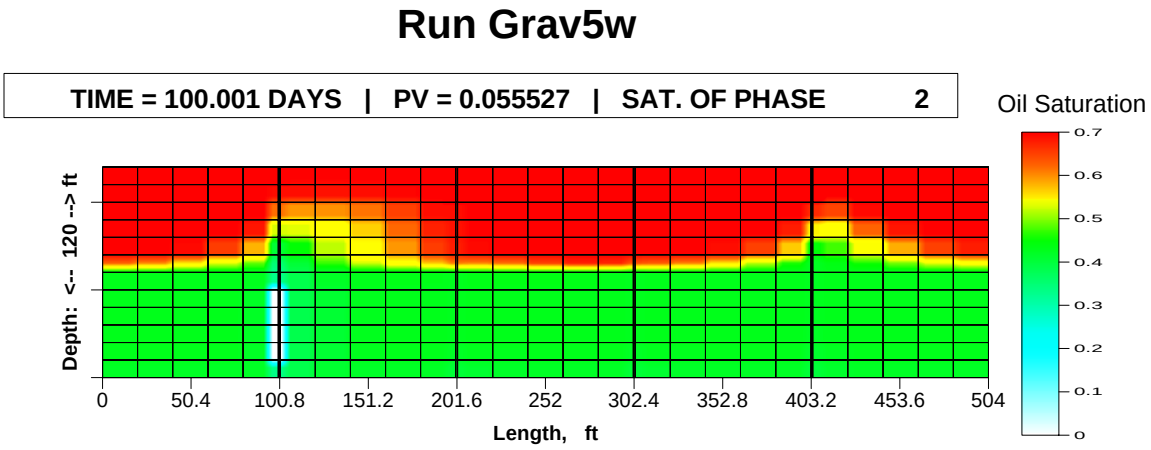

Fig. 4.30 Distribution of oil saturation for the waterflood at 100 days

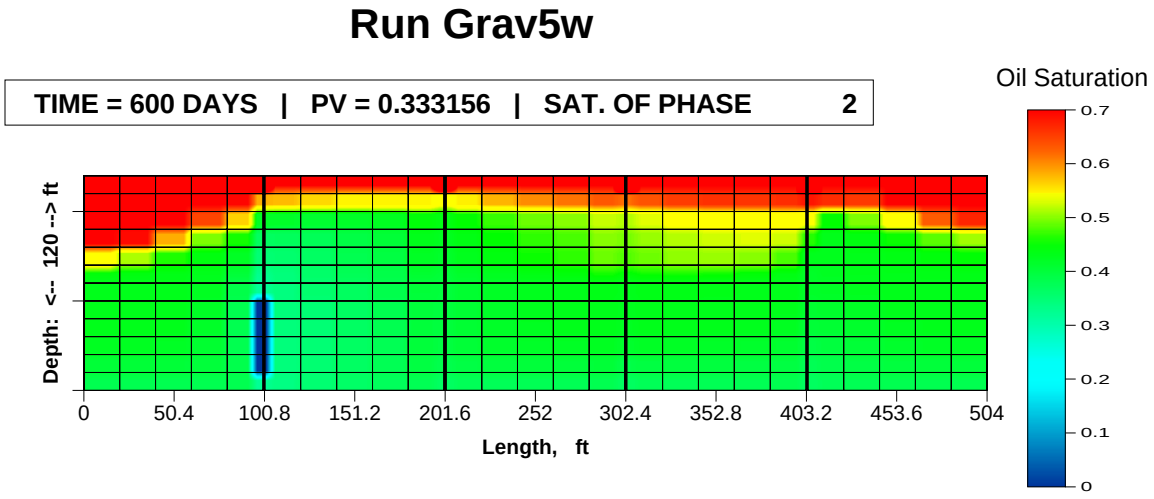

Fig. 4.31 Distribution of oil saturation for the waterflood at 600 days

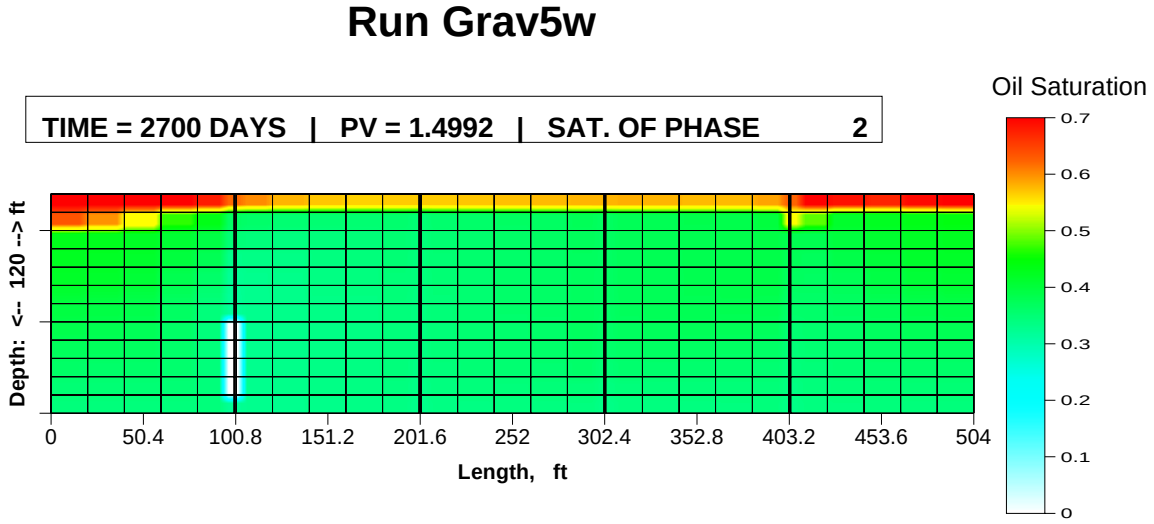

Fig. 4.32 Distribution of oil saturation for the waterflood at the end of the flood

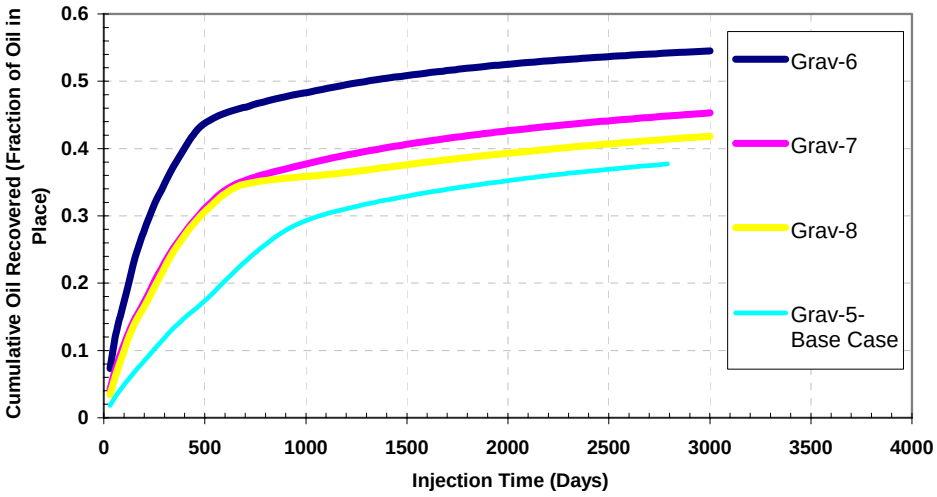

Fig. 4.33 Comparison of oil recovery for different surfactant flood sensitivity simulations